Magneto-hydrodynamic eigenvalue solver for axisymmetric equilibria based on smooth polar splines

Florian Holderied[1,2,*] and Stefan Possanner[1]

[1] *Max Planck Institute for Plasma Physics, Boltzmannstrasse 2, 85748 Garching, Germany*

[2] *Technical University of Munich, Department of Physics, James-Franck-Strasse 1, 85748 Garching, Germany*

[*] *Corresponding author: Florian Holderied, florian.holderied@ipp.mpg.de*

Abstract

We present a new eigenvalue solver for the ideal magneto-hydrodynamics (MHD) equations in axisymmetric equilibria that enables the robust and accurate description of eigenfunctions near the magnetic axis. The algorithm is based on discrete differential forms in combination with $\mathcal{C}^1$-smooth polar splines in the framework of isogeometric analysis. The symmetric discretization leads to a Hermitian Alfvén part in the MHD force operator, mirroring the self-adjointness of the continuous operator. Moreover, eigenfunctions are continuous across the magnetic axis by use of the polar spline framework. We provide comparisons to the standard tensor product approach by selected numerical examples and show that a) the polar spline framework correctly reproduces the tensor product results sufficiently far away from the magnetic axis and that b) it gives better results close to the magnetic axis with regards to back transformations to the physical (Cartesian) domain as usually needed if a coupling to a particle-in-cell code is desired.

Keywords: magneto-hydrodynamics, discrete differential forms, singular domains, polar splines

1 Introduction

The linearized ideal magneto-hydrodynamic (MHD) equations are at the center of most stability analyses concerning the design of nuclear fusion reactors such as tokamaks or stellarators. It is widely agreed upon that MHD stability is necessary for sustained power production in these reactors, even though MHD time scales are much shorter than envisioned confinement times. In its most basic form, the ideal MHD eigenvalue problem reads [15]

$$-\omega^2 \rho_{\text{eq}} \boldsymbol{U} = \mathbf{F}(\boldsymbol{U})\,, \tag{1.1}$$

where ω^2 denotes the eigenvalue, $\boldsymbol{U}$ (in some suitable space to be defined) is an eigen-solution and $\mathbf{F}$ stands for the *MHD force operator*[1],

$$\mathbf{F}(\boldsymbol{U}) = i\omega \left\{ \nabla p(\boldsymbol{U}) - \left[\nabla \times \boldsymbol{B}(\boldsymbol{U})\right] \times \boldsymbol{B}_{\text{eq}} - \boldsymbol{J}_{\text{eq}} \times \boldsymbol{B}(\boldsymbol{U}) \right\}\,, \tag{1.2}$$

where

$$i\omega\, p(\boldsymbol{U}) = \nabla \cdot (p_{\text{eq}}\, \boldsymbol{U}) + (\gamma - 1)\, p_{\text{eq}}\, \nabla \cdot \boldsymbol{U}\,, \tag{1.3}$$

$$i\omega\, \boldsymbol{B}(\boldsymbol{U}) = \nabla \times (\boldsymbol{B}_{\text{eq}} \times \boldsymbol{U})\,, \tag{1.4}$$

and $\boldsymbol{J}_{\text{eq}} = \nabla \times \boldsymbol{B}_{\text{eq}}$ denotes the equilibrium current density and $\gamma = 5/3$ the heat capacity ratio of an ideal gas (we set the vacuum permeability $\mu_0 = 1$ for the time being). The equilibrium is characterized

[1] Note that $\mathbf{F}$ is independent of ω when plugging (1.3) and (1.4) in (1.2).

by the force balance $\boldsymbol{J}_{\rm eq} \times \boldsymbol{B}_{\rm eq} = \nabla p_{\rm eq}$. Equation (1.1) is also called the *normal mode equation*, as it stems from the assumption that MHD unknowns have a time dependence $\sim \mathrm{e}^{-i\omega t}$.

To obtain unique solutions to the normal mode equation (1.1), suitable boundary conditions must be defined. In this article, we shall only consider fixed boundary modes, characterized by vanishing normal components of $\boldsymbol{U}$ at the boundary of the considered domain,

$$\boldsymbol{U} \cdot \boldsymbol{n} = 0\,, \tag{1.5}$$

where $\boldsymbol{n}$ is a outward pointing unit vector normal to the surface of the computational domain. Together with the assumption that $\boldsymbol{B}_{\rm eq} \cdot \boldsymbol{n} = 0$, it is easily verified that (1.4) ensures $\boldsymbol{B} \cdot \boldsymbol{n} = 0$. Physically speaking, we consider a plasma which is surrounded by a perfectly conducting wall.

It can be shown that the force operator $\mathbf{F}$ is self-adjoint, which means that eigenvalues ω^2 are purely real. As a consequence, stability transitions ($\mathrm{Im}(\omega) = 0 \to \mathrm{Im}(\omega) > 0$) occur at $\omega = 0$, which is beneficial for computations since the real part of the transition point is known a priori [17]. From a numerical point of view it would thus make a lot of sense to have a discrete, self-adjoint operator force operator, i.e. a Hermitian eigenvalue problem.

There exist many sophisticated solvers for the solution of (1.1) in axissymmetric equilibria (where Fourier modes in toroidal direction decouple), among the best-known being PEST [16], ERATO [18], GATO [4], as well as KINX [12] to include divertor configurations, the code in [29] and MARS [5] which include resistive effects, CASTOR [21] which can also handle 3D stellarator configurations and LIGKA [23], which includes energetic particle effects. The conventional approach is to expand the eigen-solution $\boldsymbol{U}$ in a suitable, finite set of basis functions, usually Fourier basis in the poloidal direction and spline or polynomial basis in the radial direction of the poloidal plane, and to solve the ensuing discrete eigenvalue problem. A complication arises from the geometry of the problem, which has a polar point at the magnetic axis where the Jacobian determinant of the mapping between logical and physical coordinates vanishes. This usually requires some kind of work-around when computing the push-forward of the solution to physical coordinates.

In this work we propose a new MHD eigenvalue solver that produces physical (i.e. pushed-forward) solutions which are continuous across the magnetic axis, the continuity being enforced directly through the basis functions in which $\boldsymbol{U}$ is represented. Moreover, compared to conventional approaches which usually start from a symmetrized energy functional derived from (1.1), we directly solve the system of linearized MHD equations composed of the fluid momentum balance equation, pressure equation and induction equation and hence treat the perturbed fluid velocity $\boldsymbol{U}$, the perturbed pressure p and the perturbed magnetic field $\boldsymbol{B}$ as independent variables. This is advantageous in a sense that the resulting discretized operators can directly be used in an initial value solver for the linear ideal MHD equations and/or some extended model (e.g. hybrid MHD-kinetic models). As a consequence of this strategy, our discretization leads to a "partly Hermitian" force operator, meaning that the Alfvén part $\big[\nabla \times \boldsymbol{B}(\boldsymbol{U})\big] \times \boldsymbol{B}_{\rm eq}$ of $\mathbf{F}$ is self-adjoint on the discrete level, while the other parts are left non-Hermitian and will be treated in a future work. With regards to time integration, the Hermitian Alfvén part ensures exact conservation of energy for Alfvénic modes if supplemented with a suitable time integrator (e.g. Crank-Nicolson [10]) and it is expected that this is beneficial with respect to long-term numerical stability.

In more detail, our solver is based on *discrete differential forms* in combination with *smooth polar splines*. Discrete differential forms, or finite element exterior calculus (FEEC) [2, 3], is a framework for geometric discretization of PDEs which allows to encode properties such as curl grad $= 0$ and div curl $= 0$ into conforming finite element (FE) spaces. More broadly, FEEC discretizations ensure a discrete version of Stokes theorem, which is extremely beneficial when local conservation laws are in play. On mapped domains, discrete differential forms are particularly powerful when used in the context of isogeometric-analysis (IGA) [9]. In the IGA approach, the mapping describing the geometry of the problem is represented in the same set of basis functions as the solution fields. The theory for IGA in FEEC has been worked out in [7] using tensor product B-spline basis functions. Later, this theory was extended to include also domains with a polar singularity [28, 27], leading to the notion of "smooth polar splines". These polar splines, while constructed as linear combinations of tensor product B-splines supported in the vicinity of the polar point (magnetic axis), can be made as regular

as desired when pushed-forward to physical coordinates. In this work we use $\mathcal{C}^1$-polar splines for practical reasons, as higher regularity would demand more computational resources without expecting significant improvements in the results. $\mathcal{C}^1$-regularity is necessary, however, to guarantee the continuity of the eigen-solutions of problem (1.1).

Our contribution is the formulation of a *commuting* de Rham diagram in case when the sub-complex is spanned by 2D smooth polar spline bases presented in [27], which are supplemented with a single toroidal Fourier harmonic in order to be applicable to 3D axisymmetric systems (a sub-complex applicable to general 3D configurations based on a third B-spline basis in toroidal direction was constructed in [25]). For this we define new polar projection operators that project into the polar spline spaces, such that the commuting property holds. We achieve this by formulating "polar degrees of freedom" (polar DOFs), i.e. linear functionals on functions from the de Rham sequence that define the conforming polar sub-complex. Just as the polar basis functions are linear combinations of tensor product basis functions, the polar DOFs can be constructed as linear combinations of tensor product DOFs. We provide explicit expressions for all reduction matrices needed in the process.

The article is organized as follows: First, the ideal MHD eigenvalue problem (1.1) is formulated in terms of differential forms followed by the derivation of a weak formulation suitable for a finite element discretization. The resulting weak formulation at the end of Section 2 is the basis for the presented methodologies. For this, we first review the construction of finite-dimensional subspaces of the continuous function spaces appearing in the weak formulations using $\mathcal{C}^1$-smooth polar splines introduced in [27]. Based on this, Section 4 deals with the construction of commuting projectors from the continuous spaces on the finite-dimensional subspaces. In Section 5, we apply the methods to the continuous weak formulation to obtain a discrete eigenvalue problem that can be solved for a finite set of eigenfrequencies and eigenfunctions. Finally, in Section 6, we discuss two numerical examples. On the one hand, we investigate the behavior of eigenfunctions close to the magnetic axis and, on the other hand, we perform a benchmark study with existing codes.

2 MHD with differential forms

As a first step, we shall write the MHD eigenvalue problem (1.1) in terms of differential forms (we refer to e.g. [14] for a thorough introduction to differential geometry). Consider the *logical domain* $\hat{\Omega} = [0,1]^3$ with logical coordinates $(s,\theta,\varphi) \in \hat{\Omega}$. The *physical domain* $\Omega \subset \mathbb{R}^3$ is the image of $\hat{\Omega}$ under the mapping

$$F : \hat{\Omega} \to \Omega,\ (s,\theta,\varphi) \mapsto (x,y,z) = F(s,\theta,\varphi). \tag{2.1}$$

Hence, $\boldsymbol{x} := (x,y,z)$ are global or "Cartesian" coordinates of Ω and $\boldsymbol{\eta} := (s,\theta,\varphi)$ are local, curvilinear coordinates of Ω. For the time being, the map F is assumed to be $\mathcal{C}^1$ everywhere (we can relax this assumption later when dealing with polar domains). The Jacobian matrix, its determinant and the metric tensor are denoted by DF, $\sqrt{g} := |\det(DF)|$ and $G := DF^\top DF$, respectively. Scalar functions like the plasma pressure or mass density can be written either as 0-forms or as 3-forms. On the other hand, vector-valued functions like the magnetic field can be written either as vector fields (contra-variant), as 1-forms (co-variant) or as 2-forms (pseudo-vectors). Table 1 summarizes the relevant transformation formulae which we refer to as *pull-back* ($\Omega \to \hat{\Omega}$) and *push-forward* ($\hat{\Omega} \to \Omega$) operations. The differential operators grad, curl and div transform as

$$\nabla f = DF^{-\top}\, \hat{\nabla} \hat{f}^0\,, \tag{2.2a}$$

$$\nabla \times \boldsymbol{V} = \frac{1}{\sqrt{g}}\, DF\, \hat{\nabla} \times (G\, \hat{\boldsymbol{V}}) = \frac{1}{\sqrt{g}}\, DF\, \hat{\nabla} \times \hat{\boldsymbol{V}}^1\,, \tag{2.2b}$$

$$\nabla \cdot \boldsymbol{V} = \frac{1}{\sqrt{g}}\, \hat{\nabla} \cdot (\sqrt{g}\, \hat{\boldsymbol{V}}) = \frac{1}{\sqrt{g}}\, \hat{\nabla} \cdot \hat{\boldsymbol{V}}^2\,, \tag{2.2c}$$

where $\nabla = [\,\partial_x, \partial_y, \partial_z\,]$ and $\hat{\nabla} = [\,\partial_s, \partial_\theta, \partial_\varphi\,]$ act on Cartesian and logical coordinates, respectively. From (2.2) it is immediately evident that the gradient acts on 0-forms and transforms as a 1-form, the curl acts on 1-forms and transforms as a 2-form, and the divergence acts on 2-forms and transforms as

Table 1: Summary of pull-back and push-forward transformations between generic scalar and vector-valued functions $f = f(\boldsymbol{x})$ and $\boldsymbol{V} = [V_x(\boldsymbol{x}), V_y(\boldsymbol{x}), V_z(\boldsymbol{x})]$, respectively, and differential k-forms ($0 \leq k \leq 3$) under the map $F : \hat{\Omega} \to \Omega,\ \boldsymbol{\eta} \mapsto \boldsymbol{x} = F(\boldsymbol{\eta})$.

	pull-back	push-forward
0-form	$\hat{f}^0(\boldsymbol{\eta}) = f(F(\boldsymbol{\eta}))$	$f(F(\boldsymbol{\eta})) = \hat{f}^0(\boldsymbol{\eta})$
1-form (co-variant)	$\hat{\boldsymbol{V}}^1 = \begin{bmatrix} \hat{V}_1^1(\boldsymbol{\eta}) \\ \hat{V}_2^1(\boldsymbol{\eta}) \\ \hat{V}_3^1(\boldsymbol{\eta}) \end{bmatrix} = DF^\top \begin{bmatrix} V_x(F(\boldsymbol{\eta})) \\ V_y(F(\boldsymbol{\eta})) \\ V_z(F(\boldsymbol{\eta})) \end{bmatrix}$	$\begin{bmatrix} V_x(F(\boldsymbol{\eta})) \\ V_y(F(\boldsymbol{\eta})) \\ V_z(F(\boldsymbol{\eta})) \end{bmatrix} = DF^{-\top} \begin{bmatrix} \hat{V}_1^1(\boldsymbol{\eta}) \\ \hat{V}_2^1(\boldsymbol{\eta}) \\ \hat{V}_3^1(\boldsymbol{\eta}) \end{bmatrix}$
2-form (pseudo-vector)	$\hat{\boldsymbol{V}}^2 = \begin{bmatrix} \hat{V}_1^2(\boldsymbol{\eta}) \\ \hat{V}_2^2(\boldsymbol{\eta}) \\ \hat{V}_3^2(\boldsymbol{\eta}) \end{bmatrix} = \sqrt{g}\, DF^{-1} \begin{bmatrix} V_x(F(\boldsymbol{\eta})) \\ V_y(F(\boldsymbol{\eta})) \\ V_z(F(\boldsymbol{\eta})) \end{bmatrix}$	$\begin{bmatrix} V_x(F(\boldsymbol{\eta})) \\ V_y(F(\boldsymbol{\eta})) \\ V_z(F(\boldsymbol{\eta})) \end{bmatrix} = \frac{1}{\sqrt{g}}\, DF \begin{bmatrix} \hat{V}_1^2(\boldsymbol{\eta}) \\ \hat{V}_2^2(\boldsymbol{\eta}) \\ \hat{V}_3^2(\boldsymbol{\eta}) \end{bmatrix}$
3-form	$\hat{f}^3(\boldsymbol{\eta}) = \sqrt{g}\, f(F(\boldsymbol{\eta}))$	$f(F(\boldsymbol{\eta})) = \frac{1}{\sqrt{g}}\, \hat{f}^3(\boldsymbol{\eta})$
vector field (contra-variant)	$\hat{\boldsymbol{V}} = \begin{bmatrix} \hat{V}_1(\boldsymbol{\eta}) \\ \hat{V}_2(\boldsymbol{\eta}) \\ \hat{V}_3(\boldsymbol{\eta}) \end{bmatrix} = DF^{-1} \begin{bmatrix} V_x(F(\boldsymbol{\eta})) \\ V_y(F(\boldsymbol{\eta})) \\ V_z(F(\boldsymbol{\eta})) \end{bmatrix}$	$\begin{bmatrix} V_x(F(\boldsymbol{\eta})) \\ V_y(F(\boldsymbol{\eta})) \\ V_z(F(\boldsymbol{\eta})) \end{bmatrix} = DF \begin{bmatrix} \hat{V}_1(\boldsymbol{\eta}) \\ \hat{V}_2(\boldsymbol{\eta}) \\ \hat{V}_3(\boldsymbol{\eta}) \end{bmatrix}$

a 3-form (compare with push-forward operations in Table 1). Cross products are transformed using the formula $M\boldsymbol{V} \times M\boldsymbol{W} = \det(M)\, M^{-\top}(\boldsymbol{V} \times \boldsymbol{W})$ for some invertible matrix $M \in \mathbb{R}^{3\times 3}$. For example, the cross product of two 2-forms transforms as

$$\boldsymbol{V} \times \boldsymbol{W} = \frac{1}{\sqrt{g}}\, DF^{-\top} \left(\hat{\boldsymbol{V}}^2 \times \hat{\boldsymbol{W}}^2 \right). \tag{2.3}$$

Using the transformation formulae listed in Table 1 together with (2.2) and (2.3) it is straightforward to write the MHD eigenvalue problem (1.1) in terms of differential forms. We choose to express ρ_{eq}, p_{eq} and p as 3-forms and $\boldsymbol{J}_{\text{eq}}$, $\boldsymbol{B}_{\text{eq}}$, $\boldsymbol{B}$ and $\boldsymbol{U}$ as a 2-forms. While the choices for the 3-forms, the current density and the magnetic fields are motivated by physics arguments, namely being (flux) densities, the reason for the choice of $\boldsymbol{U}$ being a 2-form is the boundary condition (1.5). It is easily understood that the second and the third basis vector of 2-forms (columns of $DF/\sqrt{g}$) are always tangential to the surface at $s = 1$. Therefore, forcing the first component of a 2-form to zero at the boundary directly leads to the boundary condition (1.5). Using the fact that equilibrium quantities are independent of the angle-like coordinate φ in axisymmetric systems, we consider a single Fourier mode with wave number $k = 2\pi \cdot n$ ($n \in \mathbb{Z}$) in φ-direction for the perturbed fields. Hence, we introduce the following notations[2]:

$$\rho^{\text{eq}} := \hat{\rho}^3_{\text{eq}}(s,\theta)\,, \qquad p^{\text{eq}} := \hat{p}^3_{\text{eq}}(s,\theta)\,, \qquad \mathbf{B}^{\text{eq}} := \hat{\boldsymbol{B}}^2_{\text{eq}}(s,\theta)\,, \qquad \mathbf{J}^{\text{eq}} := \hat{\boldsymbol{J}}^2_{\text{eq}}(s,\theta)\,, \tag{2.4}$$

$$\hat{\boldsymbol{U}}^2 = \mathbf{U}(s,\theta)\, \mathrm{e}^{ik\varphi}\,, \qquad \hat{p}^3 = p(s,\theta)\, \mathrm{e}^{ik\varphi}\,, \qquad \hat{\boldsymbol{B}}^2 = \mathbf{B}(s,\theta)\, \mathrm{e}^{ik\varphi}\,. \tag{2.5}$$

Note that we use the superscript $(\cdot)^{\text{eq}}$ for the equilibrium forms to avoid confusions with the "physical" equilibrium fields (e.g. $p_{\text{eq}} = p_{\text{eq}}(\boldsymbol{x})$ but $p^{\text{eq}} = \hat{p}^3_{\text{eq}}(s,\theta)$). The unknown functions $\mathbf{U}$, p and $\mathbf{B}$ are

[2] We remark the slight abuse of notation for p. Until now, $p = p(\boldsymbol{x})$ has denoted the pressure as a function of the Cartesian coordinates (x, y, z), whereas in the remainder of this article, $p = p(s,\theta)$ shall denote the "poloidal" part of the 3-form pressure $\hat{p}^3$.

defined on the *poloidal domain* $(s,\theta) \in \hat{\Omega}_P = [0,1]^2$ and are generally complex-valued. The "poloidal" gradient operator is $\hat{\nabla}_P := [\partial_s, \partial_\theta, ik]$ and can be used in (2.2) in place of $\hat{\nabla}$ when using the ansatz (2.5). Finally, although not appearing in (1.1), we additionally define the variables

$$\hat{f}^0 = f(s,\theta)\, \mathrm{e}^{ik\varphi}, \qquad \hat{\boldsymbol{A}}^1 = \mathbf{A}(s,\theta)\, \mathrm{e}^{ik\varphi}\,, \tag{2.6}$$

which will serve as dummy variables for 0-forms and 1-forms in the remainder of this article.

We choose to write the MHD momentum conservation law in weak form. In this way we mimic the implementation used in the STRUPHY hybrid code and preserve certain symmetries of the MHD operator [19], such as the skew-symmetry in the shear-Alfvén subsystem. For this, we define the "poloidal" L^2-scalar products

$$(f,h)_{0,P} := \int_{\hat{\Omega}_P} f\, h^* \sqrt{g}\, \mathrm{d}s\, \mathrm{d}\theta\,, \tag{2.7a}$$

$$(\mathbf{A},\mathbf{C})_{1,P} := \int_{\hat{\Omega}_P} \mathbf{A}^\top G^{-1}\, \mathbf{C}^* \sqrt{g}\, \mathrm{d}s\, \mathrm{d}\theta\,, \tag{2.7b}$$

$$(\mathbf{B},\mathbf{K})_{2,P} := \int_{\hat{\Omega}_P} \mathbf{B}^\top G\, \mathbf{K}^* \frac{1}{\sqrt{g}}\, \mathrm{d}s\, \mathrm{d}\theta\,, \tag{2.7c}$$

$$(p,r)_{3,P} := \int_{\hat{\Omega}_P} p\, r^* \frac{1}{\sqrt{g}}\, \mathrm{d}s\, \mathrm{d}\theta\,, \tag{2.7d}$$

where $(\cdot)^*$ denotes the complex conjugate. Let us remark that we once more used the assumption of axial symmetry meaning that the metric tensor G and its determinant g are real-valued and independent of the angle-like coordinate φ. Details shall be discussed in Section 3.2. Furthermore, let us introduce the function spaces

$$V^0 := H^2(\hat{\Omega}_P) \xrightarrow{\hat{\nabla}_P} V^1 := \boldsymbol{H}^1(\mathrm{curl}, \hat{\Omega}_P) \xrightarrow{\hat{\nabla}_P \times} V^2 := \boldsymbol{H}^1(\hat{\Omega}_P) \xrightarrow{\hat{\nabla}_P \cdot} V^3 := L^2(\hat{\Omega}_P)\,, \tag{2.8}$$

which form a de Rham complex with enhanced smoothness compared to the more common L^2 de Rham complex with minimal regularity (also called Stokes complex, see e.g. [20] for more details). The enhanced smoothness is needed for obtaining a well-posed weak formulation of the linearized MHD equations, which shall be given in a moment. To properly account for boundary conditions at $s = 1$ ($\partial\Omega$), we additionally define the spaces

$$V_0^0 := \left\{ f \in V^0,\ f(s=1,\theta) = 0 \quad \forall\, \theta \right\}\,, \tag{2.9a}$$

$$V_0^1 := \left\{ \mathbf{A} \in V^1,\ A_2(s=1,\theta) = 0,\ A_3(s=1,\theta) = 0 \quad \forall\, \theta \right\}\,, \tag{2.9b}$$

$$V_0^2 := \left\{ \mathbf{B} \in V^2,\ B_1(s=1,\theta) = 0 \quad \forall\, \theta \right\}\,, \tag{2.9c}$$

which ensure that elements in V_0^1 that are pushed-forward according to Table 1 have vanishing tangential components on $\partial\Omega$. Moreover, as explained previously, elements in V_0^2 that are pushed-forward have vanishing normal components on $\partial\Omega$.

To finally obtain the weak eigenvalue formulation, we multiply (1.1) with the test function $\boldsymbol{K}^*$ (which lives in the same space as $\boldsymbol{U}$), integrate over the computational domain Ω and perform integration by parts in the first and second term on the right-hand side of the MHD momentum balance equation. This is followed by transformation to differential forms (with the help of Table 1, (2.2) and (2.3)) and insertion of the ansatz (2.5). This leads to the following weak eigenvalue problem: find

non-trivial $\omega \in \mathbb{C}$ and $(\mathbf{U},\, p,\, \mathbf{B}) \in V_0^2 \times V^3 \times V_0^2$ such that

$$i\omega \left(\frac{\rho^{\mathrm{eq}}}{\sqrt{g}}\, \mathbf{U},\, \mathbf{K} \right)_{2,P} = -\left(p,\, \hat{\nabla}_P \cdot \mathbf{K} \right)_{3,P} - \left(\mathbf{B},\, \hat{\nabla}_P \times \left(\frac{1}{\sqrt{g}}\, \mathbf{B}^{\mathrm{eq}} \times \mathbf{K} \right) \right)_{2,P} - \left(\mathbf{K},\, G^{-1}\, (\mathbf{J}^{\mathrm{eq}} \times \mathbf{B}) \right)_{2,P} \qquad \forall\, \mathbf{K} \in V_0^2\,, \tag{2.10a}$$

$$i\omega\, p = \hat{\nabla}_P \cdot \left(\frac{p^{\mathrm{eq}}}{\sqrt{g}}\, \mathbf{U} \right) + (\gamma - 1) \frac{p^{\mathrm{eq}}}{\sqrt{g}}\, \hat{\nabla}_P \cdot \mathbf{U} \qquad \text{in } V^3\,, \tag{2.10b}$$

$$i\omega\, \mathbf{B} = \hat{\nabla}_P \times \left(\frac{1}{\sqrt{g}}\, \mathbf{B}^{\mathrm{eq}} \times \mathbf{U} \right) \qquad \text{in } V_0^2\,. \tag{2.10c}$$

The two boundary terms appearing on the right-hand side of (2.10a) when integrating by parts vanish due to the choice $\mathbf{K} \in V_0^2$ and the assumption that $\boldsymbol{B}_{\mathrm{eq}} \cdot \boldsymbol{n} = 0$. Moreover, we assume the equilibrium fields ρ^{eq} and p^{eq} and the components of $\mathbf{B}^{\mathrm{eq}}$ and $\mathbf{J}^{\mathrm{eq}}$ to be in $\mathcal{C}^\infty$ for simplicity. As already stated in the Introduction, system (2.10) is the basis for the methodologies presented in this article and the aim is to find a corresponding discrete version.

3 Discrete differential forms on polar domains

3.1 Review on tensor product B-splines

Let $\Omega_s = \Omega_\theta = [0,1]$ with partitions defined by $0 = s_0 < s_1 \ldots < s_{n_s - q_s} = 1$ and $0 = \theta_0 < \theta_1 \ldots < \theta_{n_\theta} = 1$ such that the number of cells (or elements) is $n_s - q_s$ and n_θ, respectively. Uni-variate B-spline bases of degree $q_s \geq 1$ and $q_\theta \geq 1$ are defined via the knot sequences

$$T_s := (\underbrace{0, \ldots, 0}_{q_s \text{ times}}, s_0, s_1, \ldots, s_{n_s - q_s - 1}, s_{n_s - q_s}, \underbrace{1, \ldots, 1}_{q_s \text{ times}})\,, \tag{3.1}$$

$$T_\theta := (\underbrace{\theta_{-q_\theta}, \ldots, \theta_{-1}}_{q_\theta \text{ points}}, \theta_0, \theta_1, \ldots, \theta_{n_\theta - 1}, \theta_{n_\theta}, \underbrace{\theta_{n_\theta + 1}, \ldots, \theta_{n_\theta + q_\theta}}_{q_\theta \text{ points}})\,. \tag{3.2}$$

For details on B-splines, see e.g. [11, 24]. We construct *clamped* B-splines in Ω_s and *periodic* B-splines in Ω_θ. In the periodic case, we have $\theta_{-i} = \theta_{n_\theta - i} - 1$ and $\theta_{n_\theta + i} = \theta_i + 1$ for $i \in \{1, \ldots, q_\theta\}$ and the multiplicity of each knot is 1. The knot sequence T_θ containing $n_\theta + 2q_\theta + 1$ distinct cell interfaces yields $n_\theta + q_\theta$ shifted B-splines of identical shape that are $\mathcal{C}^{q_\theta - 1}$ everywhere. The last q_θ B-splines are identified with the first q_θ B-splines to ensure periodicity. This yields the final number of n_θ linearly independent periodic B-spline basis functions in Ω_θ, denoted by $N_i^{q_\theta}(\theta)$ with $i \in \{0, \ldots, n_\theta - 1\}$. In the clamped case, the knot sequence T_s with $n_s + q_s + 1$ points yields n_s B-splines, where all, except for the first and the last B-spline, are $\mathcal{C}^{q_s - 1}$ everywhere. Hence, we obtain n_s linearly independent clamped B-spline basis functions in Ω_s, denoted by $N_i^{q_s}(s)$ with $i \in \{0, \ldots, n_s - 1\}$. Since the first and the last knot have multiplicity $q_s + 1$, the first and the last B-spline are interpolatory at $s = 0$ and $s = 1$, respectively:

$$N_0^{q_s}(0) = N_{n_s - 1}^{q_s}(1) = 1\,, \qquad N_{i>0}^{q_s}(0) = N_{i<n_s - 1}^{q_s}(1) = 0\,. \tag{3.3}$$

This allows for an efficient construction of spaces of the form (2.9) by simply removing contributions from the last spline $N_{n_s - 1}^{q_s}(s)$. The derivatives of B-splines $N_i^{q_s}(s)$ and $N_i^{q_\theta}(\theta)$ can be expressed as

$$\frac{\mathrm{d}}{\mathrm{d}s} N_i^{q_s}(s) = q_s \left(\frac{N_i^{q_s - 1}(s)}{T_{s,i+q_s} - T_{s,i}} - \frac{N_{i+1}^{q_s - 1}(s)}{T_{s,i+q_s+1} - T_{s,i+1}} \right)\,, \quad N_0^{q_s - 1}(s) = N_{n_s}^{q_s - 1}(s) = 0\,, \tag{3.4}$$

$$\frac{\mathrm{d}}{\mathrm{d}\theta} N_i^{q_\theta}(\theta) = q_\theta \left(\frac{N_i^{q_\theta - 1}(\theta)}{T_{\theta,i+q_\theta} - T_{\theta,i}} - \frac{N_{i+1}^{q_\theta - 1}(\theta)}{T_{\theta,i+q_\theta+1} - T_{\theta,i+1}} \right)\,, \tag{3.5}$$

where $N_i^{q_s-1}(s)$ and $N_i^{q_\theta-1}(\theta)$ are lower degree B-splines created from the same knot sequences (3.1) and (3.2), respectively. It is convenient to define the lower degree, re-scaled B-splines (also called M-splines)

$$D_i^{q_s}(s) := q_s \frac{N_{i+1}^{q_s-1}(s)}{T_{s,i+q_s+1} - T_{s,i+1}}, \qquad D_i^{q_\theta}(\theta) := q_\theta \frac{N_{i+1}^{q_\theta-1}(\theta)}{T_{\theta,i+q_\theta+1} - T_{\theta,i+1}}, \tag{3.6}$$

where $i \in \{0, \dots, d_s - 1\}$ with $d_s = n_s - 1$ for $D_i^{q_s}(s)$. In the periodic case the last $q_\theta - 1$ M-splines that have a non-vanishing support in Ω_θ are once more identified with the first $q_\theta - 1$ M-splines. This yields the total number of $d_\theta = n_\theta$ linearly independent periodic M-splines. Using (3.6) the recursion formulae for the derivatives (3.4) become

$$\frac{\mathrm{d}}{\mathrm{d}s} N_i^{q_s}(s) = D_{i-1}^{q_s}(s) - D_i^{q_s}(s), \qquad D_{-1}^{q_s}(s) = D_{n_s-1}^{q_s}(s) = 0, \tag{3.7}$$

$$\frac{\mathrm{d}}{\mathrm{d}\theta} N_i^{q_\theta}(\theta) = D_{i-1}^{q_\theta}(\theta) - D_i^{q_\theta}(\theta). \tag{3.8}$$

Finally, we define the so-called Greville points [13], denoted by $(\mathfrak{s}_i)_{i=0}^{n_s-1}$ and $(\mathfrak{t}_i)_{i=0}^{n_\theta-1}$:

$$\mathfrak{s}_i := \frac{1}{q_s} \sum_{j=i+1}^{i+q_s} T_{s,j}, \qquad \mathfrak{t}_i := \frac{1}{q_\theta} \sum_{j=i+1}^{i+q_\theta} T_{\theta,j}. \tag{3.9}$$

These points will serve as interpolation points in Section 4 when projection operators on B-spline spaces based on interpolation and histopolation are introduced. A Greville point is generally located close the maximum of the B-spline with the same index. Typical examples of uni-variate B-spline bases are plotted in Figure 1 for the clamped (top left) and the periodic (bottom left) case. The corresponding lower degree, re-scaled B-splines (here called M-splines) are plotted in the right column. The splines are created from equally spaced cell interfaces (here called break points) and the Greville points (3.9) are shown as well (red dots).

Based on the introduced uni-variate B-spline bases in both directions s and θ, we define the following function spaces:

$$V_h^{s,0} := \left\{ f(s) = \sum_{i=0}^{n_s-1} f_i N_i^{q_s}(s), \quad f_i \in \mathbb{C} \right\}, \qquad \dim V_h^{s,0} = n_s, \tag{3.10a}$$

$$V_h^{s,1} := \left\{ f(s) = \sum_{i=0}^{d_s-1} f_i D_i^{q_s}(s), \quad f_i \in \mathbb{C} \right\}, \qquad \dim V_h^{s,1} = d_s = n_s - 1, \tag{3.10b}$$

$$V_h^{\theta,0} := \left\{ g(\theta) = \sum_{i=0}^{n_\theta-1} g_i N_i^{q_\theta}(\theta), \quad g_i \in \mathbb{C} \right\}, \qquad \dim V_h^{\theta,0} = n_\theta, \tag{3.10c}$$

$$V_h^{\theta,1} := \left\{ g(\theta) = \sum_{i=0}^{d_\theta-1} g_i D_i^{q_\theta}(\theta), \quad g_i \in \mathbb{C} \right\}, \qquad \dim V_h^{\theta,1} = d_\theta = n_\theta. \tag{3.10d}$$

For $f_h \in V_h^{s,0}$ and $g_h \in V_h^{\theta,0}$ we have for the derivatives, thanks to (3.7) and (3.8),

$$f_h' = \sum_{i=0}^{n_s-1} f_i (D_{i-1}^{q_s} - D_i^{q_s}) = \sum_{i=0}^{d_s-1} (f_{i+1} - f_i) D_i^{q_s} \quad \in V_h^{s,1}, \tag{3.11}$$

$$g_h' = \sum_{i=0}^{n_\theta-1} g_i (D_{i-1}^{q_\theta} - D_i^{q_\theta}) = \sum_{i=0}^{d_\theta-1} (g_{i+1} - g_i) D_i^{q_\theta} \quad \in V_h^{\theta,1}. \tag{3.12}$$

Hence, we can define the derivative matrices $\mathbb{G}^s \in \mathbb{R}^{d_s \times n_s}$ and $\mathbb{G}^\theta \in \mathbb{R}^{d_\theta \times n_\theta}$ with entries

$$\mathbb{G}_{ij}^s := \begin{cases} -1 & \text{for} \quad j = i, \\ 1 & \text{for} \quad j = i+1, \\ 0 & \text{else}, \end{cases} \qquad \mathbb{G}_{ij}^\theta := \begin{cases} -1 & \text{for} \quad j = i, \\ 1 & \text{for} \quad j = \mathrm{mod}(i+1, n_\theta), \\ 0 & \text{else}, \end{cases} \tag{3.13}$$

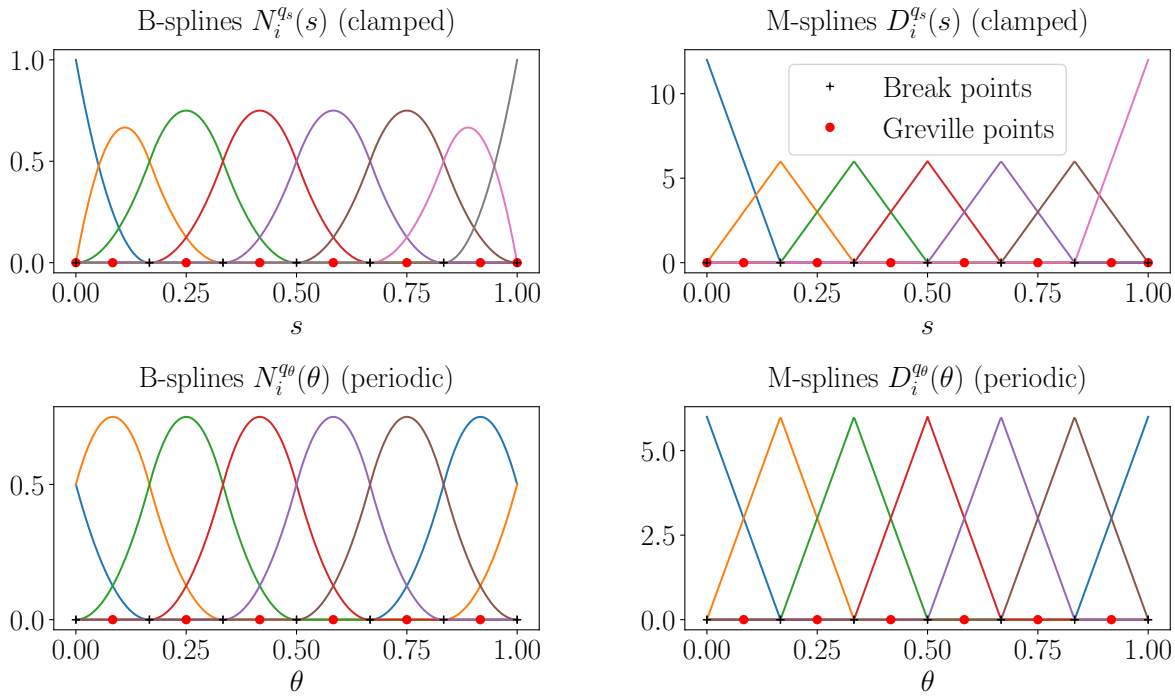

Figure 1: B-spline basis functions of degree $q_s = q_\theta = 2$ on a uniform grid with $n_s - q_s = n_\theta = 6$ cells defined by equally spaced break points (black crosses). Shown are clamped (top left) and periodic (bottom left) B-splines. The corresponding lower degree ($q_s - 1 = q_\theta - 1 = 1$), re-scaled B-splines (here called M-splines) are plotted for the clamped (top right) and the periodic (bottom right) case. The corresponding Greville points (3.9) are shown as well (red dots).

respectively. By additionally stacking FE coefficients and basis functions on top of each other (bold symbols),

$$\mathbf{f} := (f_i)_{i=0}^{n_s-1}\,, \qquad \mathbf{N}^s := (N_i^{q_s})_{i=0}^{n_s-1}\,, \qquad \mathbf{D}^s := (D_i^{q_s})_{i=0}^{d_s-1}\,, \tag{3.14}$$

$$\mathbf{g} := (g_i)_{i=0}^{n_\theta-1}\,, \qquad \mathbf{N}^\theta := (N_i^{q_\theta})_{i=0}^{n_\theta-1}\,, \qquad \mathbf{D}^\theta := (D_i^{q_\theta})_{i=0}^{d_\theta-1}\,, \tag{3.15}$$

functions $f_h \in V_h^{s,0}$ and $g_h \in V_h^{\theta,0}$ and their derivatives $f_h' \in V_h^{s,1}$ and $g_h' \in V_h^{\theta,1}$ can compactly be written as

$$f_h = \mathbf{f}^\top \mathbf{N}^s\,, \qquad f_h' = (\mathbb{G}^s\,\mathbf{f})^\top \mathbf{D}^s\,, \tag{3.16}$$

$$g_h = \mathbf{g}^\top \mathbf{N}^\theta\,, \qquad g_h' = (\mathbb{G}^\theta\,\mathbf{g})^\top \mathbf{D}^\theta\,, \tag{3.17}$$

respectively.

To represent two-dimensional functions, let us define the tensor product spaces

$$V_h^0 := \left\{ f_h(s,\theta) = \sum_{i=0}^{n_s-1} \sum_{j=0}^{n_\theta-1} f_{(ij)}\, N_i^{q_s}(s) N_j^{q_\theta}(\theta)\,, \quad f_{(ij)} \in \mathbb{C} \right\}\,, \qquad \dim V_h^0 = n_s n_\theta\,, \tag{3.18a}$$

$$V_h^{1,1} := \left\{ f_h(s,\theta) = \sum_{i=0}^{d_s-1} \sum_{j=0}^{n_\theta-1} f_{(ij)}\, D_i^{q_s}(s) N_j^{q_\theta}(\theta)\,, \quad f_{(ij)} \in \mathbb{C} \right\}\,, \qquad \dim V_h^{1,1} = d_s n_\theta\,, \tag{3.18b}$$

$$V_h^{1,2} := \left\{ f_h(s,\theta) = \sum_{i=0}^{n_s-1} \sum_{j=0}^{d_\theta-1} f_{(ij)}\, N_i^{q_s}(s) D_j^{q_\theta}(\theta)\,, \quad f_{(ij)} \in \mathbb{C} \right\}\,, \qquad \dim V_h^{1,2} = n_s d_\theta\,, \tag{3.18c}$$

$$V_h^3 := \left\{ f_h(s,\theta) = \sum_{i=0}^{d_s-1} \sum_{j=0}^{d_\theta-1} f_{(ij)}\, D_i^{q_s}(s) D_j^{q_\theta}(\theta)\,, \quad f_{(ij)} \in \mathbb{C} \right\}\,, \qquad \dim V_h^3 = d_s d_\theta\,. \tag{3.18d}$$

Two-dimensional indices are "flattened" in row-major ordering. Hence, in the definition of the spaces, we introduced the *flattened-index notation* (ij) which enables us to stack tensor product basis functions (and coefficients) in the following way:

$$\begin{aligned} &\boldsymbol{\Lambda}^0 := (\Lambda^0_{(ij)}) \in \mathbb{R}^{n_s n_\theta}\,, \qquad \Lambda^0_{(ij)} := N_i^{q_s} N_j^{q_\theta}\,, \\ &\quad \text{with} \quad (ij) = n_\theta\, i + j\,, \qquad 0 \le i < n_s\,, \quad 0 \le j < n_\theta\,, \end{aligned} \tag{3.19}$$

$$\begin{aligned} &\boldsymbol{\Lambda}^3 := (\Lambda^3_{(ij)}) \in \mathbb{R}^{d_s d_\theta}\,, \qquad \Lambda^3_{(ij)} := D_i^{q_s} D_j^{q_\theta}\,, \\ &\quad \text{with} \quad (ij) = d_\theta\, i + j\,, \qquad 0 \le i < d_s\,, \quad 0 \le j < d_\theta\,. \end{aligned} \tag{3.20}$$

Moreover, we introduce the two product spaces

$$V_h^1 := V_h^{1,1} \times V_h^{1,2} \times V_h^0\,, \qquad \dim V_h^1 = d_s n_\theta + n_s d_\theta + n_s n_\theta\,, \tag{3.21a}$$

$$V_h^2 := V_h^{1,2} \times V_h^{1,1} \times V_h^3\,, \qquad \dim V_h^2 = n_s d_\theta + d_s n_\theta + d_s d_\theta\,, \tag{3.21b}$$

with their respective stacked vector valued basis functions

$$\vec{\boldsymbol{\Lambda}}^1 := [\,\vec{\boldsymbol{\Lambda}}^{1,1}, \vec{\boldsymbol{\Lambda}}^{1,2}, \vec{\boldsymbol{\Lambda}}^{1,3}\,]\,, \qquad \vec{\boldsymbol{\Lambda}}^2 := [\,\vec{\boldsymbol{\Lambda}}^{2,1}, \vec{\boldsymbol{\Lambda}}^{2,2}, \vec{\boldsymbol{\Lambda}}^{2,3}\,]\,, \tag{3.22}$$

where

$$\vec{\boldsymbol{\Lambda}}^{1,\mu} := (\vec{\Lambda}^{1,\mu}_{(ij)})\,, \qquad \vec{\Lambda}^{1,1}_{(ij)} := \begin{bmatrix} D_i^{q_s} N_j^{q_\theta} \\ 0 \\ 0 \end{bmatrix}\,, \quad \vec{\Lambda}^{1,2}_{(ij)} := \begin{bmatrix} 0 \\ N_i^{q_s} D_j^{q_\theta} \\ 0 \end{bmatrix}\,, \quad \vec{\Lambda}^{1,3}_{(ij)} := \begin{bmatrix} 0 \\ 0 \\ N_i^{q_s} N_j^{q_\theta} \end{bmatrix}\,, \tag{3.23}$$

$$\vec{\boldsymbol{\Lambda}}^{2,\mu} := (\vec{\Lambda}^{2,\mu}_{(ij)})\,, \qquad \vec{\Lambda}^{2,1}_{(ij)} := \begin{bmatrix} N_i^{q_s} D_j^{q_\theta} \\ 0 \\ 0 \end{bmatrix}\,, \quad \vec{\Lambda}^{2,2}_{(ij)} := \begin{bmatrix} 0 \\ D_i^{q_s} N_j^{q_\theta} \\ 0 \end{bmatrix}\,, \quad \vec{\Lambda}^{2,3}_{(ij)} := \begin{bmatrix} 0 \\ 0 \\ D_i^{q_s} D_j^{q_\theta} \end{bmatrix}\,. \tag{3.24}$$

We point to the difference between the bases $\boldsymbol{\Lambda}^k$ $(k = 0, 3)$ and $\vec{\boldsymbol{\Lambda}}^k$ $(k = 1, 2)$, the former being used for scalar functions while the latter is used for vector valued functions with values in $\mathbb{C}^3$. The components $\mu = 1, 2, 3$ indicated by the arrow are usually written with an upper index, whereas FE indices referring to the bold symbol are lower indices. Discrete functions can now compactly be written as

$$V_h^0 \ni f_h = \mathcal{S}_0[\,\mathbf{f}\,] = \mathbf{f}^\top \boldsymbol{\Lambda}^0\,, \qquad \mathbf{f} := \quad (f_{(ij)}) \quad \in \mathbb{C}^{n_s n_\theta}\,, \tag{3.25}$$

$$V_h^1 \ni \mathbf{A}_h = \mathcal{S}_1[\,\vec{\mathbf{a}}\,] = \vec{\mathbf{a}}^\top \vec{\boldsymbol{\Lambda}}^1\,, \qquad \vec{\mathbf{a}} := \begin{bmatrix} \mathbf{a}^1 := (a^1_{(ij)}) \\ \mathbf{a}^2 := (a^2_{(ij)}) \\ \mathbf{a}^3 := (a^3_{(ij)}) \end{bmatrix} \in \mathbb{C}^{(d_s n_\theta + n_s d_\theta + n_s n_\theta)}\,, \tag{3.26}$$

$$V_h^2 \ni \mathbf{B}_h = \mathcal{S}_2[\,\vec{\mathbf{b}}\,] = \vec{\mathbf{b}}^\top \vec{\boldsymbol{\Lambda}}^2\,, \qquad \vec{\mathbf{b}} := \begin{bmatrix} \mathbf{b}^1 := (b^1_{(ij)}) \\ \mathbf{b}^2 := (b^2_{(ij)}) \\ \mathbf{b}^3 := (b^3_{(ij)}) \end{bmatrix} \in \mathbb{C}^{(n_s d_\theta + d_s n_\theta + d_s d_\theta)}\,, \tag{3.27}$$

$$V_h^3 \ni p_h = \mathcal{S}_3[\,\mathbf{p}\,] = \mathbf{p}^\top \boldsymbol{\Lambda}^3\,, \qquad \mathbf{p} := \quad (p_{(ij)}) \quad \in \mathbb{C}^{d_s d_\theta}\,, \tag{3.28}$$

where the operators $\mathcal{S}_k : \mathbb{C}^{\dim V_h^k} \to V_h^k$ $(0 \le k \le 3)$ map FE coefficients to the corresponding spline space V_h^k. With regards to derivatives (grad, curl and div), let us introduce the tensor product matrices

$$\mathbb{D}^s := \mathbb{G}^s \otimes \mathbb{1}^\theta\,, \qquad \mathbb{D}^\theta := \mathbb{1}^s \otimes \mathbb{G}^\theta\,, \tag{3.29}$$

where $\otimes$ denotes the Kronecker product of two matrices. The size of the identity matrices $\mathbb{1}$ will be adapted to the corresponding space it acts on; hence $\mathbb{1}^s = \mathbb{1}_{n_s}$ or $\mathbb{1}^s = \mathbb{1}_{d_s}$ and accordingly for $\mathbb{1}^\theta$. Thus, the following derivatives are easily computed in view of (3.11) and (3.12),

$$\hat{\nabla}_P f_h = (\mathbb{G}\,\mathbf{f})^\top \vec{\mathbf{\Lambda}}^1 \in V_h^1\,, \qquad \mathbb{G} := \begin{bmatrix} \mathbb{D}^s \\ \mathbb{D}^\theta \\ ik\,\mathbb{1} \end{bmatrix}\,, \tag{3.30}$$

$$\hat{\nabla}_P \times \mathbf{A}_h = (\mathbb{C}\,\vec{\mathbf{a}})^\top \vec{\mathbf{\Lambda}}^2 \in V_h^2\,, \qquad \mathbb{C} := \begin{bmatrix} 0 & -ik\,\mathbb{1} & \mathbb{D}^\theta \\ ik\,\mathbb{1} & 0 & -\mathbb{D}^s \\ -\mathbb{D}^\theta & \mathbb{D}^s & 0 \end{bmatrix}\,, \tag{3.31}$$

$$\hat{\nabla}_P \cdot \mathbf{B}_h = (\mathbb{D}\,\vec{\mathbf{b}})^\top \mathbf{\Lambda}^3 \in V_h^3\,, \qquad \mathbb{D} := \left[\begin{array}{c|c|c} \mathbb{D}^s & \mathbb{D}^\theta & ik\,\mathbb{1} \end{array}\right]\,, \tag{3.32}$$

where $\mathbb{1} = \mathbb{1}^s \otimes \mathbb{1}^\theta$ with appropriate sizes of $\mathbb{1}^s$ and $\mathbb{1}^\theta$ as explained before. Note that we use the same symbol $\mathbb{C}$ for the discrete curl matrix (3.31) and the space of complex numbers. By construction, it is immediately evident that

$$\mathbb{C}\,\mathbb{G} = 0\,, \qquad \mathbb{D}\,\mathbb{C} = 0\,, \tag{3.33}$$

which allows the construction of the discrete cochain complex

$$V_h^0 \xrightarrow{\mathbb{G}} V_h^1 \xrightarrow{\mathbb{C}} V_h^2 \xrightarrow{\mathbb{D}} V_h^3\,, \tag{3.34}$$

meaning that the image of the previous operator (either $\mathbb{G}$ or $\mathbb{C}$) is in the kernel of the next operator (either $\mathbb{C}$ or $\mathbb{D}$).

3.2 Mappings with polar singularity

Let us make two generic assumptions on the mapping $F : (s, \theta, \varphi) \mapsto (x, y, z) = F(s, \theta, \varphi)$ introduced in Section 2:

1. Axial symmetry: the metric tensor $G = DF^\top DF$ is independent of the angle-like coordinate φ.
2. There is a polar singularity at $s = 0$, i.e. for fixed $\varphi = \varphi_0$ the function $F(0, \theta, \varphi_0)$ is independent of θ such that the Jacobian determinant $\det DF(s = 0, \theta) = 0$ but $\det DF(s > 0, \theta) \neq 0$.

As prototypical examples we consider mappings of the form

$$F_{\text{cyl}}(s, \theta, \varphi) := \begin{bmatrix} R(s, \theta) \\ 2\pi R_0\, \varphi \\ Z(s, \theta) \end{bmatrix}\,, \qquad F_{\text{tor}}(s, \theta, \varphi) := \begin{bmatrix} R(s, \theta)\cos(2\pi\varphi) \\ R(s, \theta)\sin(2\pi\varphi) \\ Z(s, \theta) \end{bmatrix}\,, \tag{3.35}$$

where the second mapping F_{tor} represents a toroidal configuration with φ being the geometrical toroidal angle. In contrast to that, the first mapping F_{cyl} represents a straight configuration with length $2\pi R_0$ such that φ plays the role of the (normalized) axial coordinate of a cylindrical configuration (typically z, but y in the present case). In both cases the "poloidal" mapping F_{pol} is such that

$$F_{\text{pol}} : (s, \theta) \mapsto (R, Z), \qquad DF_{\text{pol}}\big|_{s=0} = \begin{bmatrix} \frac{\partial R}{\partial s} & \frac{\partial R}{\partial \theta} \\ \frac{\partial Z}{\partial s} & \frac{\partial Z}{\partial \theta} \end{bmatrix}\Bigg|_{s=0} = \begin{bmatrix} \frac{\partial R}{\partial s}\big|_{s=0} & 0 \\ \frac{\partial Z}{\partial s}\big|_{s=0} & 0 \end{bmatrix}\,. \tag{3.36}$$

The simplest example would be the standard square-to-disc mapping

$$R(s, \theta) = R_0 + a\, s \cos(2\pi\theta)\,, \tag{3.37a}$$

$$Z(s, \theta) = Z_0 + a\, s \sin(2\pi\theta)\,, \tag{3.37b}$$

where (R_0, Z_0) is the center of the disc and a its radius. In case of the toroidal mapping (3.35), R_0 and a have the meaning of the major and minor radius of the torus, respectively. However, other mappings with more complicated poloidal cross sections can be considered as well as long as (3.36) holds. In view of applications in fusion research, the functions $R(s,\theta)$ and $Z(s,\theta)$ are usually chosen in a way that (s,θ) become *magnetic flux coordinates*, i.e. for fixed $s = s_0$, the curve $\gamma(\theta) = (R(s_0,\theta), Z(s_0,\theta))$ defines a closed magnetic flux surface corresponding to a given MHD equilibrium. A common choice for the angle-like coordinate θ is then to define it in a way that magnetic field lines become straight when plotted in the (θ,φ)-plane. However, other choices can be made as well.

With regards to differential forms that are obtained by pull-back operations under polar mappings with the above stated properties, one can deduce the following properties for differential forms at the pole:

$$\text{polar 0-forms}: \quad f(s=0,\theta) = f_0 \qquad \forall\,\theta\,, \tag{3.38a}$$

$$\text{polar 1-forms}: \quad A_2(s=0,\theta) = 0\,, \quad A_3(s=0,\theta) = A_0 \qquad \forall\,\theta\,, \tag{3.38b}$$

$$\text{polar 2-forms}: \quad B_1(s=0,\theta) = 0\,, \quad B_3(s=0,\theta) = 0 \qquad \forall\,\theta\,, \tag{3.38c}$$

$$\text{polar 3-forms}: \quad p(s=0,\theta) = 0 \qquad \forall\,\theta\,. \tag{3.38d}$$

The polar spline framework for discrete differential forms laid out in [27] is designed in way that it meets the requirements (3.38) while keeping the discrete cochain complex property (3.34). Moreover, the push-forward of a polar spline is sufficiently regular at the pole ($\mathcal{C}^1$ for 0-forms in this work for instance). The framework is based on the isogeometric approach, which means that the mapping F_{pol} must be represented in the *same* B-spline basis that is used to construct the space V_h^0 in (3.18a), i.e.

$$V_h^0 \ni R_h(s,\theta) = \mathcal{S}_0[\,\mathbf{R}\,] = R_0 + \sum_{i=1}^{n_s-1} \sum_{j=0}^{n_\theta-1} R_{(ij)}\, N_i^{q_s}(s) N_j^{q_\theta}(\theta)\,, \tag{3.39a}$$

$$V_h^0 \ni Z_h(s,\theta) = \mathcal{S}_0[\,\mathbf{Z}\,] = Z_0 + \sum_{i=1}^{n_s-1} \sum_{j=0}^{n_\theta-1} Z_{(ij)}\, N_i^{q_s}(s) N_j^{q_\theta}(\theta)\,. \tag{3.39b}$$

The FE coefficients $\mathbf{R} := (R_{(ij)})$ and $\mathbf{Z} := (Z_{(ij)})$ are called the *control points* of the poloidal mapping; they can be obtained by interpolation of given analytical expressions like (3.37), or, once more in view of fusion research, by interpolation of a given poloidal magnetic flux function $\psi = \psi(R,Z)$, e.g. obtained by an MHD equilibrium code, in a way that (s,θ) become magnetic flux coordinates. Note that in (3.39) we used that $R_{(0j)} = R_0$ and $Z_{(0j)} = Z_0$ $\forall j$ representing the pole (R_0, Z_0) on the physical domain.

3.3 Discrete polar 0-forms

The details of constructing the $\mathcal{C}^1$-continuous polar basis for the V_h^0-space from spline mappings such as (3.39) are given in [28, 26] and will not be repeated here. We start directly from the result and review the derivation of basis functions for the other spaces in the discrete de Rham sequence, namely V_h^k $(0 \le k \le 3)$. These spaces will be $\mathcal{C}^0$ at the pole $s = 0$ because a) first derivatives are, and b) mixed first derivatives will turn out to be zero. According to [28], a $\mathcal{C}^1$-continuous polar differential 0-form f_h is represented as

$$f_h(s,\theta) = \sum_{\ell=0}^{2} f_\ell \underbrace{\sum_{i=0}^{1} \sum_{j=0}^{n_\theta-1} \chi_{ij}^{\ell} N_i^{q_s}(s) N_j^{q_\theta}(\theta)}_{=:\overline{\Lambda}_\ell^0(s,\theta)} + \sum_{i>1,j} f_{(\overline{ij})} N_i^{q_s}(s) N_j^{q_\theta}(\theta)\,, \tag{3.40}$$

where the meaning of $(\overline{ij})$ is given in (3.46). The three new polar basis functions are denoted by $\overline{\Lambda}_\ell^0$ with $\ell = 0,1,2$; they are obtained by linear combination of $i = 0$ and $i = 1$ tensor product basis functions. The dimension of the polar subspace is thus

$$\overline{n}^0 := (n_s - 2)\, n_\theta + 3\,. \tag{3.41}$$

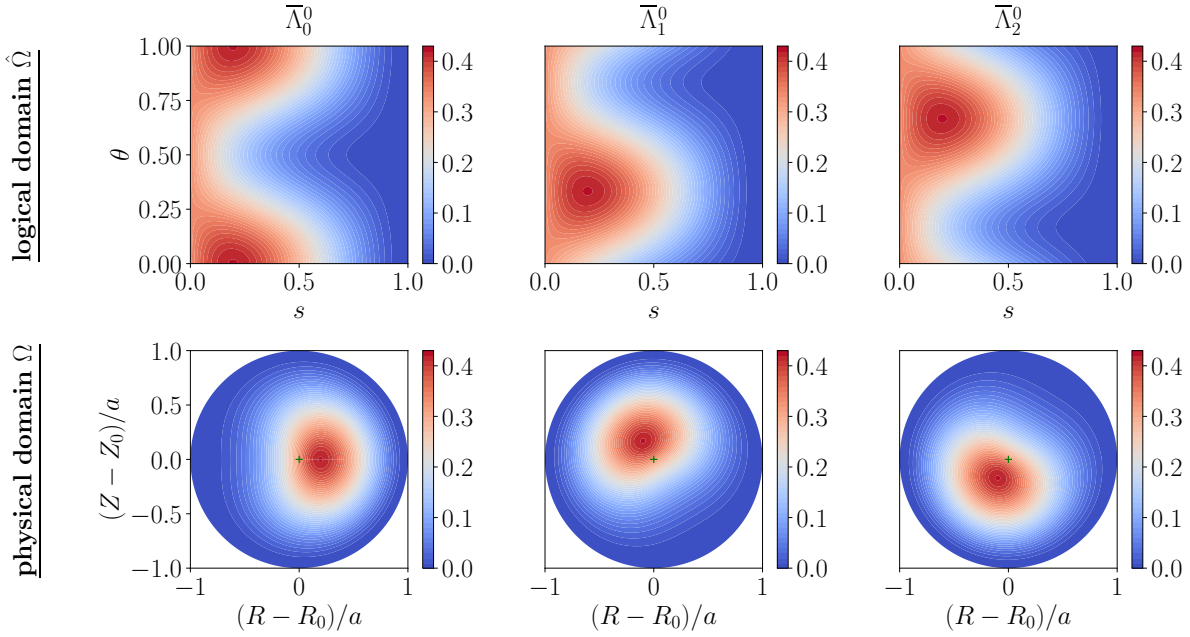

.

Figure 2: The three new basis functions $\overline{\Lambda}^0_0$, $\overline{\Lambda}^0_1$ and $\overline{\Lambda}^0_2$ for the example $q_s = q_\theta = 3$, $n_s = 4$ and $n_\theta = 12$ on the logical domain (upper row) and physical domain (lower row) using the generic mapping F_{cyl} in (3.35) with (3.37), $R_0 = 2$ and $a = 1$. Any linear combination of these three basis functions is single-valued at the pole and continuously differentiable across the pole. The pole (R_0, Z_0) is marked with a cross

Using the abbreviations $\Delta R_{1j} := R_{(1j)} - R_0$ and $\Delta Z_{1j} := Z_{(1j)} - Z_0$, the polar extraction coefficients are given by

$$\ell = 0: \qquad \chi^0_{0j} := \frac{1}{3}, \qquad \chi^0_{1j} := \frac{1}{3} + \frac{2}{3\tau}\Delta R_{1j}, \tag{3.42a}$$

$$\ell = 1: \qquad \chi^1_{0j} := \frac{1}{3}, \qquad \chi^1_{1j} := \frac{1}{3} - \frac{1}{3\tau}\Delta R_{1j} + \frac{\sqrt{3}}{3\tau}\Delta Z_{1j}, \tag{3.42b}$$

$$\ell = 2: \qquad \chi^2_{0j} := \frac{1}{3}, \qquad \chi^2_{1j} := \frac{1}{3} - \frac{1}{3\tau}\Delta R_{1j} - \frac{\sqrt{3}}{3\tau}\Delta Z_{1j}\,. \tag{3.42c}$$

They are the barycentric coordinates of the control points $R_{(ij)}$ and $Z_{(ij)}$ with $i = 0$ and $i = 1$ with respect to an equilateral triangle with vertices

$$v_1 := (\tau + R_0, 0), \quad v_2 := \left(R_0 - \frac{\tau}{2}, Z_0 + \frac{\sqrt{3}}{2}\tau\right), \quad v_3 := \left(R_0 - \frac{\tau}{2}, Z_0 - \frac{\sqrt{3}}{2}\tau\right). \tag{3.43}$$

The parameter τ is chosen such that the triangle encloses the pole (R_0, Z_0) and the first ring of control points (R_{1j}, Z_{1j}). This leads to the definition

$$\tau := \max\left[\max_j\left(-2\Delta R_{1j}\right), \max_j\left(\Delta R_{1j} - \sqrt{3}\,\Delta Z_{1j}\right), \max_j\left(\Delta R_{1j} + \sqrt{3}\,\Delta Z_{1j}\right)\right]. \tag{3.44}$$

The three new basis functions are plotted in Figure 2 for cubic B-splines both on the logical (upper row) and physical (lower row) domain using the generic mapping F_{cyl} in (3.35) with (3.37) (cylinder). Unlike pure tensor product basis functions, each of the new polar basis functions has a support that overlaps the pole. Moreover, using the property (3.3) of clamped B-splines, it is easily verified that (3.40) satisfies

$$f_h(s = 0, \theta) = \frac{1}{3}(f_0 + f_1 + f_2), \tag{3.45}$$

i.e. polar 0-forms are by construction single-valued at the pole such that the requirement (3.38a) is met. Similar to the tensor product basis functions (3.19), we introduce the stacking notation

$$\begin{aligned} \overline{\boldsymbol{\Lambda}}^0 &:= \left(\overline{\Lambda}^0_0, \overline{\Lambda}^0_1, \overline{\Lambda}^0_2, \overline{\Lambda}^0_{(\overline{ij})}\right) \in \mathbb{R}^{\overline{n}^0}, \qquad \overline{\Lambda}^0_{(\overline{ij})} := N_i^{q_s} N_j^{q_\theta}, \\ &\text{with} \quad (\overline{ij}) = n_\theta\,(i-2) + j + 3\,, \qquad 1 < i < n_s\,, \quad 0 \le j < n_\theta\,. \end{aligned} \tag{3.46}$$

Hence, the new set of basis functions $\overline{\boldsymbol{\Lambda}}^0$ contains as its first three entries the three new polar basis functions, followed by standard tensor product basis functions with index $i > 1$. Based on this new set of basis functions, the polar subspace $\overline{V}^0_h$ is readily defined as

$$\overline{V}^0_h := \operatorname{span}\left(\overline{\boldsymbol{\Lambda}}^0\right) \subset \overline{V}^0_h\,, \qquad \dim \overline{V}^0_h = \overline{n}^0\,, \tag{3.47}$$

and moreover, similar to (3.25), polar spline functions $f_h \in \overline{V}^0_h$ can compactly be written as

$$f_h = \overline{\mathcal{S}}_0[\,\overline{\mathbf{f}}\,] = \overline{\mathbf{f}}^\top \overline{\boldsymbol{\Lambda}}^0\,, \qquad \overline{\mathbf{f}} := \left(f_0, f_1, f_2, f_{(\overline{ij})}\right) \in \mathbb{C}^{\overline{n}^0}\,. \tag{3.48}$$

Finally, we define the *polar extraction operator*

$$\mathbb{E}^0 := \begin{bmatrix} \mathbb{X}^0 & 0 \\ 0 & \mathbb{1}_{(n_s-2)n_\theta} \end{bmatrix} \in \mathbb{R}^{\overline{n}^0 \times n_s n_\theta}\,, \qquad \mathbb{X}^0 \in \mathbb{R}^{3\times 2n_\theta}\,, \quad \mathbb{X}^0_{\ell j} := \begin{cases} \chi^\ell_{0j} & 0 \le j < n_\theta\,, \\ \chi^\ell_{1(j-n_\theta)} & n_\theta \le j < 2n_\theta\,, \end{cases} \tag{3.49}$$

where the matrix $\mathbb{X}^0$ performs the linear combination of the first $2n_\theta$ tensor product basis functions in $\boldsymbol{\Lambda}^0$ to yield the three new polar splines $\overline{\Lambda}^0_\ell$ ($\ell = 0, 1, 2$). Therefore, the complete new basis $\overline{\boldsymbol{\Lambda}}^0 = \mathbb{E}^0 \boldsymbol{\Lambda}^0$ and

$$f_h = \overline{\mathbf{f}}^\top \overline{\boldsymbol{\Lambda}}^0 = \overline{\mathbf{f}}^\top \mathbb{E}^0 \boldsymbol{\Lambda}^0 = \mathbf{f}^\top \boldsymbol{\Lambda}^0\,. \tag{3.50}$$

Consequently, for given polar FE coefficients $\overline{\mathbf{f}}$, the corresponding tensor product FE coefficients are obtained via $\mathbf{f} = (\mathbb{E}^0)^\top \overline{\mathbf{f}}$. It should be noted that the inverse operation, i.e. going from $\mathbf{f}$ to $\overline{\mathbf{f}}$, is not unique and can be achieved through any kind of projection $V^0_h \to \overline{V}^0_h$. Such a projection has been identified in [26], for instance. In other words, $\overline{V}^0_h$ is a subspace of V^0_h comprised of those elements with FE coefficients of the form $\mathbf{f} = (\mathbb{E}^0)^\top \overline{\mathbf{f}}$ for any $\overline{\mathbf{f}} \in \mathbb{C}^{\overline{n}^0}$.

3.4 Discrete polar gradient operator and 1-forms

When applying the "poloidal" gradient operator $\hat{\nabla}_P$ to a polar 0-form, the result must be a polar 1-form whose coefficients are obtained via the application of the *polar gradient matrix* $\overline{\mathbb{G}}$, formally

$$\hat{\nabla}_P f_h = \begin{bmatrix} \partial_s f_h \\ \partial_\theta f_h \\ ik\, f_h \end{bmatrix} = (\,\overline{\mathbb{G}}\,\overline{\mathbf{f}}\,)^\top \vec{\overline{\boldsymbol{\Lambda}}}^1\,. \tag{3.51}$$

The goal of this section is to identify on the one hand the suitable basis $\vec{\overline{\boldsymbol{\Lambda}}}^1$ and on the other hand the form of the polar gradient matrix $\overline{\mathbb{G}}$.

Let us start by computing the partial derivatives of (3.40). Using the recursion formulae (3.7) and (3.8) in both directions s and θ we obtain

$$\frac{\partial f_h}{\partial s} = \sum_{\ell=0}^{2} f_\ell \sum_{i=0}^{1} \sum_{j=0}^{n_\theta-1} \chi^\ell_{ij} (D^{q_s}_{i-1} - D^{q_s}_i) N^{q_\theta}_j + \sum_{i>1,j} f_{(\overline{ij})} (D^{q_s}_{i-1} - D^{q_s}_i) N^{q_\theta}_j\,, \tag{3.52}$$

$$\frac{\partial f_h}{\partial \theta} = \sum_{\ell=0}^{2} f_\ell \sum_{i=0}^{1} \sum_{j=0}^{n_\theta-1} \chi^\ell_{ij} N^{q_s}_i (D^{q_\theta}_{j-1} - D^{q_\theta}_j) + \sum_{i>1,j} f_{(\overline{ij})} N^{q_s}_i (D^{q_\theta}_{j-1} - D^{q_\theta}_j)\,. \tag{3.53}$$

We can sort this in terms of tensor product basis functions that span the space V_h^1:

$$\frac{\partial f_h}{\partial s} = \sum_{\ell=0}^{2} f_\ell \sum_{j=0}^{n_\theta-1} (\chi^\ell_{1j} - \chi^\ell_{0j}) D_0^{q_s} N_j^{q_\theta} + \sum_{j=0}^{n_\theta-1} \left(f_{(\overline{2j})} - \sum_{\ell=0}^{2} f_\ell \chi^\ell_{1j} \right) D_1^{q_s} N_j^{q_\theta} + \sum_{i>1,j} (f_{(\overline{i+1j})} - f_{(\overline{ij})}) D_i^{q_s} N_j^{q_\theta} \,, \tag{3.54}$$

$$\frac{\partial f_h}{\partial \theta} = \sum_{\ell=0}^{2} f_\ell \sum_{i=0}^{1} \sum_{j=0}^{d_\theta-1} (\chi^\ell_{ij+1} - \chi^\ell_{ij}) N_i^{q_s} D_j^{q_\theta} + \sum_{i>1,j} (f_{(\overline{ij+1})} - f_{(\overline{ij})}) N_i^{q_s} D_j^{q_\theta} \,. \tag{3.55}$$

Before further simplifying these expressions, we note some important properties of the extraction coefficients (3.42):

1. $\chi^\ell_{0j+1} - \chi^\ell_{0j} = 0 \qquad \forall\, j, \ell \,,$ (3.56)
2. $\sum_{\ell=0}^{2} f_\ell \, (\chi^\ell_{1j} - \chi^\ell_{0j}) = \sum_{\ell=1}^{2} (f_\ell - f_0)(\chi^\ell_{1j} - \chi^\ell_{0j}) \qquad \forall\, j \,,$ (3.57)
3. $\sum_{\ell=0}^{2} f_\ell \, (\chi^\ell_{1j+1} - \chi^\ell_{1j}) = \sum_{\ell=1}^{2} (f_\ell - f_0)(\chi^\ell_{1j+1} - \chi^\ell_{1j}) \qquad \forall\, j \,,$ (3.58)
4. $\sum_{\ell=0}^{2} \chi^\ell_{1j} = 1 \qquad \forall\, j \,.$ (3.59)

By substituting the first three relations (3.56)-(3.58) into the derivatives (3.54) and (3.55), the first two components of the gradient of f_h can be written as

$$\begin{aligned} \begin{bmatrix} \partial_s f_h \\ \partial_\theta f_h \end{bmatrix} &= \sum_{\ell=1}^{2} (f_\ell - f_0) \sum_{j=0}^{n_\theta-1} \begin{bmatrix} (\chi^\ell_{1j} - \chi^\ell_{0j}) D_0^{q_s} N_j^{q_\theta} \\ (\chi^\ell_{1j+1} - \chi^\ell_{1j}) N_1^{q_s} D_j^{q_\theta} \end{bmatrix} + \sum_{j=0}^{n_\theta-1} \left(f_{(\overline{2j})} - \sum_{\ell=0}^{2} f_\ell \chi^\ell_{1j} \right) \begin{bmatrix} D_1^{q_s} N_j^{q_\theta} \\ 0 \end{bmatrix} \\ &+ \sum_{i>1,j} (f_{(\overline{i+1j})} - f_{(\overline{ij})}) \begin{bmatrix} D_i^{q_s} N_j^{q_\theta} \\ 0 \end{bmatrix} + \sum_{i>1,j} (f_{(\overline{ij+1})} - f_{(\overline{ij})}) \begin{bmatrix} 0 \\ N_i^{q_s} D_j^{q_\theta} \end{bmatrix} . \end{aligned} \tag{3.60}$$

Here, one should keep in mind that $d_\theta = n_\theta$. This representation of the gradient is intuitive because each term is multiplied by a difference of FE coefficients $\overline{\mathbf{f}}$. Due to the property (3.59) this means that the gradient is evidently zero if all entries of $\overline{\mathbf{f}}$ are identical. From the partition of unity property of B-splines it then follows that constant functions are in the kernel of the polar gradient operator. The first term on the right-hand side of (3.60) leads to the definition of two new basis functions:

$$\vec{\Lambda}_0^{1,2} := \sum_{j=0}^{n_\theta-1} \begin{bmatrix} (\chi^1_{1j} - \chi^1_{0j}) D_0^{q_s} N_j^{q_\theta} \\ (\chi^1_{1j+1} - \chi^1_{1j}) N_1^{q_s} D_j^{q_\theta} \\ 0 \end{bmatrix} , \qquad \vec{\Lambda}_1^{1,2} := \sum_{j=0}^{n_\theta-1} \begin{bmatrix} (\chi^2_{1j} - \chi^2_{0j}) D_0^{q_s} N_j^{q_\theta} \\ (\chi^2_{1j+1} - \chi^2_{1j}) N_1^{q_s} D_j^{q_\theta} \\ 0 \end{bmatrix} . \tag{3.61}$$

Note that these basis functions are vector valued (in $\mathbb{R}^3$) and that we will attribute them to the *second component of polar 1-forms*, which will become clear when discussing projection operators in Section 4. The other basis functions are standard tensor product basis functions. The dimensions are thus

$$\overline{n}^{1,1} := (d_s - 1)\, n_\theta \,, \qquad \overline{n}^{1,2} := (n_s - 2)\, d_\theta + 2 \,. \tag{3.62}$$

The two new basis functions are plotted in Figure 3 both on the logical (upper row) and physical (lower row) domain (push-forward with $DF^{-\top}$, see Table 1) using the generic mapping F_{cyl} in (3.35) with

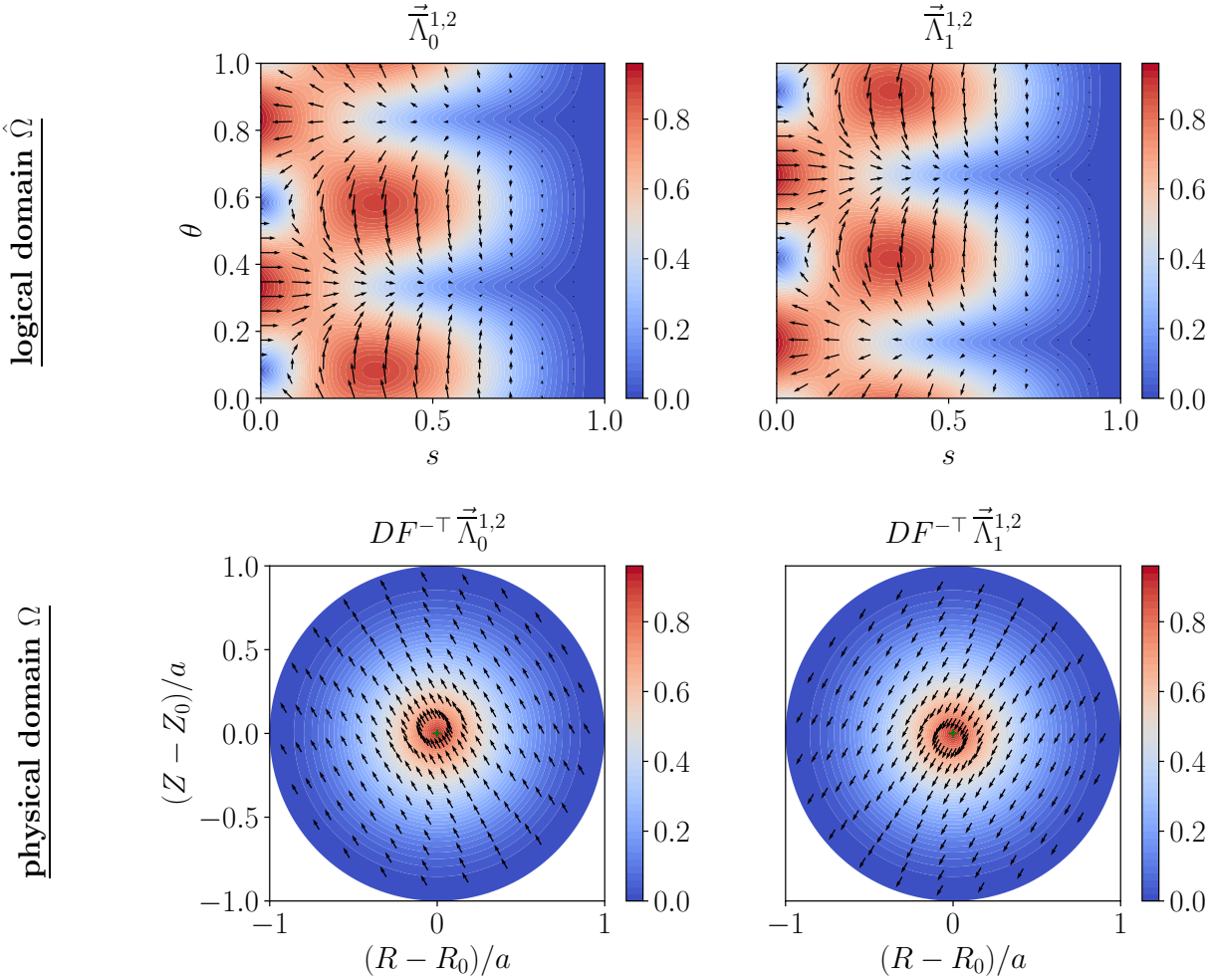

Figure 3: The two new vector valued basis functions $\vec{\Lambda}_0^{1,2}$ (left column) and $\vec{\Lambda}_1^{1,2}$ (right column) (3.61) on the logical domain (uppper row) and physical domain (lower row) for the example $q_s = q_\theta = 3$, $n_s = 4$ and $n_\theta = 12$ using the generic mapping F_{cyl} in (3.35) with (3.37) (cylinder). The arrows' absolute values are color-coded. Arrows on the physical domain are normalized to the same value for better visibility and arrows at $s = 0$ pointing in the negative direction are not visible on the logical domain.

(3.37) (cylinder). It is seen that both basis functions have no θ-dependence on the physical domain. Moreover, we note that

$$\left(\vec{\Lambda}_0^{1,2} \cdot \vec{e}_2\right)(s = 0, \theta) = \left(\vec{\Lambda}_1^{1,2} \cdot \vec{e}_2\right)(s = 0, \theta) = 0 \qquad \forall\, \theta\,, \tag{3.63}$$

where $\vec{e}_2 = [0, 1, 0]$. Hence, when using these two basis functions for discrete polar 1-forms, they correctly mimic the requirement (3.38b) for the second component of continuous polar 1-forms. Similar to the tensor product basis functions (3.22) we introduce the notation

$$\vec{\mathbf{\Lambda}}^1 := \left[\vec{\mathbf{\Lambda}}^{1,1}, \vec{\mathbf{\Lambda}}^{1,2}, \vec{\mathbf{\Lambda}}^{1,3}\right], \tag{3.64}$$

where

$$\vec{\overline{\mathbf{\Lambda}}}^{1,1} := \left(\vec{\overline{\Lambda}}^{1,1}_{(\overline{ij})}\right) \in \mathbb{R}^{\overline{n}^{1,1}}\,, \qquad \vec{\overline{\Lambda}}^{1,1}_{(\overline{ij})} := \begin{bmatrix} D_i^{q_s} N_j^{q_\theta} \\ 0 \\ 0 \end{bmatrix}\,, \tag{3.65a}$$

$$\text{with} \quad (\overline{ij}) = n_\theta\,(i-1) + j\,, \qquad 0 < i < d_s\,, \quad 0 \le j < n_\theta\,,$$

$$\vec{\overline{\mathbf{\Lambda}}}^{1,2} := \left(\vec{\overline{\Lambda}}^{1,2}_0, \vec{\overline{\Lambda}}^{1,2}_1, \vec{\overline{\Lambda}}^{1,2}_{(\overline{ij})}\right) \in \mathbb{R}^{\overline{n}^{1,2}}\,, \qquad \vec{\overline{\Lambda}}^{1,2}_{(\overline{ij})} := \begin{bmatrix} 0 \\ N_i^{q_s} D_j^{q_\theta} \\ 0 \end{bmatrix}\,, \tag{3.65b}$$

$$\text{with} \quad (\overline{ij}) = d_\theta\,(i-2) + j + 2\,, \qquad 1 < i < n_s\,, \quad 0 \le j < d_\theta\,,$$

$$\vec{\overline{\mathbf{\Lambda}}}^{1,3} := \left(\vec{\overline{\Lambda}}^{1,3}_0, \vec{\overline{\Lambda}}^{1,3}_1, \vec{\overline{\Lambda}}^{1,3}_2, \vec{\overline{\Lambda}}^{1,3}_{(\overline{ij})}\right) \in \mathbb{R}^{\overline{n}^0}\,, \quad \vec{\overline{\Lambda}}^{1,3}_{\ell=0,1,2} := \begin{bmatrix} 0 \\ 0 \\ \overline{\Lambda}^0_{l=0,1,2} \end{bmatrix}\,, \quad \vec{\overline{\Lambda}}^{1,3}_{(\overline{ij})} := \begin{bmatrix} 0 \\ 0 \\ N_i^{q_s} N_j^{q_\theta} \end{bmatrix}\,, \tag{3.65c}$$

$$\text{with} \quad (\overline{ij}) = n_\theta\,(i-2) + j + 3\,, \qquad 1 < i < n_s\,, \quad 0 \le j < n_\theta\,.$$

Based on this new set of basis functions, the polar subspace $\overline{V}^1_h$ is readily defined as

$$\overline{V}^1_h := \operatorname{span}\left(\vec{\overline{\mathbf{\Lambda}}}^1\right) \subset V^1_h\,, \qquad \dim \overline{V}^1_h = \overline{n}^{1,1} + \overline{n}^{1,2} + \overline{n}^0 =: \overline{n}^1\,, \tag{3.66}$$

and moreover, similar to (3.26), polar spline functions $\mathbf{A}_h \in \overline{V}^1_h$ can compactly be written as

$$\mathbf{A}_h = \overline{\mathcal{S}}_1[\vec{\overline{\mathbf{a}}}] := \vec{\overline{\mathbf{a}}}^\top \vec{\overline{\mathbf{\Lambda}}}^1\,, \qquad \vec{\overline{\mathbf{a}}} := \begin{bmatrix} \overline{\mathbf{a}}^1 := (a^1_{(\overline{ij})}) \\ \overline{\mathbf{a}}^2 := (a^2_0, a^2_1, a^2_{(\overline{ij})}) \\ \overline{\mathbf{a}}^3 := (a^3_0, a^3_1, a^3_2, a^3_{(\overline{ij})}) \end{bmatrix} \in \mathbb{C}^{\overline{n}^1}\,. \tag{3.67}$$

With regards to (3.49), we define in a block-wise fashion the polar extraction operator

$$\mathbb{E}^{1,\mathrm{pol}} := \begin{bmatrix} 0 & \mathbb{1}_{(d_s-1)\,n_\theta} & 0 & 0 \\ \mathbb{X}^{1,1} & 0 & \mathbb{X}^{1,2} & 0 \\ 0 & 0 & 0 & \mathbb{1}_{(n_s-2)\,d_\theta} \end{bmatrix} \in \mathbb{R}^{(\overline{n}^{1,1}+\overline{n}^{1,2})\times(d_s n_\theta + n_s d_\theta)}\,, \tag{3.68}$$

where the $\mathbb{X}^{1,1} \in \mathbb{R}^{2\times n_\theta}$ acts on the first n_θ tensor product basis functions in $\vec{\mathbf{\Lambda}}^{1,1}$ and $\mathbb{X}^{1,2} \in \mathbb{R}^{2\times 2d_\theta}$ acts on the first $2d_\theta$ tensor product basis functions in $\vec{\mathbf{\Lambda}}^{1,2}$ to yield the two new polar splines (3.61). The entries can be deduced from (3.61) and read

$$\mathbb{X}^{1,1}_{\ell j} := \chi^{\ell+1}_{1j} - \chi^{\ell+1}_{0j}\,, \qquad \mathbb{X}^{1,2}_{\ell j} := \begin{cases} 0 & 0 \le j < d_\theta\,, \\ \chi^{\ell+1}_{1(j-d_\theta+1)} - \chi^{\ell+1}_{1(j-d_\theta)} & d_\theta \le j < 2d_\theta\,. \end{cases} \tag{3.69}$$

The full extraction operator for obtaining the basis in (3.67) reads

$$\mathbb{E}^1 := \begin{bmatrix} \mathbb{E}^{1,\mathrm{pol}} & 0 \\ 0 & \mathbb{E}^0 \end{bmatrix}\,. \tag{3.70}$$

Therefore, the complete new basis $\vec{\overline{\mathbf{\Lambda}}}^1 = \mathbb{E}^1 \vec{\mathbf{\Lambda}}^1$ and

$$\mathbf{A}_h = \vec{\overline{\mathbf{a}}}^\top \vec{\overline{\mathbf{\Lambda}}}^1 = \vec{\overline{\mathbf{a}}}^\top \mathbb{E}^1 \vec{\mathbf{\Lambda}}^1 = \vec{\mathbf{a}}^\top \vec{\mathbf{\Lambda}}^1\,. \tag{3.71}$$

Consequently, for given polar FE coefficients $\vec{\overline{\mathbf{a}}}$, the corresponding tensor product FE coefficients are obtained via $\vec{\mathbf{a}} = (\mathbb{E}^1)^\top \vec{\overline{\mathbf{a}}}$.

In view of (3.60), we shall write the poloidal gradient of $f_h \in \overline{V}_h^0$ compactly as

$$\hat{\nabla}_P f_h = (\,\overline{\mathbb{G}}\,\overline{\mathbf{f}}\,)^\top \vec{\mathbf{\Lambda}}^1\,, \qquad \overline{\mathbb{G}} := \begin{bmatrix} \overline{\mathbb{D}}^s \\ \overline{\mathbb{D}}^\theta \\ ik\,\mathbb{1} \end{bmatrix}, \tag{3.72}$$

with the derivative matrices

$$\overline{\mathbb{D}}^s := \begin{bmatrix} \mathbb{D}^{1\chi} & \mathbb{G}^s_{-2} \otimes \mathbb{1}_{n_\theta} \end{bmatrix} \in \mathbb{R}^{\overline{n}^{1,1} \times \overline{n}^0}\,, \qquad \overline{\mathbb{D}}^\theta := \begin{bmatrix} \mathbb{D}^{\chi\chi} & 0 \\ 0 & \mathbb{D}^\theta \end{bmatrix} \in \mathbb{R}^{\overline{n}^{1,2} \times \overline{n}^0}\,, \tag{3.73}$$

with blocks

$$\mathbb{D}^{1\chi} \in \mathbb{R}^{\overline{n}^{1,1} \times 3}\,, \qquad \mathbb{D}^{1\chi}_{(\overline{ij})\ell} := \begin{cases} -\chi^\ell_{1j} & \text{for } i = 1\,, \\ 0 & \text{else}\,, \end{cases} \tag{3.74}$$

$$\mathbb{G}^s_{-2} := (\mathbb{G}^s_{ij})_{i>0, j>1} \in \mathbb{R}^{(d_s-1)\times(n_s-2)}\,, \tag{3.75}$$

$$\mathbb{D}^{\chi\chi} \in \mathbb{R}^{2\times 3}\,, \qquad \mathbb{D}^{\chi\chi} := \begin{bmatrix} -1 & 1 & 0 \\ -1 & 0 & 1 \end{bmatrix}, \tag{3.76}$$

and $\mathbb{D}^\theta$ has been defined in (3.29) and is used here with $\mathbb{1}^s = \mathbb{1}_{n_s-2}$.

3.5 Discrete polar curl operator and 2-forms

When applying the "poloidal" curl operator $\hat{\nabla}_P \times$ to a polar 1-form (3.67), the result must be a poloidal 2-form whose coefficients are obtained via the application of the *polar curl matrix* $\overline{\mathbb{C}}$, formally

$$\hat{\nabla}_P \times \mathbf{A}_h = \begin{bmatrix} \partial_\theta A_{h,3} - ik\,A_{h,2} \\ ik\,A_{h,1} - \partial_s A_{h,3} \\ \partial_s A_{h,2} - \partial_\theta A_{h,1} \end{bmatrix} = (\,\overline{\mathbb{C}}\,\vec{\overline{\mathbf{a}}}\,)^\top \vec{\mathbf{\Lambda}}^2\,. \tag{3.77}$$

The goal of this section is to identify on the one hand the suitable basis $\vec{\mathbf{\Lambda}}^2$ and on the other hand the form of the polar curl matrix $\overline{\mathbb{C}}$.

Since $A_{h,3} = (\overline{\mathbf{a}}^3)^\top \overline{\mathbf{\Lambda}}^0$, we already computed $\partial_s A_{h,3}$ and $\partial_\theta A_{h,3}$ in (3.60) of the previous section. Therefore, from (3.61),

$$\vec{\Lambda}^{2,1}_0 := \vec{\Lambda}^{1,2}_0 \times \vec{\boldsymbol{e}}_3\,, \qquad \vec{\Lambda}^{2,1}_1 := \vec{\Lambda}^{1,2}_1 \times \vec{\boldsymbol{e}}_3\,, \tag{3.78}$$

where $\vec{\boldsymbol{e}}_3 = [\,0, 0, 1\,]$. Note that we attribute these basis functions to the *first component of polar 2-forms*. The dimensions are thus

$$\overline{n}^{2,1} := \overline{n}^{1,2} = (n_s - 2)\,d_\theta + 2\,, \qquad \overline{n}^{2,2} := \overline{n}^{1,1} = (d_s - 1)\,n_\theta =: \overline{n}^3\,, \tag{3.79}$$

The two new basis functions are plotted in Figure 4 both on the logical (upper row) and physical (lower row) domain (push-forward with $DF/\sqrt{g}$, see Table 1) using the generic mapping F_{cyl} in (3.35) with (3.37) (cylinder). It is seen that both basis functions have no θ-dependence on the physical domain. Moreover, we note that

$$\left(\vec{\Lambda}^{2,1}_0 \cdot \vec{\boldsymbol{e}}_1\right)(s = 0, \theta) = \left(\vec{\Lambda}^{2,1}_1 \cdot \vec{\boldsymbol{e}}_1\right)(s = 0, \theta) = 0 \quad \forall\, \theta\,, \tag{3.80}$$

where $\vec{\boldsymbol{e}}_1 = [\,1, 0, 0\,]$. Hence, when using these two basis functions for discrete polar 2-forms, they correctly mimic the requirement (3.38c) for the first component of continuous polar 2-forms. Similar to the tensor product basis (3.22) we introduce the notation

$$\vec{\mathbf{\Lambda}}^2 := \left[\vec{\mathbf{\Lambda}}^{2,1}, \vec{\mathbf{\Lambda}}^{2,2}, \vec{\mathbf{\Lambda}}^{2,3}\right], \tag{3.81}$$

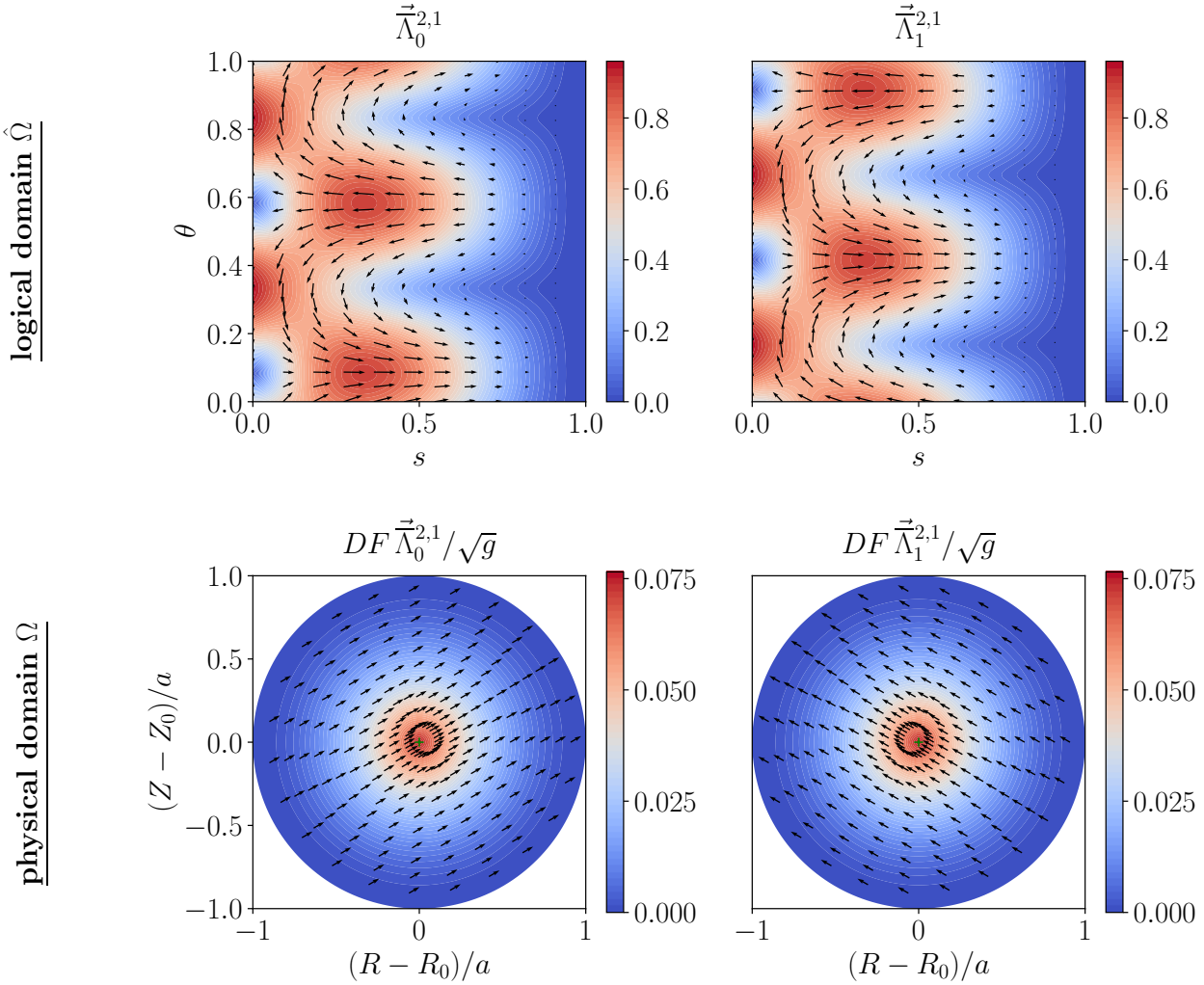

Figure 4: The two new vector valued basis functions $\vec{\Lambda}_0^{2,1}$ (left column) and $\vec{\Lambda}_1^{2,1}$ (right column) (3.78) on the logical domain (uppper row) and physical domain (lower row) for the example $q_s = q_\theta = 3$, $n_s = 4$ and $n_\theta = 12$ using the generic mapping F_{cyl} in (3.35) with (3.37)) (cylinder). The arrows' absolute values are color-coded. Arrows on the physical domain are normalized to the same value for better visibility and arrows tangential to the surface $s = 0$ are not visible on the logical domain.

where

$$\vec{\mathbf{\Lambda}}^{2,1} := \left(\vec{\Lambda}_0^{2,1}, \vec{\Lambda}_1^{2,1}, \vec{\Lambda}_{(\overline{ij})}^{2,1}\right) \in \mathbb{R}^{\overline{n}^{2,1}}, \qquad \vec{\Lambda}_{(\overline{ij})}^{2,1} := \begin{bmatrix} N_i^{q_s} D_j^{q_\theta} \\ 0 \\ 0 \end{bmatrix}, \tag{3.82a}$$

$$\text{with} \quad (\overline{ij}) = d_\theta\,(i-2) + j + 2\,, \qquad 1 < i < n_s\,, \quad 0 \le j < d_\theta\,,$$

$$\vec{\mathbf{\Lambda}}^{2,2} := \left(\vec{\Lambda}_{(\overline{ij})}^{2,2}\right) \in \mathbb{R}^{\overline{n}^{2,2}}, \qquad \vec{\Lambda}_{(\overline{ij})}^{2,2} := \begin{bmatrix} 0 \\ D_i^{q_s} N_j^{q_\theta} \\ 0 \end{bmatrix}, \tag{3.82b}$$

$$\text{with} \quad (\overline{ij}) = n_\theta\,(i-1) + j\,, \qquad 0 < i < d_s\,, \quad 0 \le j < n_\theta\,,$$

$$\vec{\mathbf{\Lambda}}^{2,3} := \left(\vec{\Lambda}_{(\overline{ij})}^{2,3}\right) \in \mathbb{R}^{\overline{n}^{3}}, \qquad \vec{\Lambda}_{(\overline{ij})}^{2,3} := \begin{bmatrix} 0 \\ 0 \\ D_i^{q_s} D_j^{q_\theta} \end{bmatrix}, \tag{3.82c}$$

$$\text{with} \quad (\overline{ij}) = d_\theta\,(i-1) + j\,, \qquad 0 < i < d_s\,, \quad 0 \le j < d_\theta\,.$$

The third component $\vec{\mathbf{\Lambda}}^{2,3}$ has been determined from (3.77): the relevant partial derivatives of $A_{h,1} = \vec{\mathbf{A}}_h \cdot \vec{\boldsymbol{e}}_1$ and $A_{h,2} = \vec{\mathbf{A}}_h \cdot \vec{\boldsymbol{e}}_2$ read

$$\begin{aligned}
\frac{\partial A_{h,2}}{\partial s} &= \sum_{\ell=0}^{1} a_\ell^2 \sum_{j=0}^{d_\theta-1} (\chi_{1j+1}^{\ell+1} - \chi_{1j}^{\ell+1})(D_0^{q_s} - D_1^{q_s}) D_j^{q_\theta} + \sum_{i>1,j} a_{(\overline{ij})}^2 (D_{i-1}^{q_s} - D_i^{q_s}) D_j^{q_\theta} \\
&= \sum_{\ell=0}^{1} a_\ell^2 \sum_{j=0}^{d_\theta-1} (\chi_{1j+1}^{\ell+1} - \chi_{1j}^{\ell+1}) D_0^{q_s} D_j^{q_\theta} + \sum_{j=0}^{d_\theta-1} \left[a_{(\overline{2j})}^2 - \sum_{\ell=0}^{1} a_\ell^2 (\chi_{1j+1}^{\ell+1} - \chi_{1j}^{\ell+1}) \right] D_1^{q_s} D_j^{q_\theta} \\
&\quad + \sum_{i>1,j} (a_{(\overline{i+1j})}^2 - a_{(\overline{ij})}^2) D_i^{q_s} D_j^{q_\theta} \,,
\end{aligned} \tag{3.83}$$

$$\begin{aligned}
\frac{\partial A_{h,1}}{\partial \theta} &= \sum_{\ell=0}^{1} a_\ell^2 \sum_{j=0}^{n_\theta-1} (\chi_{1j}^{\ell+1} - \chi_{0j}^{\ell+1}) D_0^{q_s} (D_{j-1}^{q_\theta} - D_j^{q_\theta}) + \sum_{i>0,j} a_{(\overline{ij})}^1 D_i^{q_s} (D_{j-1}^{q_\theta} - D_j^{q_\theta}) \\
&= \sum_{\ell=0}^{1} a_\ell^2 \sum_{j=0}^{d_\theta-1} (\chi_{1j+1}^{\ell+1} - \chi_{0j+1}^{\ell+1} - \chi_{1j}^{\ell+1} + \chi_{0j}^{\ell+1}) D_0^{q_s} D_j^{q_\theta} + \sum_{i>0,j} (a_{(\overline{ij+1})}^1 - a_{(\overline{ij})}^1) D_i^{q_s} D_j^{q_\theta} \\
&= \sum_{\ell=0}^{1} a_\ell^2 \sum_{j=0}^{d_\theta-1} (\chi_{1j+1}^{\ell+1} - \chi_{1j}^{\ell+1}) D_0^{q_s} D_j^{q_\theta} + \sum_{i>0,j} (a_{(\overline{ij+1})}^1 - a_{(\overline{ij})}^1) D_i^{q_s} D_j^{q_\theta} \,,
\end{aligned} \tag{3.84}$$

respectively, where we used (3.56) to obtain the last line. Taking the difference yields

$$\begin{aligned}
\frac{\partial A_{h,2}}{\partial s} - \frac{\partial A_{h,1}}{\partial \theta} &= \sum_{j=0}^{d_\theta-1} \left[a_{(\overline{2j})}^2 - \sum_{\ell=0}^{1} a_\ell^2 (\chi_{1j+1}^{\ell+1} - \chi_{1j}^{\ell+1}) - a_{(\overline{1j+1})}^1 + a_{(\overline{1j})}^1 \right] D_1^{q_s} D_j^{q_\theta} \\
&\quad + \sum_{i>1,j} (a_{(\overline{i+1j})}^2 - a_{(\overline{ij})}^2 - a_{(\overline{ij+1})}^1 + a_{(\overline{ij})}^1) D_i^{q_s} D_j^{q_\theta} \,,
\end{aligned} \tag{3.85}$$

which reveals the basis $\vec{\mathbf{\Lambda}}^{2,3}$ of the third component of 2-forms, namely being the standard tensor product basis functions without the $i = 0$ ones such that the second requirement in (3.38c) is satisfied. Based on the new set of basis functions, the polar subspace $\overline{V}_h^2$ is readily defined as

$$\overline{V}_h^2 := \operatorname{span}\left(\vec{\mathbf{\Lambda}}^2 \right) \subset \overline{V}_h^2 \,, \qquad \dim \overline{V}_h^2 = \overline{n}^{2,1} + \overline{n}^{2,2} + \overline{n}^3 =: \overline{n}^2 \,, \tag{3.86}$$

and moreover, similar to (3.27), polar spline function $\mathbf{B}_h \in \overline{V}_h^2$ can compactly be written as

$$\mathbf{B}_h = \overline{\mathcal{S}}_2[\vec{\mathbf{b}}] = \vec{\mathbf{b}}^\top \vec{\mathbf{\Lambda}}^2 \,, \qquad \vec{\mathbf{b}} := \begin{bmatrix} \overline{\mathbf{b}}^1 := (b_0^1, b_1^1, b_{(\overline{ij})}^1) \\ \overline{\mathbf{b}}^2 := (b_{(\overline{ij})}^2) \\ \overline{\mathbf{b}}^3 := (b_{(\overline{ij})}^3) \end{bmatrix} \in \mathbb{C}^{\overline{n}^2} \,. \tag{3.87}$$

With regards to (3.68), we define in a block-wise fashion the polar extraction operator

$$\mathbb{E}^{2,\mathrm{pol}} := \begin{bmatrix} \mathbb{X}^{1,2} & 0 & -\mathbb{X}^{1,1} & 0 \\ 0 & \mathbb{1}_{(n_s-2)\,d_\theta} & 0 & 0 \\ 0 & 0 & 0 & \mathbb{1}_{(d_s-1)\,n_\theta} \end{bmatrix} \in \mathbb{R}^{(\overline{n}^{2,1}+\overline{n}^{2,2}) \times (n_s d_\theta + d_s n_\theta)} \,, \tag{3.88}$$

where $\mathbb{X}^{1,1}$ and $\mathbb{X}^{1,2}$ were defined in (3.69). The full extraction operator for obtaining the basis in (3.82) finally reads

$$\mathbb{E}^2 := \begin{bmatrix} \mathbb{E}^{2,\mathrm{pol}} & 0 \\ 0 & \mathbb{E}^3 \end{bmatrix} \,, \qquad \mathbb{E}^3 := \begin{bmatrix} 0 & \mathbb{1}_{(d_s-1)d_\theta} \end{bmatrix} \in \mathbb{R}^{\overline{n}^3 \times d_s d_\theta} \,. \tag{3.89}$$

Therefore, the complete new basis $\vec{\overline{\mathbf{\Lambda}}}^2 = \mathbb{E}^2 \vec{\mathbf{\Lambda}}^2$ and

$$\mathbf{B}_h = \vec{\mathbf{b}}^\top \vec{\overline{\mathbf{\Lambda}}}^2 = \vec{\mathbf{b}}^\top \mathbb{E}^2 \vec{\mathbf{\Lambda}}^2 = \vec{\mathbf{b}}^\top \vec{\mathbf{\Lambda}}^2 \,. \tag{3.90}$$

Consequently, for given polar FE coefficients $\vec{\mathbf{b}}$, the corresponding tensor product FE coefficients are obtained via $\vec{\mathbf{b}} = (\mathbb{E}^2)^\top \vec{\mathbf{b}}$.

In view of (3.77) and (3.85), we shall write the poloidal curl of $\mathbf{A}_h \in \overline{V}_h^1$ compactly as

$$\hat{\nabla}_P \times \mathbf{A}_h = (\,\overline{\mathbb{C}}\,\vec{\mathbf{a}}\,)^\top \vec{\overline{\mathbf{\Lambda}}}^2 \,, \qquad \overline{\mathbb{C}}\,\vec{\mathbf{a}} := \left[\begin{array}{c|c|c} 0 & -ik\,\mathbb{1} & \overline{\mathbb{D}}^\theta \\ ik\,\mathbb{1} & 0 & -\overline{\mathbb{D}}^s \\ -\mathbb{D}^\theta & \overline{\mathbb{S}} & 0 \end{array}\right] \left[\begin{array}{c} \overline{\mathbf{a}}^1 \\ \overline{\mathbf{a}}^2 \\ \overline{\mathbf{a}}^3 \end{array}\right] , \tag{3.91}$$

where $\mathbb{D}^\theta$ has been defined in (3.29) and is used here with $\mathbb{1}^s = \mathbb{1}_{d_s-1}$ and the derivative matrices $\overline{\mathbb{D}}$ have been defined in (3.73) and need to be used here with appropriate sizes of the identity matrices $\mathbb{1}$. Moreover,

$$\overline{\mathbb{S}} := \left[\mathbb{D}^{2\chi} \quad \mathbb{G}^s_{-2} \otimes \mathbb{1}_{d_\theta}\right] \in \mathbb{R}^{\overline{n}^3 \times \overline{n}^{1,2}} \,, \tag{3.92}$$

where

$$\mathbb{D}^{2\chi} \in \mathbb{R}^{\overline{n}^3 \times 2} \,, \qquad \mathbb{D}^{2\chi}_{(\overline{ij})\ell} := \begin{cases} -(\chi^{\ell+1}_{1j+1} - \chi^{\ell+1}_{1j}) & i = 1 \,, \\ 0 & \text{else} \,, \end{cases} \tag{3.93}$$

and $\mathbb{G}^s_{-2}$ has been defined in (3.75).

Proposition 1. *We have* $\overline{\mathbb{C}}\,\overline{\mathbb{G}} = 0$.

Proof. The matrix product of interest reads

$$\overline{\mathbb{C}}\,\overline{\mathbb{G}} = \left[\begin{array}{c|c|c} 0 & -ik\,\mathbb{1} & \overline{\mathbb{D}}^\theta \\ ik\,\mathbb{1} & 0 & -\overline{\mathbb{D}}^s \\ -\mathbb{D}^\theta & \overline{\mathbb{S}} & 0 \end{array}\right] \left[\begin{array}{c} \overline{\mathbb{D}}^s \\ \overline{\mathbb{D}}^\theta \\ ik\,\mathbb{1} \end{array}\right] .$$

The first two rows yield zero immediately. In the last row we must show that

$$-\mathbb{D}^\theta\,\overline{\mathbb{D}}^s + \overline{\mathbb{S}}\,\overline{\mathbb{D}}^\theta = 0 \,,$$

where

$$\mathbb{D}^\theta = \mathbb{1}_{d_s-1} \otimes \mathbb{G}^\theta \quad \in \mathbb{R}^{\overline{n}^3 \times \overline{n}^{1,1}} \,, \qquad \overline{\mathbb{D}}^s = \left[\mathbb{D}^{1\chi} \quad \mathbb{G}^s_{-2} \otimes \mathbb{1}_{n_\theta}\right] \quad \in \mathbb{R}^{\overline{n}^{1,1} \times \overline{n}^0} \,,$$

$$\overline{\mathbb{S}} = \left[\mathbb{D}^{2\chi} \quad \mathbb{G}^s_{-2} \otimes \mathbb{1}_{d_\theta}\right] \quad \in \mathbb{R}^{\overline{n}^3 \times \overline{n}^{1,2}} \,, \qquad \overline{\mathbb{D}}^\theta = \begin{bmatrix} \mathbb{D}^{\chi\chi} & 0 \\ 0 & \mathbb{D}^\theta \end{bmatrix} \quad \in \mathbb{R}^{\overline{n}^{1,2} \times \overline{n}^0} \,.$$

and the single blocks

$$\mathbb{G}^\theta \in \mathbb{R}^{d_\theta \times n_\theta} \,, \qquad \mathbb{G}^s_{-2} \in \mathbb{R}^{(d_s-1)\times(n_s-2)} \,, \qquad \mathbb{D}^{1\chi} \in \mathbb{R}^{\overline{n}^{1,1}\times 3} \,, \qquad \mathbb{D}^{2\chi} \in \mathbb{R}^{\overline{n}^3 \times 2} \,, \qquad \mathbb{D}^{\chi\chi} \in \mathbb{R}^{2\times 3} \,.$$

Therefore,

$$-\mathbb{D}^\theta\,\overline{\mathbb{D}}^s + \overline{\mathbb{S}}\,\overline{\mathbb{D}}^\theta = -\left[\mathbb{D}^\theta\,\mathbb{D}^{1\chi} \quad \mathbb{G}^s_{-2} \otimes \mathbb{G}^\theta\right] + \left[\mathbb{D}^{2\chi}\,\mathbb{D}^{\chi\chi} \quad \mathbb{G}^s_{-2} \otimes \mathbb{G}^\theta\right] .$$

It remains to show the equality of the first block:

$$\mathbb{D}^\theta\,\mathbb{D}^{1\chi}_{(\overline{ij})\ell} = \mathbb{D}^{1\chi}_{(\overline{ij+1})\ell} - \mathbb{D}^{1\chi}_{(\overline{ij})\ell} = \begin{cases} -\chi^\ell_{1j+1} + \chi^\ell_{ij} & i = 1,\ \ell = 0,1,2 \,, \\ 0 & \text{else} \,, \end{cases}$$

$$\mathbb{D}^{2\chi}\,\mathbb{D}^{\chi\chi} = \begin{cases} \chi^1_{1j+1} - \chi^1_{ij} + \chi^2_{1j+1} - \chi^2_{ij} & i = 1,\ \ell = 0 \,, \\ -\chi^\ell_{1j+1} + \chi^\ell_{ij} & i = 1,\ \ell = 1,2 \,, \\ 0 & \text{else} \,. \end{cases}$$

From the polar extraction coefficients (3.42) follows

$$\chi^1_{1j+1} - \chi^1_{ij} + \chi^2_{1j+1} - \chi^2_{ij} = -\chi^0_{1j+1} + \chi^0_{ij} \,,$$

which completes the proof. □

3.6 Discrete polar divergence operator and 3-forms

When applying the "poloidal" divergence operator $\hat{\nabla}_P \cdot ()$ to a polar 2-form (3.87), the result must be a polar 3-form whose coefficients are obtained via the application of the *polar divergence matrix* $\overline{\mathbb{D}}$, formally

$$\hat{\nabla}_P \cdot \mathbf{B}_h = \partial_s B_{h,1} + \partial_\theta B_{h,2} + ik\, B_{h,3} = (\,\overline{\mathbb{D}}\,\vec{\mathbf{b}}\,)^\top \overline{\mathbf{\Lambda}}^3 \,. \tag{3.94}$$

The goal of this section is to identify on the one hand the suitable basis $\overline{\mathbf{\Lambda}}^3$ and on the other hand the form of the polar divergence matrix $\overline{\mathbb{D}}$.

The basis is evidently given by the basis (3.82c) in which $B_{h,3}$ is displayed, thus

$$\begin{aligned} \overline{\mathbf{\Lambda}}^3 &:= \left(\overline{\Lambda}^3_{(\overline{ij})}\right) \in \mathbb{R}^{\overline{n}^3}\,, \qquad \overline{\Lambda}^3_{(\overline{ij})} := D_i^{q_s} D_j^{q_\theta}\,, \\ &\text{with} \quad (\overline{ij}) = d_\theta\,(i-1) + j\,, \qquad 0 < i < d_s\,, \quad 0 \le j < d_\theta\,. \end{aligned} \tag{3.95}$$

Based on this new set of basis functions, the polar subspace $\overline{V}^3_h$ is readily defined as

$$\overline{V}^3_h := \operatorname{span}\left(\,\overline{\mathbf{\Lambda}}^3\,\right) \subset \overline{V}^3_h\,, \qquad \dim \overline{V}^3_h = \overline{n}^3\,, \tag{3.96}$$

and moreover, similar to (3.28), polar spline functions $p_h \in \overline{V}^3_h$ can compactly be written as

$$p_h = \overline{\mathcal{S}}_3[\,\overline{\mathbf{p}}\,] = \overline{\mathbf{p}}^\top\,\overline{\mathbf{\Lambda}}^3\,, \qquad \overline{\mathbf{p}} := (p_{(\overline{ij})}) \in \mathbb{C}^{\overline{n}^3}\,. \tag{3.97}$$

The polar extraction operator $\mathbb{E}^3$ has already been defined in (3.89). Therefore, $\overline{\mathbf{\Lambda}}^3 = \mathbb{E}^3\mathbf{\Lambda}^3$ and

$$p_h = \overline{\mathbf{p}}^\top\overline{\mathbf{\Lambda}}^3 = \overline{\mathbf{p}}^\top\mathbb{E}^3\mathbf{\Lambda}^3 = \mathbf{p}^\top\mathbf{\Lambda}^3\,. \tag{3.98}$$

Consequently, for given polar FE coefficients $\overline{\mathbf{p}}$, the corresponding tensor product FE coefficients are obtained via $\mathbf{p} = (\mathbb{E}^3)^\top\overline{\mathbf{p}}$.

In order to compute the polar divergence matrix we note that the sum of the derivatives with respect to s and θ can be easily deduced from (3.85), where we take note of the minus sign in the definition of the polar 2-form basis functions (3.78):

$$\begin{aligned} \frac{\partial B_{h,1}}{\partial s} + \frac{\partial B_{h,2}}{\partial \theta} = &\sum_{j=0}^{d_\theta-1} \left[b^1_{(\overline{2j})} - \sum_{\ell=0}^{1} b^1_\ell (\chi^{\ell+1}_{1j+1} - \chi^{\ell+1}_{1j}) + b^2_{(\overline{1j+1})} - b^2_{(\overline{1j})} \right] D_1^{q_s} D_j^{q_\theta} \\ &+ \sum_{i>1,j} (b^1_{(\overline{i+1j})} - b^1_{(\overline{ij})} + b^2_{(\overline{ij+1})} - b^2_{(\overline{ij})}) D_i^{q_s} D_j^{q_\theta}\,. \end{aligned} \tag{3.99}$$

The polar divergence of $\mathbf{B}_h \in Vhpolc$ can then be written compactly as

$$\hat{\nabla}_P \cdot \mathbf{B}_h = (\,\overline{\mathbb{D}}\,\vec{\mathbf{b}}\,)^\top\overline{\mathbf{\Lambda}}^3\,, \qquad \overline{\mathbb{D}}\,\vec{\mathbf{b}} = \left[\begin{array}{c|c|c} \overline{\mathbb{S}} & \mathbb{D}^\theta & ik\,\mathbb{1} \end{array}\right] \left[\begin{array}{c} \overline{\mathbf{b}}^1 \\ \overline{\mathbf{b}}^2 \\ \overline{\mathbf{b}}^3 \end{array}\right], \tag{3.100}$$

where $\mathbb{D}^\theta$ has been defined in (3.29) and is used here with $\mathbb{1}^s = \mathbb{1}_{d_s-1}$ and $\overline{\mathbb{S}}$ has been defined in (3.92).

Proposition 2. *We have* $\overline{\mathbb{D}}\,\overline{\mathbb{C}} = 0$.

Proof. The matrix product of interest reads

$$\overline{\mathbb{D}}\,\overline{\mathbb{C}} = \left[\begin{array}{c|c|c} \overline{\mathbb{S}} & \mathbb{D}^\theta & ik\,\mathbb{1} \end{array}\right] \left[\begin{array}{c|c|c} 0 & -ik\,\mathbb{1} & \overline{\mathbb{D}}^\theta \\ ik\,\mathbb{1} & 0 & -\overline{\mathbb{D}}^s \\ -\mathbb{D}^\theta & \overline{\mathbb{S}} & 0 \end{array}\right].$$

The first two rows yield zero immediately and the relation

$$\overline{\mathbb{S}}\,\overline{\mathbb{D}}^\theta - \mathbb{D}^\theta\,\overline{\mathbb{D}}^s = 0\,,$$

has been proven in Proposition 1. □

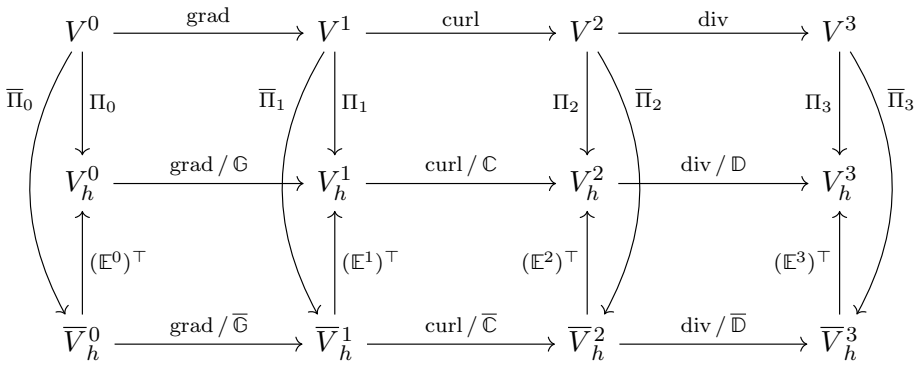

Figure 5: Commuting diagrams in 3D. Top row: continuous spaces, middle row: pure tensor product spaces, bottom row: polar spaces.

Consequently, due to the fact that $\overline{\mathbb{C}}\,\overline{\mathbb{G}} = 0$ and $\overline{\mathbb{D}}\,\overline{\mathbb{C}} = 0$ (see Propositions 1 and 2), we can construct similar to the pure tensor product case (3.34) the discrete cochain complex

$$\overline{V}_h^0 \xrightarrow{\overline{\mathbb{G}}} \overline{V}_h^1 \xrightarrow{\overline{\mathbb{C}}} \overline{V}_h^2 \xrightarrow{\overline{\mathbb{D}}} \overline{V}_h^3\,, \tag{3.101}$$

meaning that the image of the previous operator (either $\overline{\mathbb{G}}$ or $\overline{\mathbb{C}}$) is in the kernel of the next operator (either $\overline{\mathbb{C}}$ or $\overline{\mathbb{D}}$).

4 Commuting projectors

The discrete complexes (3.34) (pure tensor product splines) and (3.101) (polar splines) can be thought of as sub-complexes of the continuous version,

$$V^0 \xrightarrow{\text{grad}} V^1 \xrightarrow{\text{curl}} V^2 \xrightarrow{\text{div}} V^3\,. \tag{4.1}$$

The link between the spaces V^k, V_h^k and $\overline{V}_h^k$ $(0 \leq k \leq 3)$ is provided by projection operators $\Pi_k : V^k \to V_h^k$ and $\overline{\Pi}_k : V \to \overline{V}_h^k$, and the transpose extraction operators $(\mathbb{E}^k)^\top : \overline{V}_h^k \to V_h^k$, as displayed in Figure 5. The discrete spaces are defined here through the spline basis functions, such that there is a one-to-one correspondence between the elements (piece-wise polynomial functions) and their spline coefficients.

In this part we define the projection operators based on inter- and histopolation, such that the diagrams in Figure 5 are commuting in the following sense: at first, we shall prove the "standard" commutation relations

$$\Pi_1\,\text{grad} = \text{grad}\,\Pi_0\,, \qquad \Pi_2\,\text{curl} = \text{curl}\,\Pi_1\,, \qquad \Pi_3\,\text{div} = \text{div}\,\Pi_2\,, \tag{4.2}$$

where

$$\text{grad} = \hat{\nabla}_P\,()\,, \qquad \text{curl} = \hat{\nabla}_P \times ()\,, \qquad \text{div} = \hat{\nabla}_P \cdot ()\,. \tag{4.3}$$

The proof can be based solely on the definition of the *degrees of freedom (DOFs)* by inter- and histopolation (see below). The mechanics of the proof in the tensor product case suggests how to choose the DOFs for polar projectors in order to achieve, secondly,

$$\overline{\Pi}_1\,\text{grad} = \text{grad}\,\overline{\Pi}_0\,, \qquad \overline{\Pi}_2\,\text{curl} = \text{curl}\,\overline{\Pi}_1\,, \qquad \overline{\Pi}_3\,\text{div} = \text{div}\,\overline{\Pi}_2\,. \tag{4.4}$$

Additionally, in [25] it was shown that

$$\mathbb{G}\,(\mathbb{E}^0)^\top = (\mathbb{E}^1)^\top \overline{\mathbb{G}}\,, \qquad \mathbb{C}\,(\mathbb{E}^1)^\top = (\mathbb{E}^2)^\top \overline{\mathbb{C}}\,, \qquad \mathbb{D}\,(\mathbb{E}^2)^\top = (\mathbb{E}^3)^\top \overline{\mathbb{D}}\,. \tag{4.5}$$

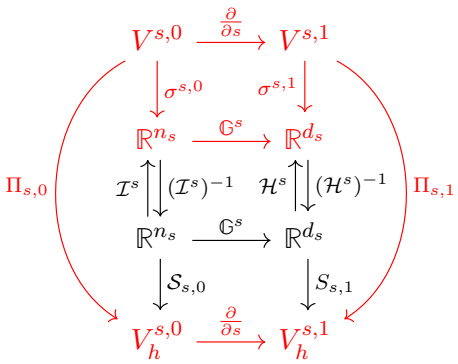

Figure 6: Commuting diagram in 1D using the notions of degrees of freedom (DOFs) $\sigma^{s,0}$ and $\sigma^{s,1}$ and finite element (FE) coefficients.

4.1 Tensor product degrees of freedom and projectors

The construction of degrees of freedom and commuting projectors in the pure tensor product setting can be found in [6], for instance, and is only repeated here in order to prepare for the polar case in the next section. A good understanding of the commuting projectors can be obtained in terms of the 1D diagram in Figure 6. We choose the s-space in this example, the θ-direction is treated in full analogy (even though the spaces are slightly different because of the boundaries). The upper row of the diagram contains the continuous function spaces $V^{s,0} = H^1(\Omega_s)$ and $V^{s,1} = L^2(\Omega_s)$ with $\Omega_s = [0, 1]$. The *degrees of freedom* (DOFs) $\sigma^{s,0} : V^{s,0} \to \mathbb{C}^{n_s}$ and $\sigma^{s,1} : V^{s,1} \to \mathbb{C}^{d_s}$ are linear functionals on the continuous spaces, with their image in the second row. The third row contains the *finite element (FE) coefficients* (in the spline bases) and the fourth row the FE spaces $V_h^{s,0} \subset V^{s,0}$ and $V_h^{s,1} \subset V^{s,1}$ spanned by the 1D spline bases and introduced in (3.10).

When dealing with inter-/histopolation, the DOFs can be defined as

$$f \in V^{s,0}: \qquad \boldsymbol{\sigma}^{s,0} := (\sigma_i^{s,0})_{i=0}^{n_s-1}, \qquad \sigma_i^{s,0}(f) := f(\mathfrak{s}_i), \tag{4.6a}$$

$$g \in V^{s,1}: \qquad \boldsymbol{\sigma}^{s,1} := (\sigma_i^{s,1})_{i=0}^{d_s-1}, \qquad \sigma_i^{s,1}(g) := \int_{\mathfrak{s}_i}^{\mathfrak{s}_{i+1}} g(s)\,\mathrm{d}s\,. \tag{4.6b}$$

Here, $\mathfrak{s} = (\mathfrak{s}_i)_{i=0}^{n_s-1}$ are the interpolation points in Ω_s, for example the Greville points of a spline basis (3.9), and $d_s = n_s - 1$ is the number of histopolation intervals. The bases of the FE spaces $V_h^{s,0}$ and $V_h^{s,1}$ appear in the inter-/histopolation matrices

$$\mathcal{I}_{ij}^s := N_j^{q_s}(\mathfrak{s}_i), \qquad \mathcal{H}_{ij}^s := \int_{\mathfrak{s}_i}^{\mathfrak{s}_{i+1}} D_j^{q_s}(s)\,\mathrm{d}s\,, \tag{4.7}$$

respectively. The interpolation points $\mathfrak{s}$ have to be chosen such that $\mathcal{I}^s$ and $\mathcal{H}^s$ are invertible (that is the reason for Greville points with splines, usually). When using for instance a quadrature rule of sufficient order for computing integrals, the matrix $\mathcal{H}^s$ is exact since M-splines are piece-wise polynomials.

The operators $\mathcal{S}_{s,0} : \mathbb{C}^{n_s} \to V_h^{s,0}$ and $\mathcal{S}_{s,1} : \mathbb{C}^{d_s} \to V_h^{s,1}$ map FE coefficients to the corresponding spline function:

$$V_h^{s,0} \ni f_h = S_{s,0}[\mathbf{f}](s) = \sum_{j=0}^{n_s-1} f_j\, N_j^{q_s}(s), \qquad \mathbf{f} = (f_j)_{j=0}^{n_s-1}, \tag{4.8a}$$

$$V_h^{s,1} \ni g_h = S_{s,1}[\mathbf{g}](s) = \sum_{j=0}^{d_s-1} g_j\, D_j^{q_s}(s) \qquad \mathbf{g} = (g_j)_{j=0}^{d_s-1}. \tag{4.8b}$$

For the DOFs (4.6) this means

$$\sigma_i^{s,0}(f_h) = \sum_{j=0}^{n_s-1} f_j \, N_j^{q_s}(\mathfrak{s}_i) = \sum_j \mathcal{I}_{ij}^s \, f_j \qquad \Rightarrow \quad \sigma^{s,0}(f_h) = \mathcal{I}^s \, \mathbf{f} \,, \tag{4.9a}$$

$$\sigma_i^{s,1}(g_h) = \sum_{j=0}^{d_s-1} g_j \int_{\mathfrak{s}_i}^{\mathfrak{s}_{i+1}} D_j^{q_s}(s) \, \mathrm{d}s = \sum_j \mathcal{H}_{ij}^s \, g_j \quad \Rightarrow \quad \sigma^{s,1}(g_h) = \mathcal{H}^s \, \mathbf{g} \,, \tag{4.9b}$$

such that it is evident that the DOFs (4.6) uniquely define an element in $V_h^{s,0}$ and $V_h^{s,1}$ provided that $\mathcal{I}^s$ and $\mathcal{H}^s$ are invertible.

Definition 1. *The projectors $\Pi_{s,0} : V^{s,0} \to V_h^{s,0}$ and $\Pi_{s,1} : V^{s,1} \to V_h^{s,1}$ are defined via the DOFs:*

$$\sigma^{s,0}(\Pi_{s,0}(f)) = \sigma^{s,0}(f) \,, \qquad \sigma^{s,1}(\Pi_{s,1}(g)) = \sigma^{s,1}(g) \,. \tag{4.10}$$

Proposition 3. *Provided that the histopolation matrix $\mathcal{H}^s$ is exact, the projectors (4.10) satisfy*

$$\Pi_{s,1}\left(\frac{\partial f}{\partial s}\right) = \frac{\partial}{\partial s}\Pi_{s,0}(f). \tag{4.11}$$

Proof. By definition both sides of the equality are in $V_h^{s,1}$. Since an element in $V_h^{s,1}$ is uniquely defined by its DOFs, we can apply $\sigma_i^{s,1}$ on both sides and show the results to be equal:

$$\sigma_i^{s,1}\left(\Pi_{s,1}\left(\frac{\partial f}{\partial s}\right)\right) \overset{(4.10)}{=} \sigma_i^{s,1}\left(\frac{\partial f}{\partial s}\right) = f(\mathfrak{s}_{i+1}) - f(\mathfrak{s}_i) = \sigma_{i+1}^{s,0}(f) - \sigma_i^{s,0}(f) \,,$$

$$\sigma_i^{s,1}\left(\frac{\partial}{\partial s}\Pi_{s,0}(f)\right) = \Pi_{s,0}(f)(\mathfrak{s}_{i+1}) - \Pi_{s,0}(f)(\mathfrak{s}_i) = \sigma_{i+1}^{s,0}(\Pi_{s,0}(f)) - \sigma_i^{s,0}(\Pi_{s,0}(f))$$

$$\overset{(4.10)}{=} \sigma_{i+1}^{s,0}(f) - \sigma_i^{s,0}(f) \,.$$

□

We note that this proof did not rely on the choice of basis functions. The DOFs defined by (4.6) and projectors defined in Definition 1 are *sufficient conditions* for the commuting property. This proof generalizes to tensor product spaces and even to the polar case in a straightforward way, as shown in the following.

Let us now shift to the spaces V^k ($0 \leq k \leq 3$) defined in (2.8). Here, one has to keep in mind that the smoothness of these spaces is strictly speaking not large enough to be able to carry out interpolation everywhere. However, in the discrete MHD eigenvalue problem in Section 5, we shall only apply projectors to functions which are continuous everywhere; a consequence of the restrictions $q_s, q_\theta \geq 2$ in the polar spline framework (see Def. 3.1 in [28]). Therefore, the projection operations are well-defined in this case. To define the DOFs, we consider the tensor product grid $(\mathfrak{s}_i, \mathfrak{t}_j)$ built from the additional 1D set of Greville points $\mathfrak{t} = (\mathfrak{t}_j)_{j=0}^{n_\theta-1}$ in θ-direction. The DOFs can then be defined as

$$f \in V^0 : \qquad \sigma_{(ij)}^0(f) := f(\mathfrak{s}_i, \mathfrak{t}_j) \,, \tag{4.12a}$$

$$\mathbf{A} = [A_1, A_2, A_3] \in V^1 : \quad \begin{cases} \sigma_{(ij)}^{1,1}(\mathbf{A}) := \displaystyle\int_{\mathfrak{s}_i}^{\mathfrak{s}_{i+1}} A_1(s, \mathfrak{t}_j) \, \mathrm{d}s \,, \\ \sigma_{(ij)}^{1,2}(\mathbf{A}) := \displaystyle\int_{\mathfrak{t}_j}^{\mathfrak{t}_{j+1}} A_2(\mathfrak{s}_i, \theta) \, \mathrm{d}\theta \,, \\ \sigma_{(ij)}^{1,3}(\mathbf{A}) := A_3(\mathfrak{s}_i, \mathfrak{t}_j) \,, \end{cases} \tag{4.12b}$$

$$\mathbf{B} = [B_1, B_2, B_3] \in V^2 : \quad \begin{cases} \sigma^{2,1}_{(ij)}(\mathbf{B}) := \int_{\mathfrak{t}_j}^{\mathfrak{t}_{j+1}} B_1(\mathfrak{s}_i, \theta)\, \mathrm{d}\theta\,, \\ \sigma^{2,2}_{(ij)}(\mathbf{B}) := \int_{\mathfrak{s}_i}^{\mathfrak{s}_{i+1}} B_2(s, \mathfrak{t}_j)\, \mathrm{d}s\,, \\ \sigma^{2,3}_{(ij)}(\mathbf{B}) := \int_{\mathfrak{s}_i}^{\mathfrak{s}_{i+1}} \int_{\mathfrak{t}_j}^{\mathfrak{t}_{j+1}} B_3(s, \theta)\, \mathrm{d}s\, \mathrm{d}\theta\,, \end{cases} \tag{4.12c}$$

$$p \in V^3 : \qquad \sigma^3_{(ij)}(p) := \int_{\mathfrak{s}_i}^{\mathfrak{s}_{i+1}} \int_{\mathfrak{t}_j}^{\mathfrak{t}_{j+1}} p(s, \theta)\, \mathrm{d}s\, \mathrm{d}\theta\,. \tag{4.12d}$$

Similar to (4.9) we have for discrete functions

$$f_h = \mathcal{S}_0[\,\mathbf{f}\,] \in V_h^0 : \qquad \sigma^0(f_h) \;= \mathcal{I}^0\,\mathbf{f}\,, \tag{4.13a}$$

$$\mathbf{A}_h = \mathcal{S}_1[\,\vec{\mathbf{a}}\,] \in V_h^1 : \qquad \sigma^1(\mathbf{A}_h) = \mathcal{I}^1\,\vec{\mathbf{a}}\,, \tag{4.13b}$$

$$\mathbf{B}_h = \mathcal{S}_2[\,\vec{\mathbf{b}}\,] \in V_h^2 : \qquad \sigma^2(\mathbf{B}_h) = \mathcal{I}^2\,\vec{\mathbf{b}}\,, \tag{4.13c}$$

$$p_h = \mathcal{S}_3[\,\mathbf{p}\,] \in V_h^3 : \qquad \sigma^3(p_h) \;= \mathcal{I}^3\,\mathbf{p}\,, \tag{4.13d}$$

where the mixed inter-/histopolation matrices $\mathcal{I}^k$ are given by

$$\mathcal{I}^0 := \mathcal{I}^s \otimes \mathcal{I}^\theta\,, \qquad \mathcal{I}^1 := \begin{bmatrix} \mathcal{H}^s \otimes \mathcal{I}^\theta & 0 & 0 \\ 0 & \mathcal{I}^s \otimes \mathcal{H}^\theta & 0 \\ 0 & 0 & \mathcal{I}^s \otimes \mathcal{I}^\theta \end{bmatrix}, \tag{4.14}$$

$$\mathcal{I}^3 := \mathcal{H}^s \otimes \mathcal{H}^\theta\,, \qquad \mathcal{I}^2 := \begin{bmatrix} \mathcal{I}^s \otimes \mathcal{H}^\theta & 0 & 0 \\ 0 & \mathcal{H}^s \otimes \mathcal{I}^\theta & 0 \\ 0 & 0 & \mathcal{H}^s \otimes \mathcal{H}^\theta \end{bmatrix}. \tag{4.15}$$

Definition 2. *The projectors $\Pi_k : V^k \to V_h^k$ $(0 \le k \le 3)$ are defined via the DOFs (4.12):*

$$\sigma^0(\Pi_0(f)) = \sigma^0(f)\,, \quad \sigma^1(\Pi_1(\mathbf{A})) = \sigma^1(\mathbf{A})\,, \quad \sigma^2(\Pi_2(\mathbf{B})) = \sigma^2(\mathbf{B})\,, \quad \sigma^3(\Pi_3(p)) = \sigma^3(p)\,. \tag{4.16}$$

Proposition 4. *Provided that the integrals in (4.12) are exact, the projectors (4.16) satisfy the commutation relations*

$$\Pi_1\,\mathrm{grad} = \mathrm{grad}\,\Pi_0\,, \qquad \Pi_2\,\mathrm{curl} = \mathrm{curl}\,\Pi_1\,, \qquad \Pi_3\,\mathrm{div} = \mathrm{div}\,\Pi_2\,. \tag{4.17}$$

Proof. We only prove the first relation $\Pi_1\,\mathrm{grad} = \mathrm{grad}\,\Pi_0$ explicitly, the other two relations can be proven accordingly. By definition both sides are in V_h^1. Since an element in V_h^1 is uniquely defined by its DOFs, we can apply σ^1 on both sides:

$$\sigma^{1,1}_{(ij)}\left(\Pi_1(\hat{\nabla}_P f)\right) \overset{(4.16)}{=} \sigma^{1,1}_{(ij)}\left(\hat{\nabla}_P f\right) = f(\mathfrak{s}_{i+1}, \mathfrak{t}_j) - f(\mathfrak{s}_i, \mathfrak{t}_j) = \sigma^0_{(i+1j)}(f) - \sigma^0_{(ij)}(f)\,,$$

$$\sigma^{1,2}_{(ij)}\left(\Pi_1(\hat{\nabla}_P f)\right) \overset{(4.16)}{=} \sigma^{1,2}_{(ij)}\left(\hat{\nabla}_P f\right) = f(\mathfrak{s}_i, \mathfrak{t}_{j+1}) - f(\mathfrak{s}_i, \mathfrak{t}_j) = \sigma^0_{(ij+1)}(f) - \sigma^0_{(ij)}(f)\,,$$

$$\sigma^{1,3}_{(ij)}\left(\Pi_1(\hat{\nabla}_P f)\right) \overset{(4.16)}{=} \sigma^{1,3}_{(ij)}\left(\hat{\nabla}_P f\right) = ik\,\sigma^0_{(ij)}(f)\,,$$

and on the other hand

$$\begin{aligned}\sigma^{1,1}_{(ij)}\left(\hat{\nabla}_P\,\Pi_0(f)\right) &= \Pi_0(f)(\mathfrak{s}_{i+1},\mathfrak{t}_j) - \Pi_0(f)(\mathfrak{s}_i,\mathfrak{t}_j)\\ &= \sigma^0_{(i+1j)}(\Pi_0(f)) - \sigma^0_{(ij)}(\Pi_0(f)) \overset{(4.16)}{=} \sigma^0_{(i+1j)}(f) - \sigma^0_{(ij)}(f)\,,\\ \sigma^{1,2}_{(ij)}\left(\hat{\nabla}_P\,\Pi_0(f)\right) &= \Pi_0(f)(\mathfrak{s}_i,\mathfrak{t}_{j+1}) - \Pi_0(f)(\mathfrak{s}_i,\mathfrak{t}_j)\\ &= \sigma^0_{(ij+1)}(\Pi_0(f)) - \sigma^0_{(ij)}(\Pi_0(f)) \overset{(4.16)}{=} \sigma^0_{(ij+1)}(f) - \sigma^0_{(ij)}(f)\,,\\ \sigma^{1,3}_{(ij)}\left(\hat{\nabla}_P\,\Pi_0(f)\right) &= ik\,\sigma^0_{(ij)}\left(\Pi_0(f)\right) \overset{(4.16)}{=} ik\,\sigma^0_{(ij)}\left(f\right)\,.\end{aligned}$$

Because this holds for any (ij) the first relation in (4.17) is proved. The proofs for the second and third relation work in full analogy. □

By identifying the projected functions with their spline coefficients as in (4.13),

$$\Pi_0(f) = \mathcal{S}_0[\,\mathbf{f}\,]\,, \qquad \Pi_1(\mathbf{A}) = \mathcal{S}_1[\,\vec{\mathbf{a}}\,]\,, \qquad \Pi_2(\mathbf{B}) = \mathcal{S}_2[\vec{\mathbf{b}}]\,, \qquad \Pi_3(p) = \mathcal{S}_3[\,\mathbf{p}\,]\,, \tag{4.18}$$

the projection problems (4.16) can be written as linear systems

$$\mathcal{I}^0\,\mathbf{f} = \sigma^0(f)\,, \qquad \mathcal{I}^1\,\vec{\mathbf{a}} = \sigma^1(\mathbf{A})\,, \qquad \mathcal{I}^2\,\vec{\mathbf{b}} = \sigma^2(\mathbf{B})\,, \qquad \mathcal{I}^3\,\mathbf{p} = \sigma^3(p)\,. \tag{4.19}$$

The solution of these linear systems can be done very efficiently because of the tensor product structure of the matrices $\mathcal{I}^k$, e.g. $(\mathcal{I}^0)^{-1} = (\mathcal{I}^s \otimes \mathcal{I}^\theta)^{-1} = (\mathcal{I}^s)^{-1} \otimes (\mathcal{I}^\theta)^{-1}$, and the costs for inverting the matrices $\mathcal{I}^s$ and $\mathcal{I}^\theta$ corresponding to 1D spline bases are negligible.

4.2 Polar degrees of freedom and projectors

In this section we derive polar DOFs that guarantee the commuting property shown in Figure 5. Figure 7 shows the grey tensor product grid with $n_s n_\theta$ interpolation points $(\mathfrak{s}_i, \mathfrak{t}_j)$ on the vertices for the DOFs σ^0 defined in (4.12a). In the polar case, only the blue points/grid are used for interpolation. The number of blue points is $(n_s - 2)\,n_\theta + 3$ which corresponds to the dimension of $\overline{V}^0_h$. The first two "rings" around the pole $(\mathfrak{s}_0, \mathfrak{t}_j)$ and $(\mathfrak{s}_1, \mathfrak{t}_j)$ are removed and three new points $(\mathfrak{s}_1, \bar{\mathfrak{t}}_0)$, $(\mathfrak{s}_1, \bar{\mathfrak{t}}_1)$ and $(\mathfrak{s}_1, \bar{\mathfrak{t}}_2)$ on the $i = 1$ ring are added for interpolation. The three angles $\{\bar{\mathfrak{t}}_0, \bar{\mathfrak{t}}_1, \bar{\mathfrak{t}}_2\} \subset \mathfrak{t}$ must be distinct and are here chosen to be part of the tensor product grid for implementation reasons. They account for the three DOFs necessary for the three new polar spline basis functions $\overline{\Lambda}^0_\ell$ around the pole. In the polar setting, we define the DOFs $\overline{\sigma}^0$ as

$$f \in V^0: \quad \begin{cases} \overline{\sigma}^0_\ell(f) := f(\mathfrak{s}_1, \bar{\mathfrak{t}}_\ell)\,, & \ell = 0, 1, 2\,, \\ \overline{\sigma}^0_{(\overline{ij})}(f) := f(\mathfrak{s}_i, \mathfrak{t}_j)\,, & 1 < i < n_s\,. \end{cases} \tag{4.20}$$

We now aim to construct the DOFs for the space $\overline{V}^1_h$ such that the commutation relations (4.4) hold. The proof of Proposition 4 serves as the blue print of how to achieve this. From Figure 7 we see that for $i > 1$ histopolation can be carried out as usual on the blue grid. However, we also need to carry out histopolation between $i = 1$ and $i = 2$ in order to get as many DOFs as basis functions in the space $\overline{V}^1_h$. In order to get the commuting property, we employ a convex combination of the DOFs for $i = 1$ and demand

$$\overline{\sigma}^{1,1}_{(\overline{1}j)}\left(\frac{\partial f}{\partial s}\,\vec{\boldsymbol{e}}_1\right) = f(\mathfrak{s}_2, \mathfrak{t}_j) - \sum_{\ell=0}^{2} w_{\ell j} f(\mathfrak{s}_1, \bar{\mathfrak{t}}_\ell)\,, \quad w_{\ell j} \in \mathbb{R}\,, \quad \sum_{\ell=0}^{2} w_{\ell j} = 1 \quad \forall\, j\,, \tag{4.21}$$

for $f \in V^0$. In the θ-direction we demand

$$\overline{\sigma}^{1,2}_\ell\left(\frac{\partial f}{\partial \theta}\,\vec{\boldsymbol{e}}_2\right) = f(\mathfrak{s}_1, \bar{\mathfrak{t}}_{\ell+1}) - f(\mathfrak{s}_1, \bar{\mathfrak{t}}_0)\,, \qquad \ell = 0, 1\,. \tag{4.22}$$

The conditions (4.21) and (4.22) can be satisfied with the following polar DOFs for the space $\overline{V}_h^1$:

$$\mathbf{A} \in V^1 : \begin{cases} \overline{\sigma}^{1,1}_{(\overline{1}j)}(\mathbf{A}) := \displaystyle\int_{\mathfrak{s}_0}^{\mathfrak{s}_2} A_1(s, \mathfrak{t}_j)\,\mathrm{d}s - \sum_{\ell=0}^{2} w_{\ell j} \int_{\mathfrak{s}_0}^{\mathfrak{s}_1} A_1(s, \bar{\mathfrak{t}}_\ell)\,\mathrm{d}s\,, \\ \overline{\sigma}^{1,1}_{(\overline{i}j)}(\mathbf{A}) := \displaystyle\int_{\mathfrak{s}_i}^{\mathfrak{s}_{i+1}} A_1(s, \mathfrak{t}_j)\,\mathrm{d}s\,, \qquad 1 < i < d_s\,, \\ \overline{\sigma}^{1,2}_{\ell}(\mathbf{A}) := \displaystyle\int_{\bar{\mathfrak{t}}_0}^{\bar{\mathfrak{t}}_{\ell+1}} A_2(\mathfrak{s}_1, \theta)\,\mathrm{d}\theta\,, \qquad \ell = 0, 1\,, \\ \overline{\sigma}^{1,2}_{(\overline{i}j)}(\mathbf{A}) := \displaystyle\int_{\mathfrak{t}_j}^{\mathfrak{t}_{j+1}} A_2(\mathfrak{s}_i, \theta)\,\mathrm{d}\theta \qquad 1 < i < n_s\,, \\ \overline{\sigma}^{1,3}(\mathbf{A}) := \overline{\sigma}^0(A_3)\,. \end{cases} \tag{4.23}$$

Let us verify that (4.21) is indeed fulfilled: from the first line in (4.23) we obtain

$$\overline{\sigma}^{1,1}_{(\overline{1}j)}\left(\frac{\partial f}{\partial s}\,\vec{e}_1\right) = f(\mathfrak{s}_2, \mathfrak{t}_j) - f(\mathfrak{s}_0, \mathfrak{t}_j) - \sum_{\ell=0}^{2} w_{\ell j}\left[f(\mathfrak{s}_1, \bar{\mathfrak{t}}_\ell) - f(\mathfrak{s}_0, \bar{\mathfrak{t}}_\ell)\right]\,. \tag{4.24}$$

Taking into account that $f(\mathfrak{s}_0 = 0, \theta)$ ($\mathfrak{s}_0 = 0$ for clamped B-splines) is independent of θ because polar 0-forms are single-valued at the pole and, moreover, that we demanded $\sum_\ell w_{\ell j} = 1$, we obtain relation (4.21). The relation (4.22) follows directly from the third line in (4.23). The polar DOFs for $\mathbf{B} \in V^2$ follow by exchanging the components in (4.23):

$$\mathbf{B} \in V^2 : \begin{cases} \overline{\sigma}^{2,1}(\mathbf{B}) := \overline{\sigma}^{1,2}(\mathbf{B})\,, \\ \overline{\sigma}^{2,2}(\mathbf{B}) := \overline{\sigma}^{1,1}(\mathbf{B})\,, \\ \overline{\sigma}^{2,3}(\mathbf{B}) := \overline{\sigma}^{3}(B_3)\,. \end{cases} \tag{4.25}$$

Here, $\overline{\sigma}^3$ is identified by looking at DOFs for $p \in V^3$ which we define to be

$$p \in V^3 : \begin{cases} \overline{\sigma}^{3}_{(\overline{1}j)}(p) := \displaystyle\int_{\mathfrak{s}_0}^{\mathfrak{s}_2} \int_{\mathfrak{t}_j}^{\mathfrak{t}_{j+1}} p(s, \theta)\,\mathrm{d}s\,\mathrm{d}\theta - \sum_{\ell=0}^{1} a_{\ell j} \int_{\mathfrak{s}_0}^{\mathfrak{s}_1} \int_{\bar{\mathfrak{t}}_0}^{\bar{\mathfrak{t}}_{\ell+1}} p(s, \theta)\,\mathrm{d}s\,\mathrm{d}\theta\,, \\ \overline{\sigma}^{3}_{(\overline{i}j)}(p) := \displaystyle\int_{\mathfrak{s}_i}^{\mathfrak{s}_{i+1}} \int_{\mathfrak{t}_j}^{\mathfrak{t}_{j+1}} p(s, \theta)\,\mathrm{d}s\,d\theta\,, \qquad 1 < i < d_s\,. \end{cases} \tag{4.26}$$

Here, we introduced the coefficients $a_{0j}, a_{1j} \in \mathbb{R}$ which have to be chosen such that the commuting property holds (see below). Note that the above DOFs are linearly independent and that the number of DOFs matches the dimension of each respective space.

Definition 3. *The projectors $\overline{\Pi}_k : V^k \to \overline{V}_h^k$ are defined via the DOFs (4.20), (4.23), (4.25) and (4.26):*

$$\overline{\sigma}^0\left(\overline{\Pi}_0(f)\right) = \overline{\sigma}^0(f)\,, \quad \overline{\sigma}^1\left(\overline{\Pi}_1(\mathbf{A})\right) = \overline{\sigma}^1(\mathbf{A})\,, \quad \overline{\sigma}^2\left(\overline{\Pi}_2(\mathbf{B})\right) = \overline{\sigma}^2(\mathbf{B})\,, \quad \overline{\sigma}^3\left(\overline{\Pi}_3(p)\right) = \overline{\sigma}^3(p)\,. \tag{4.27}$$

Proposition 5. *Provided that the integrals in (4.23), (4.25) and (4.26) are exact and that for any $(f_0, f_1, f_2) \in \mathbb{R}^3$,*

$$\sum_{\ell=0}^{1} a_{\ell j}(f_{\ell+1} - f_0) = \sum_{\ell=0}^{2} (w_{\ell j+1} - w_{\ell j}) f_\ell\,, \qquad a_{\ell j} \neq 0\,, \qquad \sum_{\ell=0}^{2} w_{\ell j} = 1\,, \tag{4.28}$$

the projectors (4.27) satisfy the commutation relations

$$\overline{\Pi}_1\,\mathrm{grad} = \mathrm{grad}\,\overline{\Pi}_0\,, \qquad \overline{\Pi}_2\,\mathrm{curl} = \mathrm{curl}\,\overline{\Pi}_1\,, \qquad \overline{\Pi}_3\,\mathrm{div} = \mathrm{div}\,\overline{\Pi}_2\,.$$

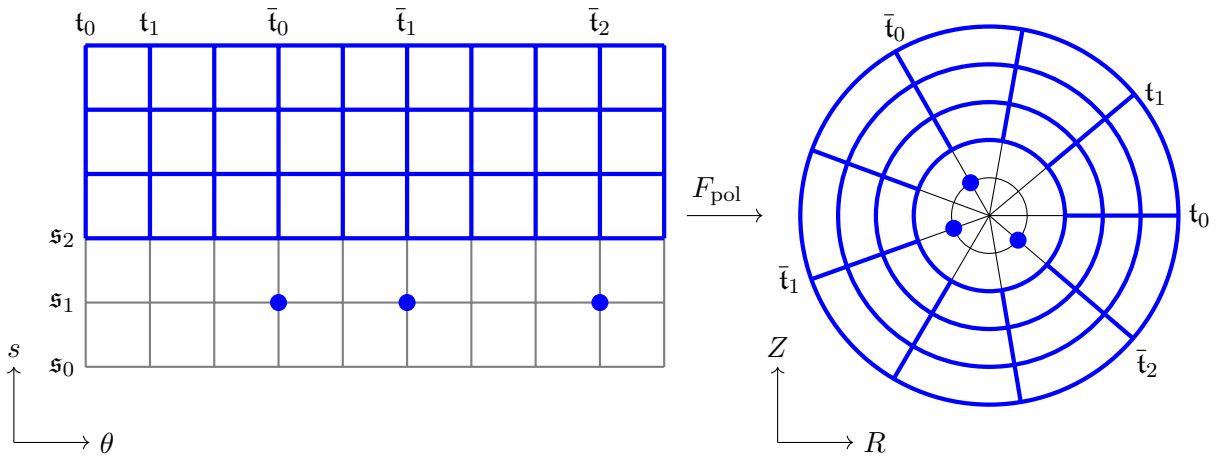

Figure 7: Only the three blue points and the vertices of the blue grid are used for interpolation in the polar setting. Note that all points on the line at $\mathfrak{s}_0 = 0$ are mapped to the pole (R_0, Z_0) under the mapping F_{pol}. However, no interpolation points are located on this line for the new blue grid.

Proof. Let us start with $\overline{\Pi}_1 \operatorname{grad} = \operatorname{grad} \overline{\Pi}_0$. By definition both sides of the equality are in $\overline{V}_h^1$. Since an element in $\overline{V}_h^1$ is uniquely defined by its DOFs, we can apply $\overline{\sigma}^1$ on both sides. The tensor product part is as usual; the new parts for $i = 1$ read

$$\begin{aligned}
\overline{\sigma}^{1,1}_{(\overline{1}j)}\left(\overline{\Pi}_1(\hat{\nabla}_P f)\right) &\overset{(4.27)}{=} \overline{\sigma}^{1,1}_{(\overline{1}j)}\left(\hat{\nabla}_P f\right) = f(\mathfrak{s}_2, \mathfrak{t}_j) - f(\mathfrak{s}_0, \mathfrak{t}_j) - \sum_{\ell=0}^{2} w_{\ell j}[\, f(\mathfrak{s}_1, \bar{\mathfrak{t}}_\ell) - f(\mathfrak{s}_0, \bar{\mathfrak{t}}_\ell)] \\
&= \overline{\sigma}^0_{(\overline{2}j)}(f) - \sum_{\ell=0}^{2} w_{\ell j}\, \overline{\sigma}^0_\ell(f)\,, \\
\overline{\sigma}^{1,2}_{\ell}\left(\overline{\Pi}_1(\hat{\nabla}_P f)\right) &\overset{(4.27)}{=} \overline{\sigma}^{1,2}_{\ell}\left(\hat{\nabla}_P f\right) = f(\mathfrak{s}_1, \bar{\mathfrak{t}}_{\ell+1}) - f(\mathfrak{s}_1, \bar{\mathfrak{t}}_0) = \overline{\sigma}^0_{\ell+1}(f) - \overline{\sigma}^0_0(f)\,, \\
\overline{\sigma}^{1,3}\left(\overline{\Pi}_1(\hat{\nabla}_P f)\right) &\overset{(4.27)}{=} \overline{\sigma}^{1,3}\left(\hat{\nabla}_P f\right) = ik\,\overline{\sigma}^0(f)\,,
\end{aligned}$$

and

$$\begin{aligned}
\overline{\sigma}^{1,1}_{(\overline{1}j)}\left(\hat{\nabla}_P\, \overline{\Pi}_0(f)\right) &= \overline{\Pi}_0(f)(\mathfrak{s}_2, \mathfrak{t}_j) - \overline{\Pi}_0(f)(\mathfrak{s}_0, \mathfrak{t}_j) - \sum_{\ell=0}^{2} w_{\ell j}\left[\,\overline{\Pi}_0(f)(\mathfrak{s}_1, \bar{\mathfrak{t}}_\ell) - \overline{\Pi}_0(f)(\mathfrak{s}_0, \bar{\mathfrak{t}}_\ell)\right] \\
&= \overline{\sigma}^0_{(\overline{2}j)}\left(\,\overline{\Pi}_0(f)\,\right) - \sum_{\ell=0}^{2} w_{\ell j}\, \overline{\sigma}^0_\ell\left(\,\overline{\Pi}_0(f)\,\right) \overset{(4.27)}{=} \overline{\sigma}^0_{(\overline{2}j)}(f) - \sum_{\ell=0}^{2} w_{\ell j} \overline{\sigma}^0_\ell(f)\,, \\
\overline{\sigma}^{1,2}_{\ell}\left(\hat{\nabla}_P\, \overline{\Pi}_0(f)\right) &= \overline{\Pi}_0(f)(\mathfrak{s}_1, \bar{\mathfrak{t}}_{\ell+1}) - \overline{\Pi}_0(f)(\mathfrak{s}_1, \bar{\mathfrak{t}}_0) = \overline{\sigma}^0_{\ell+1}\left(\,\overline{\Pi}_0(f)\,\right) - \overline{\sigma}^0_0\left(\,\overline{\Pi}_0(f)\,\right) \\
&\overset{(4.27)}{=} \overline{\sigma}^0_{\ell+1}(f) - \overline{\sigma}^0_0(f)\,, \\
\overline{\sigma}^{1,3}\left(\hat{\nabla}_P\, \overline{\Pi}_0(f)\right) &= ik\,\overline{\sigma}^0\left(\,\overline{\Pi}_0(f)\,\right) \overset{(4.27)}{=} ik\,\overline{\sigma}^0(f)\,.
\end{aligned}$$

In order to prove the second and the third commutation relation, we just need to prove the commutation for the third component of the second relation (which corresponds to the divergence of the vector curl in 2D); everything else then follows in a straightforward manner. Hence, let us look at the third component of $\overline{\Pi}_2(\operatorname{curl} \mathbf{A}) = \operatorname{curl} \overline{\Pi}_1(\mathbf{A})$. As usual, we can apply $\overline{\sigma}^{2,3}$ on both sides. The tensor

product part is as usual; the new parts for $i = 1$ read

$$\begin{aligned}
\overline{\sigma}^{2,3}_{(\overline{1}j)}\left(\overline{\Pi}_2(\hat{\nabla}_P \times \mathbf{A})\right) &\overset{(4.27)}{=} \overline{\sigma}^{2,3}_{(\overline{1}j)}\left(\hat{\nabla}_P \times \mathbf{A}\right) = \overline{\sigma}^{3}_{(\overline{1}j)}\left(\frac{\partial A_2}{\partial s} - \frac{\partial A_1}{\partial \theta}\right) \\
&= \int_{\mathfrak{t}_j}^{\mathfrak{t}_{j+1}} \left[A_2(\mathfrak{s}_2, \theta) - A_2(\mathfrak{s}_0, \theta)\right] \mathrm{d}\theta - \sum_{\ell=0}^{1} a_{\ell j} \int_{\bar{\mathfrak{t}}_0}^{\bar{\mathfrak{t}}_{\ell+1}} \left[A_2(\mathfrak{s}_1, \theta) - A_2(\mathfrak{s}_0, \theta)\right] \mathrm{d}\theta \\
&\quad - \int_{\mathfrak{s}_0}^{\mathfrak{s}_2} \left[A_1(s, \mathfrak{t}_{j+1}) - A_1(s, \mathfrak{t}_j)\right] \mathrm{d}s + \sum_{\ell=0}^{1} a_{\ell j} \int_{\mathfrak{s}_0}^{\mathfrak{s}_1} \left[A_1(s, \bar{\mathfrak{t}}_{\ell+1}) - A_1(s, \bar{\mathfrak{t}}_0)\right] \mathrm{d}s \\
&= \int_{\mathfrak{t}_j}^{\mathfrak{t}_{j+1}} A_2(\mathfrak{s}_2, \theta) \, \mathrm{d}\theta - \sum_{\ell=0}^{1} a_{\ell j} \int_{\bar{\mathfrak{t}}_0}^{\bar{\mathfrak{t}}_{\ell+1}} A_2(\mathfrak{s}_1, \theta) \, \mathrm{d}\theta \\
&\quad - \int_{\mathfrak{s}_0}^{\mathfrak{s}_2} \left[A_1(s, \mathfrak{t}_{j+1}) - A_1(s, \mathfrak{t}_j)\right] \mathrm{d}s + \sum_{\ell=0}^{2} (w_{\ell j+1} - w_{\ell j}) \int_{\mathfrak{s}_0}^{\mathfrak{s}_1} A_1(s, \bar{\mathfrak{t}}_\ell) \mathrm{d}s \\
&= \overline{\sigma}^{1,2}_{(\overline{2}j)}(\mathbf{A}) - \sum_{\ell=0}^{1} a_{\ell j} \, \overline{\sigma}^{1,2}_{\ell}(\mathbf{A}) - \overline{\sigma}^{1,1}_{(\overline{1}j+1)}(\mathbf{A}) + \overline{\sigma}^{1,1}_{(\overline{1}j)}(\mathbf{A}) \,,
\end{aligned}$$

where we used that $A_2(\mathfrak{s}_0 = 0, \theta) = 0 \ \forall \theta$. Moreover, when going from the second to the third equality sign we inserted the condition (4.28). By replacing $\mathbf{A} \to \overline{\Pi}_1(\mathbf{A})$ in the last line, we obtain

$$\begin{aligned}
\overline{\sigma}^{2,3}_{(\overline{1}j)}\left(\hat{\nabla}_P \times \overline{\Pi}_1(\mathbf{A})\right) &= \overline{\sigma}^{3}_{(\overline{1}j)}\left((\hat{\nabla}_P \times \overline{\Pi}_1(\mathbf{A})) \cdot \vec{\boldsymbol{e}}_3\right) \\
&= \overline{\sigma}^{1,2}_{(\overline{2}j)}\left(\overline{\Pi}_1(\mathbf{A})\right) - \sum_{\ell=0}^{1} a_{\ell j} \, \overline{\sigma}^{1,2}_{\ell}\left(\overline{\Pi}_1(\mathbf{A})\right) - \overline{\sigma}^{1,1}_{(\overline{1}j+1)}\left(\overline{\Pi}_1(\mathbf{A})\right) + \overline{\sigma}^{1,1}_{(\overline{1}j)}\left(\overline{\Pi}_1(\mathbf{A})\right) \\
&\overset{(4.27)}{=} \overline{\sigma}^{1,2}_{(\overline{2}j)}(\mathbf{A}) - \sum_{\ell=0}^{1} a_{\ell j} \, \overline{\sigma}^{1,2}_{\ell}(\mathbf{A}) - \overline{\sigma}^{1,1}_{(\overline{1}j+1)}(\mathbf{A}) + \overline{\sigma}^{1,1}_{(\overline{1}j)}(\mathbf{A}) \,.
\end{aligned}$$

□

Remark 1. *By comparing coefficients of f_ℓ it is easy to see that the equations (4.28) are satisfied if*

$$a_{\ell j} = w_{\ell+1 j+1} - w_{\ell+1 j} \,, \qquad \ell = 0, 1 \,. \tag{4.29}$$

This leads to the relation (3.58) if we set $w_{\ell j} = \chi^\ell_{1j}$.

In the tensor product setting, projection onto the spaces V_h^k $(0 \leq k \leq 3)$ means inverting the respective inter-/histopolation matrices $\mathcal{I}^k$, as written in (4.19). We will now identify the corresponding linear systems for the previously introduced polar projectors $\overline{\Pi}_k$. The starting point is the Definition 3 of the polar projectors via the DOFs. By expressing the projected function in the respective basis that spans $\overline{V}_h^k$, the left-hand side can be expressed in terms of new *polar inter-/histopolation matrices* $\overline{\mathcal{I}}^k$,

$$\overline{\mathcal{I}}^0 \, \overline{\mathbf{f}} = \overline{\sigma}^0(f) \,, \qquad \overline{\mathcal{I}}^1 \, \vec{\overline{\mathbf{a}}} = \overline{\sigma}^1(\mathbf{A}) \,, \qquad \overline{\mathcal{I}}^2 \, \vec{\overline{\mathbf{b}}} = \overline{\sigma}^2(\mathbf{B}) \,, \qquad \overline{\mathcal{I}}^3 \, \overline{\mathbf{p}} = \overline{\sigma}^3(p) \,. \tag{4.30}$$

In order to determine the matrices $\overline{\mathcal{I}}$, we note that the polar DOFs are linear combinations of the tensor product DOFs. Therefore, let us write the projection problems in the tensor product bases, restrict the solution to the polar subspaces via the transpose extraction operators $(\mathbb{E}^k)^\top$, and project the DOFs to get square matrices:

$$\mathbb{P}^0 \, \mathcal{I}^0 \, (\mathbb{E}^0)^\top \, \overline{\mathbf{f}} = \mathbb{P}^0 \, \sigma^0(f) \,, \tag{4.31}$$

$$\mathbb{P}^1 \, \mathcal{I}^1 \, (\mathbb{E}^1)^\top \, \vec{\overline{\mathbf{a}}} = \mathbb{P}^1 \, \sigma^1(\mathbf{A}) \,, \tag{4.32}$$

$$\mathbb{P}^2 \, \mathcal{I}^2 \, (\mathbb{E}^2)^\top \, \vec{\overline{\mathbf{b}}} = \mathbb{P}^2 \, \sigma^2(\mathbf{B}) \,, \tag{4.33}$$

$$\mathbb{P}^3 \, \mathcal{I}^3 \, (\mathbb{E}^3)^\top \, \overline{\mathbf{p}} = \mathbb{P}^3 \, \sigma^3(p) \,. \tag{4.34}$$

Here, we introduced the matrices $\mathbb{P}^k$ that map tensor product DOFs to polar DOFs, $\overline{\sigma}^k(\cdot) = \mathbb{P}^k \sigma^k(\cdot)$. These matrices perform linear combinations of tensor product DOFs and thus play a similar role as the extraction matrices for basis functions $\mathbb{E}^k$. However, while $\mathbb{E}^k$ always act on tensor product basis functions, $\mathbb{P}^k$ always act on tensor product DOFs. Their explicit form follow directly from the definitions of the polar DOFs from the previous section. From (4.20) we obtain

$$\mathbb{P}^0 := \begin{bmatrix} \mathbb{Y}^0 & 0 \\ 0 & \mathbb{1}_{(n_s-2)\,n_\theta} \end{bmatrix} \in \mathbb{R}^{\overline{n}^0 \times n_s n_\theta}\,, \qquad \mathbb{Y}^0 \in \mathbb{R}^{3\times 2n_\theta}\,, \quad \mathbb{Y}^0_{\ell j} := \begin{cases} 1 & j = n_\theta + \overline{j}_\ell\,, \\ 0 & \text{else}\,, \end{cases} \tag{4.35}$$

where $\overline{j}_\ell$ is the local index of the point $\overline{\mathfrak{t}}_\ell$ on the $i = 1$ ring such that $\mathbb{Y}^0$ selects the three interpolation points $\overline{\mathfrak{t}}_{\ell=0,1,2}$ from the entire set of interpolation points. From (4.23) we obtain

$$\mathbb{P}^1 := \begin{bmatrix} \mathbb{P}^{1,1} & 0 & 0 \\ 0 & \mathbb{P}^{1,2} & 0 \\ 0 & 0 & \mathbb{P}^0 \end{bmatrix} \in \mathbb{R}^{\overline{n}^1 \times (d_s n_\theta + n_s d_\theta + n_s n_\theta)}\,, \tag{4.36}$$

with blocks

$$\mathbb{P}^{1,1} := \begin{bmatrix} \mathbb{Y}^{1,1} & 0 \\ 0 & \mathbb{1}_{(d_s-2)\,n_\theta} \end{bmatrix} \in \mathbb{R}^{\overline{n}^{1,1} \times d_s n_\theta}\,, \qquad \mathbb{P}^{1,2} := \begin{bmatrix} \mathbb{Y}^{1,2} & 0 \\ 0 & \mathbb{1}_{(n_s-2)\,n_\theta} \end{bmatrix} \in \mathbb{R}^{\overline{n}^{1,2} \times n_s d_\theta}\,, \tag{4.37}$$

where $\mathbb{Y}^{1,1} \in \mathbb{R}^{n_\theta \times 2n_\theta}$ acts on the first $2n_\theta$ tensor product DOFs $\sigma^{1,1}_{(ij)}$ and $\mathbb{Y}^{1,2} \in \mathbb{R}^{2\times 2d_\theta}$ acts on the first $2d_\theta$ tensor product DOFs $\sigma^{1,2}_{(ij)}$:

$$\mathbb{Y}^{1,1}_{ij} := \begin{cases} \delta_{ij} - \sum_{\ell=0}^{2} \delta_{j\overline{j}_\ell} w_{\ell i} & 0 \le j < n_\theta\,, \\ \delta_{i(j-n_\theta)} & n_\theta \le j < 2n_\theta\,, \\ 0 & \text{else}\,, \end{cases} \qquad \mathbb{Y}^{1,2}_{\ell j} := \begin{cases} 1 & d_\theta + \overline{j}_0 \le j < d_\theta + \overline{j}_{\ell+1}\,, \\ 0 & \text{else}\,. \end{cases} \tag{4.38}$$

From (4.25) and (4.26) we obtain

$$\mathbb{P}^2 := \begin{bmatrix} \mathbb{P}^{1,2} & 0 & 0 \\ 0 & \mathbb{P}^{1,1} & 0 \\ 0 & 0 & \mathbb{P}^3 \end{bmatrix} \in \mathbb{R}^{\overline{n}^2 \times (n_s d_\theta + d_s n_\theta + d_s d_\theta)}\,, \qquad \mathbb{P}^3 := \begin{bmatrix} \mathbb{Y}^3 & 0 \\ 0 & \mathbb{1}_{(d_s-2)d_\theta} \end{bmatrix} \in \mathbb{R}^{\overline{n}^3 \times d_s d_\theta}\,, \tag{4.39}$$

where $\mathbb{Y}^3 \in \mathbb{R}^{d_\theta \times 2d_\theta}$ acts on the first $2d_\theta$ tensor product DOFs $\sigma^{2,3}_{(ij)} = \sigma^3_{(ij)}$,

$$\mathbb{Y}^3_{ij} := \begin{cases} \delta_{ij} & 0 \le j < \overline{j}_0 \quad \text{and} \quad \overline{j}_2 \le j < d_\theta\,, \\ \delta_{ij} - (a_{0i} + a_{1i}) & \overline{j}_0 < j \le \overline{j}_1\,, \\ \delta_{ij} - a_{1i} & \overline{j}_1 < j \le \overline{j}_2\,, \\ \delta_{i(j-d_\theta)} & d_\theta \le j < 2d_\theta\,, \\ 0 & \text{else}\,. \end{cases} \tag{4.40}$$

4.3 Convergence test

To investigate the performance of the introduced polar projection operators $\overline{\Pi}_k$ $(0 \le k \le 3)$, we conduct an L^2-convergence test by increasing the number of splines both in s- and θ- direction and increasing the spline degrees. For this purpose, we define the (exact) scalar and vector valued functions

$$f_{\text{ex}}(x, z) = (1 - x^2 - z^2)\cos(2\pi x)\cos(2\pi z)\,, \tag{4.41a}$$

$$\boldsymbol{f}_{\text{ex}}(x, z) = f_{\text{ex}}(x, z)\,\boldsymbol{e}_x + f_{\text{ex}}(x, z)\,\boldsymbol{e}_z\,, \tag{4.41b}$$

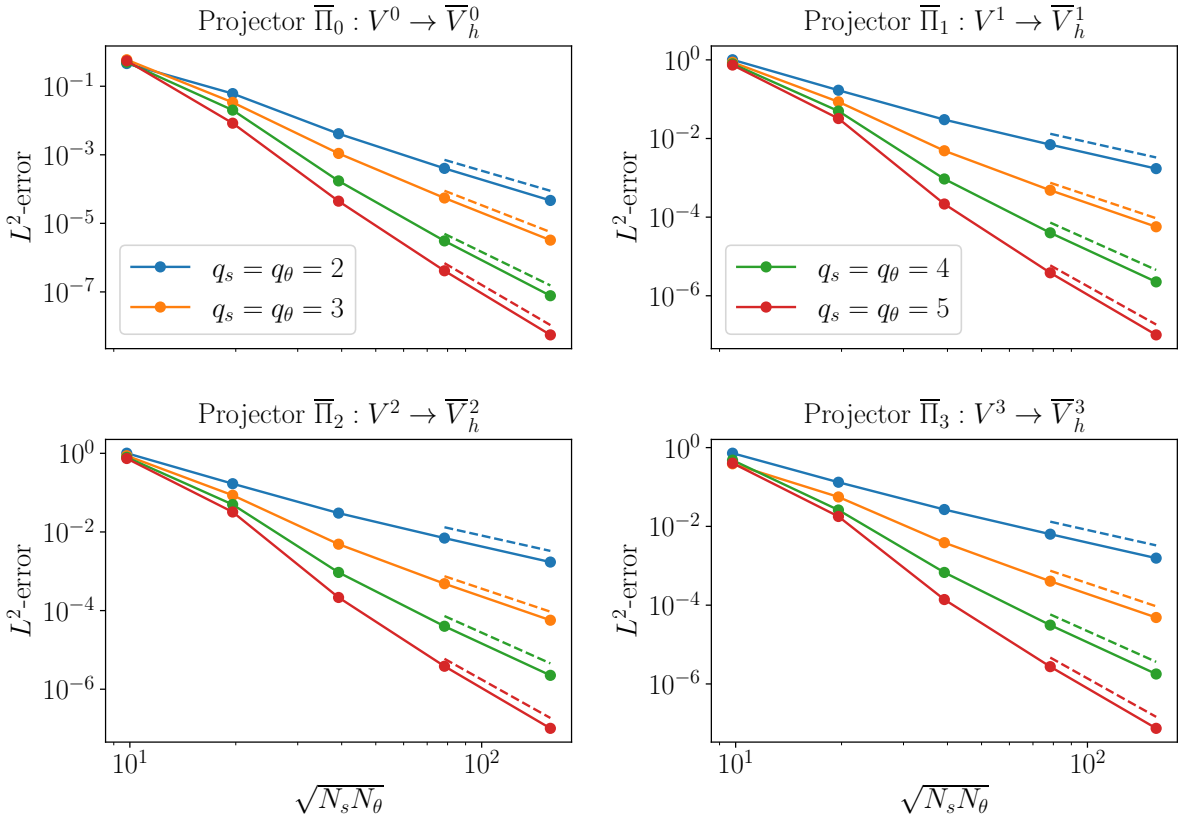

Figure 8: L^2-errors of projected polar differential k-forms ($0 \leq k \leq 3$) corresponding to the fields (4.41) for different spline degrees q_s and q_θ and different number of elements $N_s = n_s - q_s$ and $N_\theta = n_\theta$ (solid lines). Dashed lines are expected convergence rates h^{q_s+1} for $\overline{\Pi}_0$ and h^{q_s} for $\overline{\Pi}_k$ ($0 < k \leq 3$).

respectively, where $\mathbf{e}_x$ and $\mathbf{e}_z$ are Cartesian unit vectors along the respective directions. First, these fields are transformed to differential k-forms via the pull-back operations listed in Table 1 under the mapping F_{cyl} in (3.35) with (3.37) (cylinder) such that the resulting differential forms are functions of s and θ only. This is followed by projections on the spaces $\overline{V}^k_h$ ($0 \leq k \leq 3$) using the polar projection operators introduced in the previous section. The errors compared to the exact forms corresponding to the fields (4.41) are then measured in the L^2-norm based on the L^2-scalar products (2.7).

The resulting errors are shown in Figure 8 for each of the four projectors using spline degrees $q_s = q_\theta = 2, 3, 4, 5$ (solid lines). The same convergence behavior as for the pure tensor product case is observed: h^{q_s+1}-convergence for the $\overline{\Pi}_0$ projector which is based on pure interpolation and h^{q_s}-convergence for the other three projectors which are based on either mixed inter- and histopolation in case of $\overline{\Pi}_1$ and $\overline{\Pi}_2$ or pure histopolation in case of $\overline{\Pi}_3$. The parameter $h = 1/\sqrt{N_s N_\theta}$ is the geometric mean of the 1D element lengths $h_s = 1/N_s$ and $h_\theta = 1/N_\theta$ on the logical domain, where $N_s = n_s - q_s$ and $N_\theta = n_\theta$ are the number of elements in the s- and θ-direction, respectively.

5 Discrete MHD eigenvalue problem

To obtain a discrete version of the weak MHD eigenvalue problem (2.10), we replace the continuous function spaces by the corresponding polar spline subspaces introduced in Section 3. To incorporate the boundary conditions in the same way as in (2.9), we introduce *boundary operators* $\mathbb{B}^k$ ($0 \leq k < 3$) whose application on the set of basis functions spanning $\overline{V}^k_h$ form reduced bases spanning spaces $\overline{V}^k_{0,h}$ satisfying the same boundary conditions as in (2.9). E.g.

$$\overline{\mathbf{\Lambda}}^0_0 = \mathbb{B}^0\,\overline{\mathbf{\Lambda}}^0 = \mathbb{B}^0\,\mathbb{E}^0\mathbf{\Lambda}^0\,, \qquad V^0_h = \text{span}\left(\mathbf{\Lambda}^0\right)\,, \quad \overline{V}^0_h = \text{span}\left(\overline{\mathbf{\Lambda}}^0\right)\,, \quad \overline{V}^0_{0,h} = \text{span}\left(\overline{\mathbf{\Lambda}}^0_0\right)\,, \tag{5.1}$$

and similarly for $k = 1$ and $k = 2$. Thanks to the property of clamped B-splines being interpolatory at the boundaries (see (3.3)), the operators $\mathbb{B}^k$ have a simple form and just have to make sure that

basis functions in $\overline{V}_h^k$ having contributions from $N_{n_s-1}^{q_s}(s)$ are eliminated:

$$\mathbb{B}^0 := \begin{bmatrix} \mathbb{1}_{\overline{n}_0^0} & \mathbb{0}_{\overline{n}_0^0 \times n_\theta} \end{bmatrix} \in \mathbb{R}^{\overline{n}_0^0 \times \overline{n}^0}, \qquad \overline{n}_0^0 := \overline{n}^0 - n_\theta, \tag{5.2}$$

$$\mathbb{B}^1 := \begin{bmatrix} \mathbb{1}_{\overline{n}^{1,1}} & 0 & 0 & 0 \\ 0 & \mathbb{1}_{\overline{n}_0^{1,2}} & \mathbb{0}_{\overline{n}_0^{1,2} \times n_\theta} & 0 \\ 0 & 0 & 0 & \mathbb{B}^0 \end{bmatrix} \in \mathbb{R}^{\overline{n}_0^1 \times \overline{n}^1}, \quad \overline{n}_0^1 := \overline{n}^{1,1} + \overline{n}_0^{1,2} + \overline{n}_0^0, \quad \overline{n}_0^{1,2} := \overline{n}^{1,2} - d_\theta, \tag{5.3}$$

$$\mathbb{B}^2 := \begin{bmatrix} \mathbb{1}_{\overline{n}_0^{2,1}} & \mathbb{0}_{\overline{n}_0^{2,1} \times n_\theta} & 0 & 0 \\ 0 & 0 & \mathbb{1}_{\overline{n}^{2,2}} & 0 \\ 0 & 0 & 0 & \mathbb{1}_{\overline{n}^3} \end{bmatrix} \in \mathbb{R}^{\overline{n}_0^2 \times \overline{n}^2}, \quad \overline{n}_0^2 := \overline{n}_0^{2,1} + \overline{n}^{2,2} + \overline{n}^3, \quad \overline{n}_0^{2,1} := \overline{n}^{2,1} - d_\theta. \tag{5.4}$$

Discrete derivatives acting on FE coefficients of fields in the reduced spaces $\overline{V}_{0,h}^k$ can then easily be computed as matrix-matrix products

$$\overline{\mathbb{G}}_0 := \mathbb{B}^1 \, \overline{\mathbb{G}} \, (\mathbb{B}^0)^\top, \qquad \overline{\mathbb{C}}_0 := \mathbb{B}^2 \, \overline{\mathbb{C}} \, (\mathbb{B}^1)^\top, \qquad \overline{\mathbb{D}}_0 := \overline{\mathbb{D}} \, (\mathbb{B}^2)^\top. \tag{5.5}$$

Replacing next the continuous function spaces V_0^k in the weak formulation (2.10) with the subspaces $\overline{V}_{0,h}^k$ and introducing the approximations $(\mathbf{U}_h, p_h, \mathbf{B}_h) \in \overline{V}_{0,h}^2 \times \overline{V}_h^3 \times \overline{V}_{0,h}^2$ for the three trial functions and $\mathbf{K} \in \overline{V}_{0,h}^2$ for the test function,

$$\mathbf{U} \approx \mathbf{U}_h = \overline{\mathcal{S}}_{2,0}[\vec{\mathbf{u}}], \qquad p \approx p_h = \overline{\mathcal{S}}_3[\overline{\mathbf{p}}], \qquad \mathbf{B} \approx \mathbf{B}_h = \overline{\mathcal{S}}_{2,0}[\vec{\mathbf{b}}], \qquad \mathbf{K} \approx \mathbf{K}_h = \overline{\mathcal{S}}_{2,0}[\vec{\mathbf{k}}], \tag{5.6}$$

the following discrete eigenvalue problem is obtained: find non-trivial $\omega \in \mathbb{C}$ and $(\vec{\mathbf{u}}, \overline{\mathbf{p}}, \vec{\mathbf{b}}) \in \mathbb{R}^{\overline{n}_0^2} \times \mathbb{R}^{\overline{n}^3} \times \mathbb{R}^{\overline{n}_0^2}$ such that

$$i\omega \, \overline{\mathbb{M}}^\rho \, \vec{\mathbf{u}} = -\overline{\mathbb{D}}_0^\dagger \, \overline{\mathbb{M}}^3 \, \overline{\mathbf{p}} - \overline{\mathcal{T}}^\top \, (\overline{\mathcal{I}}_0^1)^{-\top} \, \overline{\mathbb{C}}_0^\dagger \, \overline{\mathbb{M}}^2 \, \vec{\mathbf{b}} - \overline{\mathbb{M}}^J \, \vec{\mathbf{b}}, \tag{5.7a}$$

$$i\omega \, \overline{\mathbf{p}} = \overline{\mathbb{D}}_0 \, (\overline{\mathcal{I}}_0^2)^{-1} \, \overline{\mathcal{F}} \, \vec{\mathbf{u}} + (\gamma - 1) \, (\overline{\mathcal{I}}_0^3)^{-1} \, \overline{\mathcal{K}} \, \overline{\mathbb{D}}_0 \, \vec{\mathbf{u}}, \tag{5.7b}$$

$$i\omega \, \vec{\mathbf{b}} = \overline{\mathbb{C}}_0 \, (\overline{\mathcal{I}}_0^1)^{-1} \, \overline{\mathcal{T}} \, \vec{\mathbf{u}}. \tag{5.7c}$$

The matrices $\overline{\mathbb{D}}_0^\dagger$ and $\overline{\mathbb{C}}_0^\dagger$ are the conjugate transposed matrices of $\overline{\mathbb{D}}_0$ and $\overline{\mathbb{C}}_0$, respectively, and appear when applied to the test function $\mathbf{K}_h$ rather than to one of the trail functions in the weak momentum balance equation. Moreover, we introduced the mass matrices

$$\overline{\mathbb{M}}^2 := \mathbb{E}_0^2 \, \mathbb{M}^2 \, (\mathbb{E}_0^2)^\top, \quad \mathbb{M}^2 := (\mathbb{M}_{\mu\nu}^2)_{\mu,\nu=1}^3, \quad \mathbb{M}_{\mu\nu,(ij)(mn)}^2 := \int_{\hat{\Omega}_P} \Lambda_{(ij)}^{2,\mu} \, G_{\mu\nu} \, \Lambda_{(mn)}^{2,\nu} \frac{1}{\sqrt{g}} \, \mathrm{d}s \, \mathrm{d}\theta, \tag{5.8}$$

$$\overline{\mathbb{M}}^3 := \mathbb{E}^3 \, \mathbb{M}^3 \, (\mathbb{E}^3)^\top, \qquad \mathbb{M}_{(ij)(mn)}^3 := \int_{\hat{\Omega}_P} \Lambda_{(ij)}^3 \, \Lambda_{(mn)}^3 \frac{1}{\sqrt{g}} \, \mathrm{d}s \, \mathrm{d}\theta, \tag{5.9}$$

$$\overline{\mathbb{M}}^\rho := \mathbb{E}_0^2 \, \mathbb{M}^\rho \, (\mathbb{E}_0^2)^\top, \quad \mathbb{M}^\rho := (\mathbb{M}_{\mu\nu}^\rho)_{\mu,\nu=1}^3, \quad \mathbb{M}_{\mu\nu,(ij)(mn)}^\rho := \int_{\hat{\Omega}_P} \Lambda_{(ij)}^{2,\mu} \, G_{\mu\nu} \, \Lambda_{(mn)}^{2,\nu} \, \rho^{\mathrm{eq}} \frac{1}{g} \, \mathrm{d}s \, \mathrm{d}\theta, \tag{5.10}$$

$$\overline{\mathbb{M}}^J := \mathbb{E}_0^2 \, \mathbb{M}^J \, (\mathbb{E}_0^2)^\top, \quad \mathbb{M}^J := (\mathbb{M}_{\mu\nu}^J)_{\mu,\nu=1}^3, \quad \mathbb{M}_{\mu\nu,(ij)(mn)}^J := \int_{\hat{\Omega}_P} \Lambda_{(ij)}^{2,\mu} \, \epsilon_{\mu\alpha\nu} \, \Lambda_{(mn)}^{2,\nu} \, J_\alpha^{\mathrm{eq}} \frac{1}{\sqrt{g}} \, \mathrm{d}s \, \mathrm{d}\theta, \tag{5.11}$$

where $\mathbb{E}_0^k := \mathbb{B}^k \, \mathbb{E}^k$ $(0 \leq k < 3)$ as in (5.1). The mass matrices $\overline{\mathbb{M}}$ are obtained from the pure tensor product mass matrices $\mathbb{M}$ by applying the respective polar extraction operator from the left-hand side and its transposed from the right-hand side. In (5.11), $\epsilon_{\mu\alpha\nu}$ are the components of the Levi-Civita

tensor and $\Lambda^{k,\mu}_{(ij)} = \vec{\Lambda}^{k,\mu}_{(ij)} \cdot \vec{e}_\mu$ for $k = 1, 2$ and $\mu = 1, 2, 3$. Furthermore, we introduced the matrices

$$\overline{\mathcal{T}} := \mathbb{P}^1_0 \, \mathcal{T} \, (\mathbb{E}^2_0)^\top \,, \quad \mathcal{T} = (\mathcal{T}_{\mu\nu})^3_{\mu\nu=1} \,, \quad \mathcal{T}_{\mu\nu,(ij)(mn)} := \sigma^{1,\mu}_{(ij)} \left[\frac{1}{\sqrt{g}} \left(\mathbf{B}^{\mathrm{eq}} \times \vec{\Lambda}^{2,\nu}_{(mn)} \right) \right] , \tag{5.12}$$

$$\overline{\mathcal{F}} := \mathbb{P}^2_0 \, \mathcal{F} \, (\mathbb{E}^2_0)^\top \,, \quad \mathcal{F} = (\mathcal{F}_{\mu\nu})^3_{\mu\nu=1} \,, \quad \mathcal{F}_{\mu\nu,(ij)(mn)} := \sigma^{2,\mu}_{(ij)} \left[\frac{p^{\mathrm{eq}}}{\sqrt{g}} \, \vec{\Lambda}^{2,\nu}_{(mn)} \right] , \tag{5.13}$$

$$\overline{\mathcal{K}} := \mathbb{P}^3 \, \mathcal{K} \, (\mathbb{E}^3)^\top \,, \qquad \mathcal{K}_{(ij)(mn)} := \sigma^3_{(ij)} \left[\frac{p^{\mathrm{eq}}}{\sqrt{g}} \, \Lambda^3_{(mn)} \right] , \tag{5.14}$$

which appear in (5.7) at places where a projector $\overline{\Pi}_k$ is applied. Here, $\mathbb{P}^k_0 := \mathbb{B}^k \, \mathbb{P}^k$ $(0 \leq k < 3)$ and $\overline{\mathcal{I}}^k_0 := \mathbb{P}^k_0 \, \mathcal{I}^k \, (\mathbb{E}^k_0)^\top$.

The discrete MHD eigenvalue problem can finally be written in the same form as its continuous counterpart (1.1). This is achieved by inserting (5.7b) and (5.7c) in (5.7a) which leads to the compact form

$$-\omega^2 \, \overline{\mathbb{M}}^\rho \, \vec{\mathbf{u}} = \mathbb{F} \, \vec{\mathbf{u}} \,, \tag{5.15}$$

where the discrete force operator on the right-hand side reads

$$\mathbb{F} := -\overline{\mathbb{D}}^\dagger \, \overline{\mathbb{M}}^3 \left[\, \overline{\mathbb{D}}_0 \, (\overline{\mathcal{I}}^2_0)^{-1} \, \overline{\mathcal{F}} + (\gamma - 1) \, (\overline{\mathcal{I}}^3_0)^{-1} \, \overline{\mathcal{K}} \, \overline{\mathbb{D}}_0 \, \right] - \mathbb{A} - \overline{\mathbb{M}}^J \, \overline{\mathbb{C}}_0 \, (\overline{\mathcal{I}}^1_0)^{-1} \, \overline{\mathcal{T}} \,, \tag{5.16}$$

$$\mathbb{A} := \overline{\mathcal{T}}^\top (\overline{\mathcal{I}}^1_0)^{-\top} \, \overline{\mathbb{C}}^\dagger_0 \, \overline{\mathbb{M}}^2 \, \overline{\mathbb{C}}_0 \, (\overline{\mathcal{I}}^1_0)^{-1} \, \overline{\mathcal{T}} \,, \tag{5.17}$$

with $\mathbb{A} = \mathbb{A}^\dagger$ being Hermitian. Hence, inverting the mass matrix $\overline{\mathbb{M}}^\rho$ and subsequently solving for the eigenvalues ω^2 and eigenvectors $\vec{\mathbf{u}}$ yields the complete ideal MHD spectrum corresponding to some given equilibrium state.

6 Numerical tests

6.1 Cylindrical magnetosonic eigenmodes

As a first test case we consider a cylindrical geometry with radius a and length $2\pi R_0$ (see mapping F_{cyl} in (3.35) with (3.37)). For this geometry, analytical solutions to the MHD equilibrium force balance are available. It is important to keep in mind, however, that the geometry in the IGA framework is not an exact disc (in the poloidal plane) but rather represented by the spline functions (3.39). Hence, it constitutes and additional source of numerical error, especially when comparisons of numerical results to analytical results, which are based on the assumption of an exact disc, are performed. Such an analytical result to the ideal MHD eigenvalue problem can be derived for the case of a homogeneous plasma with $\rho_{\mathrm{eq}} = \rho_0$ and $p_{\mathrm{eq}} = p_0$ which is placed in a constant axial magnetic field $\boldsymbol{B}_{\mathrm{eq}} = B_0 \, \boldsymbol{e}_y$ [17]. This yields two types of solutions with eigenfrequencies

$$\omega^2 = \begin{cases} v_{\mathrm{A}}^2 k^2 \,, \\ \dfrac{1}{2} \left(k^2 + \dfrac{\alpha^2_{ml}}{a^2} \right) \left((v_{\mathrm{A}}^2 + v_{\mathrm{S}}^2) \pm \sqrt{(v_{\mathrm{A}}^2 + v_{\mathrm{S}}^2)^2 - 4 v_{\mathrm{A}}^2 v_{\mathrm{S}}^2 k^2 / \left(k^2 + \dfrac{\alpha^2_{ml}}{a^2} \right)} \right) , \end{cases} \tag{6.1}$$

where $k = n/R_0$ is the "toroidal" wave number and α_{ml} is the l-th zero of the first derivative of the m-th Bessel function J_m. The characteristic velocities are the Alfvén velocity $v_{\mathrm{A}} = B_0/\sqrt{\mu_0 \rho_0}$ and the speed of sound $v_{\mathrm{S}} = \sqrt{\gamma p_0 / \rho_0}$. Hence, shear Alfvén waves are not affected by the presence of a cylindrical wall and therefore exhibit a spectrum with infinitely degenerate eigenfrequencies $\omega^2 = v_{\mathrm{A}}^2 k^2$. In contrast to that, fast $(+)$ and slow $(-)$ magnetosonic waves exhibit a discrete spectrum of eigenfrequencies characterized by two integer mode numbers $l > 0$ and $|m| \geq 0$, where m can be identified with the "poloidal" mode number in θ-direction. It is straightforward to show that in the limit $a \to \infty$ the second expression in (6.1) collapses to the standard dispersion relation for magnetosonic waves propagating parallel to the magnetic field in an infinitely extended plasma. In this case, the fast waves

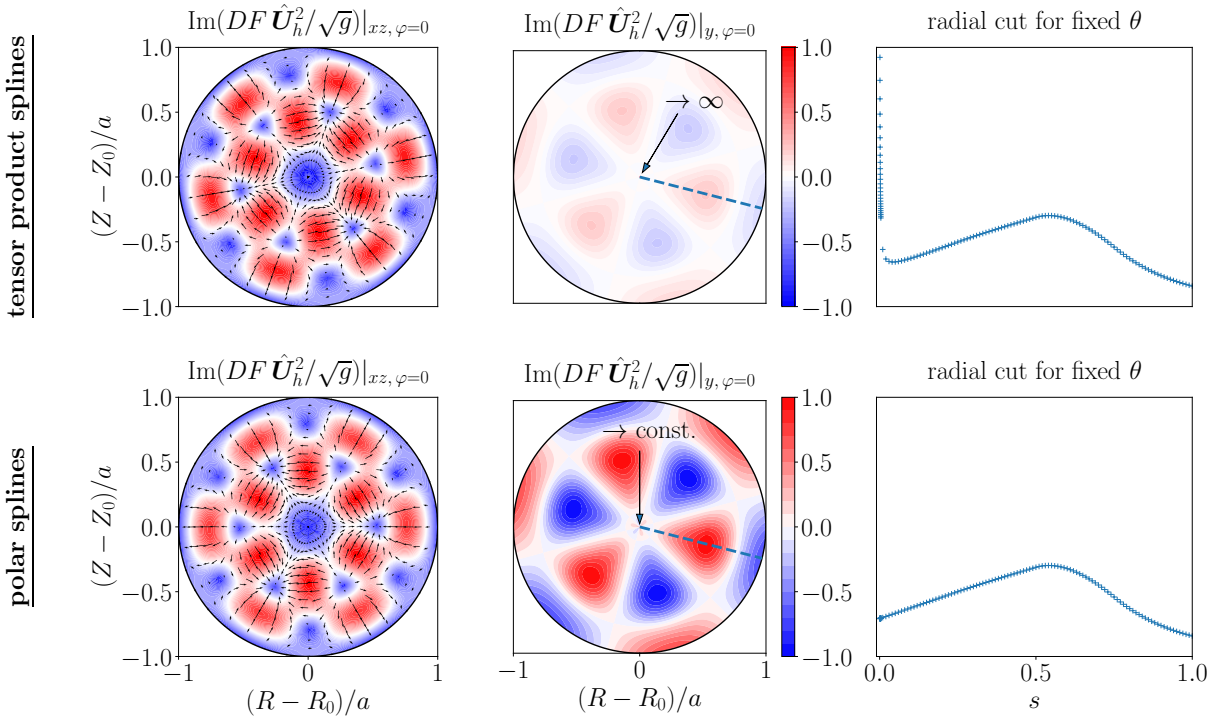

Figure 9: Normalized (to respective maximum absolute values) slow magnetosonic eigenmode (imaginary part) with mode numbers $l = 2$ and $|m| = 3$ in cylindrical geometry with a pure axial magnetic field using pure tensor product splines (upper line) and polar splines (lower line). Numerical parameters are $q_s = q_\theta = 3$, $n_s = 7$ and $n_\theta = 12$.

Table 2: Comparison of analytical (see (6.1)) and numerical eigenfrequencies for the $l = 2$, $|m| = 3$ slow magnetosonic eigenmode obtained with pure tensor product splines and polar splines ($\omega_\mathrm{A} = v_\mathrm{A}/R_0$).

	$(\omega^2 - \omega_\infty^2)/\omega_\mathrm{A}^2$	relative error
analytical	$2.118\,41 \times 10^{-5}$	-
pure tensor product splines	$2.113\,02 \times 10^{-5}$	$2.545\,86 \times 10^{-3}$
polar splines	$2.112\,72 \times 10^{-5}$	$2.687\,83 \times 10^{-3}$

(+) propagate with the Alfvén velocity and the slow waves (−) (which are then ordinary sound waves) with the speed of sound.

For parameters $a = 1\,\mathrm{m}$, $R_0 = 2\,\mathrm{m}$, $n = -1$, $B_0 = 1\,\mathrm{T}$ and $p_0 = 0.05\,B_0^2/\mu_0$ (plasma beta $\beta = 10\,\%$), we compute numerical solutions to the MHD eigenvalue problem according to (5.15) and (5.16) and compare it to the numerical spectrum obtained when using pure tensor product splines. For the latter, boundary conditions at the pole ($s = 0$) must be supplemented. In the pure tensor product spline de Rham complex (3.34) it is possible to impose the boundary conditions (3.38a), (3.38b) and the first condition in (3.38c) at $s = 0$ but not the second condition in (3.38c) and the condition (3.38d) for 3-forms. For $\mathcal{C}^1$-smooth polar splines, by contrast, the latter two are satisfied as well. To highlight the consequence of this, we investigate the $l = 2$, $|m| = 3$ slow magnetosonic eigenmode which is found in both numerical spectra. In the V_h^0 space, $n_s = 6$ cubic B-splines are used in s-direction and $n_\theta = 12$ cubic B-splines in θ-direction. It can be shown that the eigenfrequencies (6.1) corresponding to the slow magnetosonic eigenmodes converge towards the accumulation point $\omega_\infty^2 = v_\mathrm{A}^2\, v_\mathrm{S}^2\, k^2/(v_\mathrm{A}^2 + v_\mathrm{S}^2)$ for $l \to \infty$. Hence, rather than the absolute values, differences to this point are taken as a measure of accuracy.

The resulting numerical eigenfrequencies listed in Table 2 agree well with the analytical one (relative error $< 3 \times 10^{-3}$) and the difference between the pure tensor product result and the polar spline result is small. However, if the resulting eigenfunctions are plotted on the physical domain using the push-forward operation for 2-forms shown in Table 1, a very different behavior is found close to the magnetic

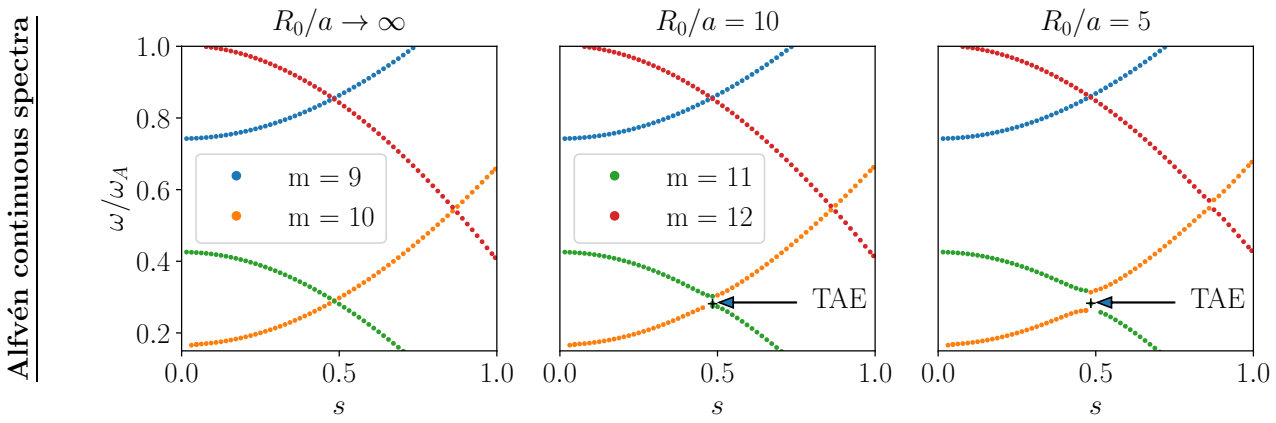

Figure 10: Numerical Alfvén continuous spectra for different aspect ratios $R_0/a \to \infty$, $R_0/a = 10$ and $R_0/a = 5$ and fixed toroidal mode number $n = -6$ ($\omega_\mathrm{A} = v_\mathrm{A}/R_0$). Numerical parameters are $q_s = q_\theta = 3$, $n_s = 64$ and $n_\theta = 96$. Shown are also the locations of toroidal Alfvén eigenmodes (TAEs) inside the gaps that form due to a coupling of the $m = 10$ and $m = 11$ branch.

axis for the axial component $U_{h,y}$. This is shown in Figure 9 where the resulting $(U_{h,x}, U_{h,z})$ vector field (left column) and $U_{h,y}$-component (middle column) are plotted using pure tensor product splines (upper row) and polar splines (lower row). While for the former the axial component diverges close to the pole due to the $1/\sqrt{g}$ factor in the push-forward operation for 2-forms ($\sqrt{g} \to 0$ for $s \to 0$), this is not the case for the polar splines where regularity in the push-forward is guaranteed. The point where the tensor product solution explodes can be pushed towards the pole $s = 0$ by increasing the resolution of the spline basis; however, this is not a viable solution when eigenfunctions need to be evaluated arbitrarily close to the pole, as for instance in particle-in-cell codes such as STRUPHY [19].

6.2 Toroidal Alfvén eigenmodes

The second test case includes effects caused by toroidal curvature and serves as a benchmark study with existing codes. The aim is to demonstrate that the presented eigenvalue solver based on FEEC and polar splines can accurately reproduce well-known numerical results. The test case is taken from [22] and is characterized by a circular toroidal geometry with minor radius $a = 1\,\mathrm{m}$ and major radius R_0 (see mapping F_tor in (3.35) with (3.37)) together with an analytical equilibrium magnetic field of the form

$$\boldsymbol{B}_\mathrm{eq} = \frac{B_0 R_0}{R}\left(\boldsymbol{e}_\varphi + \frac{r}{\overline{q}(r) R_0}\,\boldsymbol{e}_\theta\right), \qquad \overline{q}(r) = q(r)\sqrt{1 - \left(\frac{r}{R_0}\right)^2}, \tag{6.2}$$

where r is the distance from the magnetic axis at $R = R_0$ and $\boldsymbol{e}_\theta$ and $\boldsymbol{e}_\varphi$ are unit vectors (co-variant) along the poloidal and toroidal direction, respectively. Moreover, $B_0 = 3\,\mathrm{T}$ is the on-axis toroidal magnetic field and $q = q(r)$ the safety factor which is chosen to be

$$q(r) = 1.71 + 0.16\,\frac{r^2}{a^2}. \tag{6.3}$$

Finally, flat profiles for the mass density $\rho_\mathrm{eq} = \rho_0$ and the pressure $p_\mathrm{eq} = p_0 = 8.055 \times 10^{-3}\, B_0^2/\mu_0$ (on-axis plasma beta $\beta = 0.179\,\%$) are chosen. These profiles are not an exact solution to the MHD equilibrium force balance and are rather chosen in an ad hoc way mainly to capture effects coming from the characteristic $1/R$ dependence of the toroidal component of the magnetic field.

In such a configuration singular solutions corresponding to the shear Alfvén continuum exist [1]. In the cylindrical limit ($R_0/a \to \infty$) the eigenfrequencies of these continuum modes read

$$\omega^2(r) = \frac{B_0^2}{\rho_0 \mu_0}\frac{1}{R_0^2}\left(n + \frac{m}{q(r)}\right)^2 = v_\mathrm{A}^2\, k_\parallel^2(r), \tag{6.4}$$

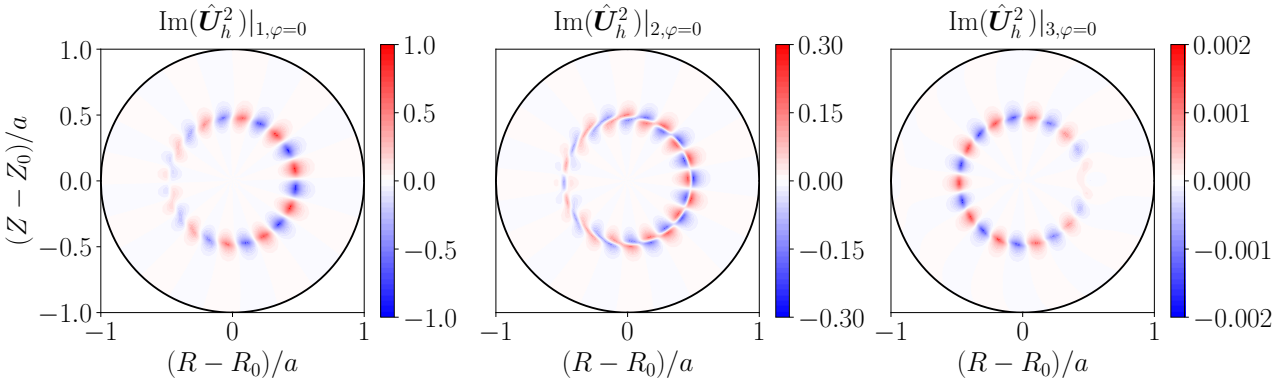

Figure 11: Normalized (to the maximum absolute value of the first component) 2-form components of a toroidal Alfvén eigenmode (TAE) with mode numbers $m = 10, 11$ and $n = -6$ in a torus with aspect ratio $R_0/a = 10$ (corresponds to the black cross in the middle plot of Figure 10).

where $v_\mathrm{A} = B_0/\sqrt{\mu_0\rho_0}$ is the on-axis Alfvén velocity. It is evident that for a fixed toroidal mode number (n), branches $\omega^2(r)$ corresponding to different poloidal mode numbers m can intersect. This degeneracy is lifted if poloidal coupling caused by toroidal curvature is present resulting in a formation of a gap i.e. a "forbidden" zone for continuum modes [8]. This feature is correctly captured by the present eigenvalue solver as shown in Figure 10 where the numerical eigenfrequencies corresponding to the shear Alfvén continuum in the range $0 < \omega/\omega_\mathrm{A} \leq 1$ are plotted ($\omega_\mathrm{A} = v_\mathrm{A}/R_0$). The toroidal mode number $n = -6$ and the "spatial location" of each eigenfrequncy is identified by looking for the singularity in the corresponding eigenfunction. On the left, the cylindrical limit with intersecting $m = 10, 11$ branches are identified while the plots in the middle and on the right show toroidicity induced gaps at the intersection points at $s = 0.5$.

Besides continuum modes, toroidicity induced global, discrete Alfvén eigenmodes (TAEs) can exist insides the gaps [8] which is also found in the numerical spectra with finite aspect ratios. Figure 11 shows the TAE mode structures for the three components of the resulting 2-form eigen-velocity for the case $R_0/a = 10$. Due to coupling of $m = 10$ and $m = 11$ modes, a ballooning-like mode structure, i.e. an asymmetry between the high-field side and low-field side is observed. The computed TAE eigenfrequency for a hydrogen plasma with number density $n_0 = 2 \times 10^{19}\,\mathrm{m}^{-3}$ is $\omega = 4.14 \times 10^{-5}\,\mathrm{rad\,s}^{-1}$ which is in good agreement with other codes (see graphs corresponding to *MHD: no background pressure gradient* in plot (a) of Figure 2 in [22]).

7 Conclusion

We presented a numerical strategy for the solution of the ideal MHD eigenvalue problem for axissymmetric equilibria on computational domains with a unique singular pole (edge that is mapped onto a single point). Our approach combines discrete differential forms with the IGA-based polar spline framework introduced by Toshniwal et al. [28, 27]. The former provides a natural discretization of grad-, curl- and div-operators in curvilinear coordinates that preserves the de Rham complex on the discrete level. The latter leads to continuous eigenfunctions on the mapped domain, including the pole. The main contribution of this work is the definition of commuting projectors for the polar de Rham diagram. These projectors are defined via polar degrees of freedom (DOFs), obtained as linear combinations of tensor product DOFs. We state several sufficient conditions for commutativity on these linear combinations and give explicit, block-wise representations of all reduction matrices needed. Finally, the new eigenvalue solver has been benchmarked with a toroidal-Alfvén eigenmode (TAE) calculation and a cylindrical test case for analytic comparison; the correct behavior of eigenfunctions near the pole is demonstrated, in contrast to the standard tensor product solver.

Future work will include detailed verifications for realistic tokamak equilibria with non-circular poloidal cross-sections and coupling to a particle-in-cell code for a kinetic minority species as shown in [19]. The latter was the original motivation for this work and it is expected that the developed

methods help improving particle pushing close to the magnetic axis.

Acknowledgements

To end this article, we would like to thank Eric Sonnendrücker and Xin Wang for general input and useful discussions throughout this work.

This work has been carried out within the framework of the EUROfusion consortium and has received funding from the Euratom research and training programme 2014-2018 and 2019-2020 under grant agreement No 633053. The views and opinions expressed herein do not necessarily reflect those of the European Commission.

References

[1] K. Appert, R. Gruber, and J. Vaclavik. Continuous spectra of a cylindrical magnetohydrodynamic equilibrium. *The Physics of Fluids*, 17(7):1471–1472, 1974.

[2] D. N. Arnold, R. S. Falk, and R. Winther. Finite element exterior calculus, homological techniques, and applications. *Acta Numerica*, 15:1–155, 2006.

[3] D. N. Arnold, R. S. Falk, and R. Winther. Finite element exterior calculus: from Hodge theory to numerical stability. *Bulletin of the American mathematical society*, 47(2):281–354, 2010.

[4] L. Bernard, F. Helton, and R. Moore. GATO: An MHD stability code for axisymmetric plasmas with internal separatrices. *Computer Physics Communications*, 24(3):377–380, 1981.

[5] A. Bondeson, G. Vlad, and H. Lütjens. Resistive toroidal stability of internal kink modes in circular and shaped tokamaks. *Physics of Fluids B: Plasma Physics*, 4(7):1889–1900, 1992.

[6] A. Buffa, J. Rivas, G. Sangalli, and R. Vázquez. Isogeometric Discrete Differential Forms in Three Dimensions. *SIAM Journal on Numerical Analysis*, 49(2):818–844, 2011.

[7] A. Buffa, G. Sangalli, and R. Vázquez. Isogeometric analysis in electromagnetics: B-splines approximation. *Computer Methods in Applied Mechanics and Engineering*, 199:1143–1152, 2010.

[8] C. Z. Cheng and M. S. Chance. Low-n shear Alfvén spectra in axisymmetric toroidal plasmas. *The Physics of Fluids*, 29(11):3695–3701, 1986.

[9] J. A. Cottrell, T. J. Hughes, and Y. Bazilevs. *Isogeometric analysis: toward integration of CAD and FEA*. John Wiley & Sons, 2009.

[10] J. Crank and P. Nicolson. A practical method for numerical evaluation of solutions of partial differential equations of the heat-conduction type. *Mathematical Proceedings of the Cambridge Philosophical Society*, 43(1):50–67, 1947.

[11] C. de Boor. *A Practical Guide to Splines*. Springer New York, NY, 2 edition, 2001.

[12] L. Degtyarev, A. Martynov, S. Medvedev, F. Troyon, L. Villard, and R. Gruber. The KINX ideal MHD stability code for axisymmetric plasmas with separatrix. *Computer Physics Communications*, 103(1):10–27, 1997.

[13] G. Farin. *Curves and Surfaces for Computer-Aided Geometric Design*. Academic Press, 1993.

[14] T. Frankel. *The Geometry of Physics: An Introduction*. Cambridge University Press, 3 edition, 2011.

[15] J. P. Freidberg. *Ideal MHD*. Cambridge University Press, 2014.

[16] R. C. Grimm, J. M. Greene, and J. L. Johnson. Computation of the Magnetohydrodynamic Spectrum in Axisymmetric Toroidal Confinement Systems. In J. KILLEEN, editor, *Controlled Fusion*, volume 16 of *Methods in Computational Physics: Advances in Research and Applications*, pages 253–280. Elsevier, 1976.

[17] R. Gruber and J. Rappaz. *Finite Element Methods in Linear Ideal Magnetohydrodynamics*. Springer, Berlin, Heidelberg, 1985.

[18] R. Gruber, F. Troyon, D. Berger, L. C. Bernard, S. Rousset, R. Schreiber, W. Kerner, W. Schneider, and K. V. Roberts. Erato stability code. *Computer Physics Communications*, 21(3):323–371, 1981.

[19] F. Holderied, S. Possanner, and X. Wang. MHD-kinetic hybrid code based on structure-preserving finite elements with particles-in-cell. *Journal of Computational Physics*, 433:110143, 2021.

[20] K. Hu, Q. Zhang, and Z. Zhang. A Family of Finite Element Stokes Complexes in Three Dimensions. *SIAM Journal on Numerical Analysis*, 60(1):222–243, 2022.

[21] W. Kerner, J. Goedbloed, G. Huysmans, S. Poedts, and E. Schwarz. CASTOR: Normal-Mode Analysis of Resistive MHD Plasmas. *Journal of Computational Physics*, 142(2):271–303, 1998.

[22] A. Könies, S. Briguglio, N. Gorelenkov, T. Fehér, M. Isaev, P. Lauber, A. Mishchenko, D. Spong, Y. Todo, W. Cooper, R. Hatzky, R. Kleiber, M. Borchardt, G. Vlad, A. Biancalani, and A. Bottino. Benchmark of gyrokinetic, kinetic MHD and gyrofluid codes for the linear calculation of fast particle driven TAE dynamics. *Nuclear Fusion*, 58(12):126027, 2018.

[23] P. Lauber, S. Günter, A. Könies, and S. Pinches. LIGKA: A linear gyrokinetic code for the description of background kinetic and fast particle effects on the MHD stability in tokamaks. *Journal of Computational Physics*, 226(1):447–465, 2007.

[24] T. Lyche, C. Manni, and H. Speleers. Foundations of Spline Theory: B-Splines, Spline Approximation, and Hierarchical Refinement. In T. Lyche, C. Manni, and H. Speleers, editors, *Splines and PDEs: From Approximation Theory to Numerical Linear Algebra*, pages 1–76. Springer, Cham, 2018.

[25] F. Patrizi. Isogeometric de Rham complex discretization in solid toroidal domains. *arXiv preprint arXiv:2106.10470*, 2021.

[26] H. Speleers and D. Toshniwal. A General Class of C^1 Smooth Rational Splines: Application to Construction of Exact Ellipses and Ellipsoids. *Computer-Aided Design*, 132:102982, 2021.

[27] D. Toshniwal and T. J. Hughes. Isogeometric discrete differential forms: Non-uniform degrees, Bézier extraction, Polar splines and flows on surfaces. *Computer Methods in Applied Mechanics and Engineering*, 376:113576, 2021.

[28] D. Toshniwal, H. Speleers, R. R. Hiemstra, and T. J. Hughes. Multi-degree smooth polar splines: A framework for geometric modeling and isogeometric analysis. *Computer Methods in Applied Mechanics and Engineering*, 316:1005–1061, 2017. Special Issue on Isogeometric Analysis: Progress and Challenges.

[29] B. Van der Holst, A. Beliën, J. Goedbloed, M. Nool, and A. Van der Ploeg. Calculation of resistive magnetohydrodynamic spectra in tokamaks. *Physics of Plasmas*, 6(5):1554–1561, 1999.